Experimental and Data Fitting Guidelines for the Determination of Polymer Crystallization Kinetics

Ricardo Arpad Pérez-Camargo,[1] Guoming Liu,[1,2*] Dujin Wang,[1,2] Alejandro J. Müller.[3,4]

[1]Beijing National Laboratory for Molecular Sciences, CAS Key Laboratory of Engineering Plastics, Institute of Chemistry, Chinese Academy of Sciences, Beijing 100190, China

[2]University of Chinese Academy of Sciences, Beijing 100049, China

[3]POLYMAT and Department of Polymers and Advanced Materials: Physics, Chemistry and Technology, Faculty of Chemistry, University of the Basque Country UPV/EHU, Donostia-San Sebastián 20018, Spain

[4]IKERBASQUE, Basque Foundation for Science, Bilbao 48013, Spain

Corresponding authors: Guoming Liu; gmliu@iccas.ac.cn

ABSTRACT

The crystallization kinetics of semicrystalline polymers is often studied with isothermal experiments and analyzed by fitting the data with analytical expressions of the Avrami and Lauritzen and Hoffman (LH) theories. To correctly carry out the analysis, precautions both in experiments and data fitting should be taken. Here, we systematically discussed the factors that influence the validity of the crystallization kinetics study. The basic concepts and fundamentals of the Avrami and LH theories were introduced at first. Then, experimental protocols were discussed in detail. To clarify the impact of various experimental parameters selected common polymers, i.e., polypropylene and polylactide, were studied using various experimental techniques (i.e., differential scanning calorimetry and polarized light optical microscopy). Common mistakes were simulated under conditions when non-ideal experimental parameters were applied. Furthermore, from a practical point of view, we show how to fit the experimental data to the Avrami and the LH theories, using an Origin ® App developed by us.

Keywords: *Isothermal crystallization, Avrami equation, Lauritzen and Hoffman theory, Thermal analysis, Step-crystallization.*

1. INTRODUCTION

Crystallization is a phase transformation of matter from an amorphous to a crystalline state. In general, crystallization involves two steps: nucleation and growth.[1] The time dependence of crystallinity is called “crystallization kinetics”. For polymers, crystallization kinetics is highly relevant to the processing and final properties of polymeric materials. Crystallization kinetics is most often followed by performing isothermal experiments, although non-isothermal approaches have also been used.[2-4] Depending on the material, isothermal crystallization can be performed at a constant temperature after the sample has been cooled from the melt or heated from the glassy state. The relevant experimental parameters are isothermal crystallization temperatures, cooling rates, times of crystallization, among other variables. The correct procedure applied to obtain the experimental data is essential before any quantitative analysis can be performed using different crystallization theories.

Crystallization theories have been developed to describe the overall crystallization process. One of the most accepted and used theories is the Avrami theory,[5-7] also known as the Johnson-Melh-Avrami-Kolmogorov model,[8] which has been reviewed in the literature.[9,10] Although it is a phenomenological model with a simple expression, it has been pointed out by Lorenzo et al.,[9] that the correct application of the Avrami theory on experimental data fitting requires selecting correct parameters, e.g., induction time, conversion range, among others. As an extension of the Avrami theory, non-isothermal approaches have also been developed, although less widely used, such as the Ozawa model.[2-4]

By analyzing the lamellar growth with secondary nucleation, the Lauritzen and Hoffman (LH) theory[11, 12] can describe, over a wide range of supercooling (ΔT) the experimental data, providing a microscopic picture of the crystallization process. Although the LH theory has been criticized[13] mainly for its inability to explain specific morphological observations and for its simplifications (or oversimplifications),[14] it is the only model that can fit the experimental data using analytical expressions and provides information regarding the activation energy barrier of nucleation. The discussion of LH theory and its modifications can be found in the literature.[15] Since many variables are included in the LH theory, there are tips on how to correctly extract parameters.

This work aims to summarize the practical aspects of polymer crystallization kinetics studied by isothermal experiments. First, we introduce the general concepts: in particular, the different terms of nucleation and crystallization. Then, we briefly describe the essentials of the Avrami theory and the LH theory, setting the bases to fit the experimental data with their expressions. Major attention is given to the correct experimental procedures for collecting isothermal crystallization data, including the influence of the crystallization temperatures, and cooling rates. Next, the factors that can affect the analysis of the Avrami theory are evaluated, not only for a continuous fit but also for a step-crystallization analysis. In the last section, we present functional elements related to data analysis using the LH theory.

1.1.General Concepts

Two processes are required for polymer crystallization: nucleation and growth. In the literature, the nucleation and growth are often named **primary nucleation** and **secondary nucleation**, respectively. These terms must not be confused with **primary and secondary crystallization**. As the first step of our discussion, we define and illustrate (see Scheme 1) the different terms mentioned above, to establish a unified criterion for them.

1.1.1. Primary Nucleation or Nucleation

The **primary nucleation or nucleation** is the formation of nuclei in the polymer where no nucleation sites exists before. The primary nucleation includes two types: **homogeneous nucleation** which arises by the spontaneous aggregation of polymer chains triggered by the supercooling applied,[16] and **heterogeneous nucleation**, which is the nucleation at the surface of heterogeneities or impurities present in the polymer.[16]

Homogeneous nucleation occurs seldomly since the formation of the new phase solely depends on fluctuations of the mother phase (i.e., melt) without the contributions of foreign elements (i.e., all the faces of the nucleus are in contact with the melt).[17, 18] The homogeneous nucleation can play a role only at very large supercooling (ΔT, e.g., 50 to 100 K[17]), often close to the glass transition of the polymer. The homogeneous nucleation can be observed when a polymer is dispersed into fine droplets that are heterogeneity free (this is usually obtained when the number of dispersed droplets is orders of magnitude higher than the number of heterogeneities present in the bulk polymer)[19-21] or using fast-scanning chip calorimeters to cover a complete range of ΔT.[22]

It has been shown that the crystallization process at large ΔT is dominated by the homogenous nucleation.[22,23]

Another special homogeneous nucleation mechanism is self-nucleation (SN). In this case, the nucleation is produced by the own ideal crystal fragments or chain segments with residual memory of any polymer.[23, 24] The SN is induced through a specific thermal treatment.[25-27] Three main SN *domains* have been defined: *Domain I* (complete melting *domain*), *Domain II* (exclusively self-nucleation *domain*), and *Domain III* (self-nucleation and annealing *domain*). Further details of the *domains* and protocol can be found in references 25-27. Here, we remark that in *Domain II*, particularly at the lowest self-nucleation temperature, the highest nucleation density is reached. Hence the T_c is shifted to the highest value, without affecting the melting behavior. This nucleation density is even higher than the nucleation caused by inherent heterogeneities and, in most cases, higher than those heterogeneities purposely added, i.e., nucleating agents. For this reason, the SN is considered a particular case of homogeneous nucleation.

The heterogeneous nucleation occurs at the surface of heterogeneities.[18] These heterogeneities include extraneous solids, cavities, container walls, among others, which enhanced the formation of stable embryos.[23] It is observed at relatively low ΔT, and it has been extensively studied in the literature.[17] The heterogeneous nucleation occurs in most polymeric materials, either from inherent impurities of the synthesis or by nucleating agents, purposely added to favor the nucleation.

Independently of the type of nucleation, the number of formed nuclei (and hence the nucleation rate) can be directly quantified through microscopy, e.g., polarized light optical microscopy, PLOM. Other experiments, like differential scanning calorimetry, DSC (see Scheme 1a, b, and c), can provide indirect information about the rate of nucleation (e.g., through the induction or incubation time, τ_0, the lag time required for the crystallization to start[28]), studying the region in which no major changes are detected.

As shown in Scheme 1a and 1b, primary nucleation occurs where essentially no heat flow can be detected (induction time), i.e., before τ_0 (see Scheme 1). In such a region, the primary nucleation is registered before any significant growth can be detected. Still, the primary nucleation process can be extended to times greater than τ_0, especially if the nucleation is sporadic.

1.1.2. Secondary nucleation or growth

Once the nucleus is formed, it will start to grow (See Schemes 1a, b and d), due to the attachment of chain segments to the growth front. This stage of crystallization is known as **secondary nucleation or growth**. If we imagine spherulites, they will grow radially, and when most of them impinge on one another, at approximately the relative half-crystallization time, $\tau_{50\%}$, this stage is considered terminated (see Schemes 1a, b and d. Note that in Schemes 1a and 1b the position of the $\tau_{50\%}$, is illustrative. Nevertheless, the values are usually close to one another). Still, some attachments of chains to the growth front events also occur in the next stage. The next stage, in which the spherulites have already started to impinge, is called **secondary crystallization**. The **growth** stage refers to the unrestrained growth of the material. The secondary nucleation is normally followed by PLOM measurements (see Section 3.3.1). Furthermore, as we show in this work, it can be also be followed by DSC[29, 30](see Section 3.3.4). It is worth noting that secondary nucleation has a lower free energy barrier than primary nucleation.[31]

1.1.3. Primary crystallization

The term **primary crystallization** includes the two previously defined nucleation and growth processes, just before the impingement of the spherulites. The primary crystallization should not be confused with primary nucleation. Schemes 1a and b show a typical calorimetric measurement of polymer isothermal crystallization. At the very beginning, no heat flow is detected, which corresponds to the process of primary nucleation before any crystallization can be measured. After that, the nuclei start to grow (see Scheme 1d), and hence there is a rapid increase in enthalpy (ΔH). The changes that occur in this stage are mainly due to growth or secondary nucleation, although primary nucleation may occur in between the growing spherulites depending on whether the primary nucleation is sporadic or instantaneous (more details in 1.2). As shown in Scheme 1b, the primary crystallization occurs approximately until reaching a relative conversion, V_c of around 50%, where spherulites start to impinge between them. Note that the impinge can sometimes occur at V_c < 50%.

1.1.4. Secondary crystallization

When the spherulites start to impinge, approximately after $\tau_{50\%}$ (see Scheme 1b and 1e, V_c~ 50%), the primary crystallization finishes. However, there are still free spaces that are not filled with crystallites. Also, a densification process may occur inside the spherulites. This includes a

"perfection" process, such as the thickening of lamellae through annealing effect and the formation of subsidiary lamellae and crystal perfection.[17,32] All these inter- and intraspherulitic crystallization processes are known as **secondary crystallization**.[32] The secondary crystallization is a slow process, as is shown in Schemes 1a and b, in which the changes in normalized ΔH and heat flow are much lower as compared to the primary crystallization. Again, it is important to note that the secondary crystallization should not be confused with the secondary nucleation because the latter corresponds to the growth of the lamellar crystals within the spherulites. Secondary nucleation refers to the attachment of chain segments to the growth front and it can occur during primary or secondary crystallization

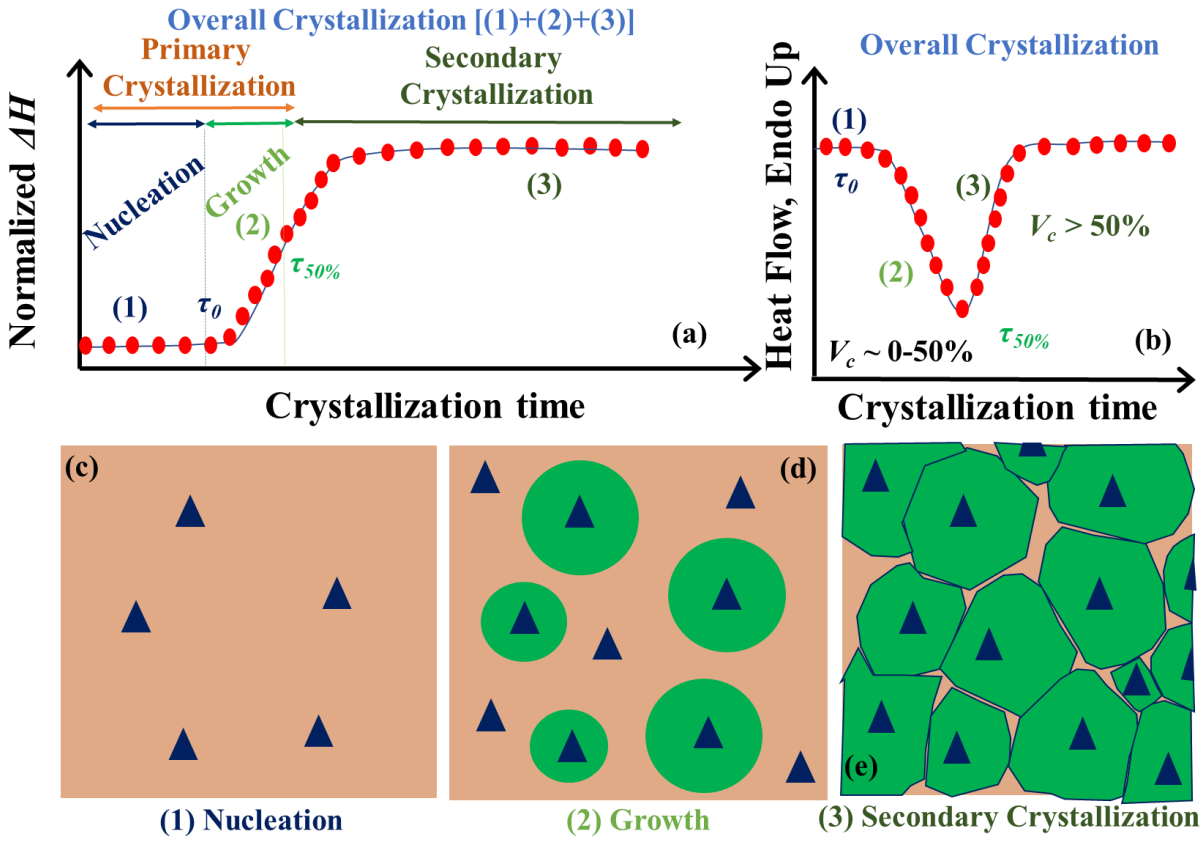

Scheme 1. Representation of a complete isothermal crystallization process through the schematic plots of (a) normalized ΔH and (b) heat flow vs. crystallization time, . In (a) and (b) the (1) nucleation, (2) growth (during this growth stage, primary nucleation may continue), and (3) secondary crystallization is indicated, which are illustrated through cartoons in (c), (d), and (e), respectively. In (c) to (e) the blue triangles represent the nucleus of the spherulites, and the green circles or polygons the growing spherulites. The vertical lines in (a) indicate the induction time, τ_0, and the half-crystallization time,$\tau_{50\%}$, which can be used as characteristic times for primary nucleation (before any growth starts) and overall crystallization (including primary nucleation and

growth) respectively. The scheme is based on reference 16. Note that in Scheme 1b, it is assumed, for illustrative purposes, that the position of $\tau_{50\%}$ coincides with the peak time (maximum heat flow). The values are usually relatively close to one another.

1.1.5. Overall crystallization

The overall crystallization includes all the above processes: primary crystallization (i.e., nucleation + growth), and secondary crystallization, as shown in Scheme 1. The overall crystallization can be recorded during isothermal DSC experiments, either continuously or by step because the crystallization process involves the release of latent heat. In the past, the crystallization process was often followed by dilatometry. Recently, besides DSC, the crystallization can be followed by wide- and small-angle X-ray scattering (WAXS and SAXS) experiments (using synchrotron radiation),[33] Fourier transformed infrared spectroscopy,[34] nuclear magnetic resonance,[35] and Raman scattering.[36] Even microhardness techniques in glassy polymers have been employed.[37,38] More details on following the crystallization process by using different experimental techniques can be seen elsewhere 36.

In this work, the terms nucleation, growth, and secondary crystallization are selected to describe the different processes of crystallization. The crystallization process has been described by different theories, among them, the Avrami and the Lauritzen and Hoffmann theories, which, despite their limitations, provide analytical expressions, widely used in the literature, to fit experimental data. Here, these theories are briefly described to set the bases for their practical use, without aiming to enter into the discussion of their validity.

1.2.Avrami theory

The Avrami theory describes the evolution of the overall crystallinity with time.[17] This involves random nucleation and growth processes.[9] As pointed out by Lorenzo et al.[9], the "free-growth" theory formulated by Göler and Sachs[39, 40] was one of the first theories that considered these terms (i.e., nucleation and growth). The Avrami theory follows such free growth approximation in a simple way that includes the time dependence of the nucleation and the time dependence of the growth taking into account the crystals dimensions. The Avrami equation assumes a constant nucleation rate (i.e., the appearance of continuous growing regions) and a constant linear growth rate (i.e., in one to three dimensions). Such considerations have their

limitations and extensions, as pointed out by Piorkowska et al.[10] The simplest form of the Avrami equations is expressed as:[5, 9]

$$1 - V_c(t) = \exp(-Kt^n) \quad (1)$$

where $V_c(t)$ is the relative volumetric transformed fraction at time t, K the overall crystallization rate constant (i.e., nucleation + growth), and n the Avrami index.

As proposed by Müller et al.,[41, 42] the n value can be expressed by the addition of two terms that represent the contribution of: the dimensionality of the growing crystals (n_{gD}) and the time dependence of the nucleation (n_n), as expressed in Equation 2.

$$n = n_{gD} + n_n \quad (2)$$

The n_{gD} values can only be integer numbers, 1, 2, and 3, corresponding to one-, two- and three-dimensional entities. In polymers, n_{gD} = 2 or 3 are commonly obtained, corresponding to either axialites (two-dimensional lamellar aggregates) or spherulites (three-dimensional aggregates superstructure). The n_n contribution should take a value of 0 or 1, where n_n = 0 corresponds to instantaneous nucleation, and n_n =1 to sporadic nucleation. However, in many cases, the nucleation is not 100% instantaneous or 100% sporadic, and it is somewhat in between 0~1. If the growth rate is not linear with time, for example, a Fickian process predicts that the growth rate is proportional to $t^{-0.5}$, and n_{gD} can have a value of 0.5.[9, 17,23]

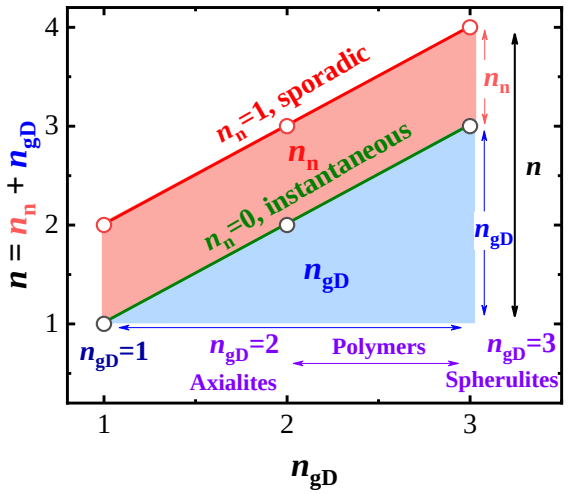

Scheme 2. Possible Avrami index (n) based on a schematic n vs. n_{gD} plot. The n_{gD} can take values between 1 and 3, and the n_n takes values between 0 and 1. The white circles represents the different n values obtained by considering the n_n and n_{gD} contributions.

Scheme 2 shows all the possibilities for the Avrami index, n, based on the n_n and n_{gD} contributions. As we mentioned before, for polymers, the n_{gD} values take values of 2 and 3, hence, an axialitic morphology that nucleated instantaneously maintains an n value of 2. On the other hand, if the polymer axialites nucleate sporadically, n will take a maximum value of 3. Similarly, a spherulitic morphology takes n values of 3 or 4 depending on the nucleation term. It is worth noting that in confined systems, n values as low as 1.0 (or even lower than 1.0) have been reported.[43] In general, as confinement increases, the n value decreases, indicating that the nucleation is the rate-determining step in overall crystallization.[44] More details related to the Avrami index are discussed in Section 3.2.5.

For the practical use of Equation 1, Lorenzo et al.[9] proposed slight modifications to include the induction time, t_0. In simple terms, the t_0 is the time at T_c that could elapse before crystallization starts. Therefore, t_0 is the time needed for primary nucleation before any growth starts, its inverse is proportional to the primary nucleation rate before growth starts.[28, 30] Thus, by considering the induction time, Equation 1 becomes the following:

$$1 - V_c(t - t_0) = \exp\left(-K(t - t_0)^n\right) \tag{3}$$

After taking logarithm at both sides of Equation 3 twice (first ln and then log), the following expression is obtained:

$$\log[-\ln[1 - V_c(t - t_0)]] = \log(K) + n\log(t - t_0) \tag{4}$$

Equation 4 is employed to construct the so-called Avrami plot.[9] From the linear fit of the Avrami plot, the slope represents n and the intercept K. More details are given in Section 3.2. The V_c in Equations 1, 3 and 4, can be calculated as:[9, 17]

$$V_c = \frac{W_c}{W_c + \left(\frac{\rho_c}{\rho_a}\right)(1 - W_c)} \quad (5)$$

where W_c is the crystalline mass fraction, ρ_c and ρ_a are the fully crystalline and fully amorphous polymer densities, respectively. When such densities are not available, it can be assumed equal ρ_a and ρ_c, e.g., a value of 1 can be assumed. In this case, the V_c is approximated to W_c. The W_c values are calculated according to Equation 6:

$$W_c = \frac{\Delta H_{(t)}}{\Delta H_{total}} \quad (6)$$

where $\Delta H_{(t)}$ is the enthalpy variation as a function of the time spent at a given T_c, and ΔH_{total} is the maximum enthalpy value reached at the end of the isothermal crystallization process. The relative errors associated with the $V_c = W_c$ approximation, i.e., $\rho_c = \rho_a$, are discussed in Section 3.2.

By applying the Avrami equation, it is possible to obtain a theoretical (i.e., obtained by using the Avrami parameters) half-crystallization time, $\tau_{50\%}$, which is the time needed for a 50% of conversion (i.e., V_c = 0.5), as follows:

$$\tau_{50\%} = \left(\frac{\ln(2)}{K}\right)^{\frac{1}{n}} \quad (7)$$

The difference between the theoretical and experimental $\tau_{50\%}$ depends on the quality of the fit close to the 50% of conversion. It is important to remark that in a heat flow vs. crystallization time curve (see Scheme 1b), the peak time (t_p) coincides with the $\tau_{50\%}$ in some special cases. Nevertheless, the values are usually relatively close to one another. Still, it is suggested to estimate the $\tau_{50\%}$ instead of t_p.

1.2.1. Dependence of nucleation with time: n_n term

Two extreme values can be taken for the n_n term; n_n = 0, and n_n = 1, which are referred to **instantaneous nucleation (n_n = 0)** and **sporadic nucleation (n_n = 1)**. In the literature, some other terms are also used, which are discussed below.

The **thermal and athermal nucleation** has been defined by Fisher et al.[45] They defined thermal nucleation as the nuclei formed randomly by thermal fluctuations throughout the crystallization. In contrast, athermal nucleation is the mechanism by which embryos are automatically promoted to nuclei, which start growing at the same time. In this context, one could consider that n_n = 1 corresponds to thermal nucleation and n_n = 0 to athermal nucleation. However, these terms are related to the process and not to its dependence with time. Therefore, we recommend employing the terms instantaneous and sporadic nucleation, as these directly refer to the nucleation time dependence.

The other set of terms on nucleation is homogeneous nucleation and heterogeneous nucleation, as defined above. A common nomenclature error in literature is to assign homogeneous nucleation to n_n = 1 and heterogeneous nucleation to n_n = 0. The terms homogeneous and heterogeneous nucleation are related to the origin of the nucleation and not to its dependence on time. Moreover, recent experiments with fast-scanning chip-calorimetry indicate that the homogenous nucleation occurs almost instantaneously at high ΔT.[22]

Here, to avoid misunderstanding, we strongly suggest adopting the terms sporadic nucleation and instantaneous nucleation to describe the n_n = 1, and n_n = 0, respectively.

1.3.Lauritzen and Hoffman Theory

The most widely employed theory to describe the growth of polymer lamellae (i.e., secondary nucleation) is the Lauritzen and Hoffman (LH) theory,[15,46] which provides analytical expressions for the linear spherulitic growth rate as a function of supercooling.[47, 48] This model has been adapted to fit overall crystallization rates obtained by DSC (i.e., including primary and secondary nucleation) and it has been widely employed for this purpose in polymer crystallization studies.[29, 48-50] Historically, other crystallization theories were also developed such as the entropy barrier (Sadler and Gilmer[51]), intramolecular nucleation (Hu et al.[52]), the multi-stage or block by block (Strobl[53]), and continuum model (Muthukumar[54]).[55, 56] But, they do not provide analytical expressions to fit experimental data, and simulations are needed instead. Here, we will focus on

the Lauritzen and Hoffman theory only from a practical point of view (i.e., as a mathematical tool), as it provides analytical expressions that can be fitted to the experimental data. We present below a brief description of the theory, and the reader is referred to reviews for more details 14, 57, 58.

The LH theory considers the formation of secondary nuclei on crystallographic surfaces. This secondary nucleus possesses chain stems of length l, and given lateral dimensions, which attach to the substrate from the undercooled melt. The attachment process involves two opposite contributions to the system's free energy: a negative one, proportional to the length of the deposing chain stem, which favors the growth, and a positive one, associated with the creation of two new fold surfaces. **These opposite contributions were used to derivate the rate of secondary nucleation. Analogous competitive factors are present for the overall crystallization process.** Here, for simplicity, the generalized (i.e., for either growth or overall crystallization processes) LH expression is presented in Equation 8:

$$A(T_c) = A_0 exp\left(-\frac{U^*}{R(T_c - T_\infty)}\right) exp\left(-\frac{K_g^A}{T_c \Delta T f}\right) \quad (8)$$

where A_0 is referred to as the growth rate constant (G_0), i.e., when the spherulitic growth rate (G) or growth rate are measured, or to the overall crystallization rate constant ($1/\tau_0$), i.e., when the overall crystallization rate ($1/\tau_{50\%}$) is calculated, e.g., from DSC measurements. The pre-exponential A_0 term includes all the parameters independent of the temperature. Equation 8 is divided into two contributions, the diffusion and nucleation terms. The first term (diffusion) between parenthesis expresses the temperature dependence of the rate of the short-range transport of the crystallizing segments, according to the Vogel-Fulcher or William-Landel-Ferry type equation.[17, 59] In this term, U^* is the activation energy for the transport of chains to the crystal surface (it can be assumed constant, and a value of 1500 cal/mol is usually employed, unless it can be estimated by rheological measurements),[23] R is the gas constant (8.314 J/mol.K), and T_c is the isothermal crystallization temperature. T_∞ is a hypothetical temperature in which chain mobility ceases, and it is usually taken as $T_\infty = T_g - 30\ (K)$. At $T_c = T_\infty$, the diffusion of the crystallizable units becomes infinitely slow. The second term (nucleation) between parentheses expresses the nucleation rate's temperature dependence. Here, ΔT is the supercooling defined as $\Delta T = T_m^0 - T_c$, where T_m^0 is the equilibrium melting temperature. Thus, this term approaches zero as $T_c = T_m^0$.

Factor f is a temperature correction term accounting for the change in the enthalpy of melting with crystallization temperature, $f = 2T_c/(T_c + T_m^0)$; and **K_g^A is a constant proportional to an energy barrier for a specific process** (indicated in the superscript A), either growth (i.e., $A = G$) or overall crystallization (i.e., $A = \tau$). Thus, **K_g^G is related to secondary nucleation, and K_g^τ is proportional to overall crystallization** (nucleation and growth). The value of K_g^A can be expressed as:[11, 12, 47]

$$K_g^A = \frac{j b_0 \sigma \sigma_e T_m^0}{k \Delta h_f} \tag{9}$$

where j is a constant determined by the operating crystallization regime, it takes a value of 4 for Regime I and III and 2 for Regime II. More details of the crystallization regimes are given in Sections 3.3.1 and 3.3.3. b_0 is the width of the chain (i.e., layer thickness perpendicular to the growth plane. For instance, in ideal PE crystals b_0 is the layer thickness perpendicular to *(110)* plane reflection, as reflected in a value of 0.411 nm[60]), σ is the lateral surface free energy, σ_e is the fold surface free energy, and as the K_g^A value it depends on the input data (e.g., growth vs. overall crystallization), k is the Boltzmann constant (1.38x10^{-23} J/K), and Δh_f is the heat of fusion of a perfect crystal. The Thomas-Stavely[61] equation allows evaluating σ (Equation 9), and hence, σ_e and q (Equation 11). q is the work done by the chain to form a fold. The q value also depends on the input data.

$$\sigma = 0.1 \Delta h_f \sqrt{a_0 b_0} \tag{10}$$

where $a_0 b_0$ is the cross-sectional area of the chain; note that a_0 and b_0 are constants related to crystallographic parameters and the growth direction in the crystal.

$$q = 2 a_0 b_0 \sigma_e \tag{11}$$

In Equation 8, the diffusion and nucleation contributions exhibited opposite dependence with temperature. For that reason, Equation 8 can be understood in terms of two competing processes.

The rate of molecular transport in the melt increases with temperature, whereas the rate of nucleation decreases with temperature.[23] Such opposite behavior produces a maximum growth (G_{max}) or overall crystallization ($1/\tau_{50\%,max}$) rate at a specific crystallization temperature ($T_{c,max}$), resulting in a bell-shaped curve.[24] It should be noted that the overall crystallization rate combines or mathematically superposed the bell-shaped behavior of both nucleation and growth processes. Recent studies have revealed that the overall crystallization behavior can display two maxima resulting from a homogenous (higher supercooling) and heterogeneous process (lower supercooling). The LH theory only can predict one maximum, corresponding either to the heterogeneous or homogeneous nucleation mechanism one. More detail is given in Section 3.6.

In summary, we have introduced the concepts of crystallization and the basics of the Avrami and LH theories. Practically, there are many tips to correctly apply the theories on experimental data, including the experimental protocol, data treatment, and fitting algorithm. The following sections illustrate those tips by performing isothermal experiments using commercial materials like polypropylene and polylactide. The experiments were performed under a wide range of conditions, from the melt, self-nucleated melt, and glassy state, continuously and by step, by PLOM and DSC. We show the ideal conditions but also simulate the most common mistakes.

2. EXPERIMENTAL PART

This section will present the materials and procedures employed in this paper. Each procedure will be present in detail, especially those performed in the DSC.

2.1.Materials

We selected several common polymers with different crystallization kinetics. Polypropylene samples with and without nucleating agents were supplied by Repsol ® and Borealis ®, respectively. The sample without a nucleating agent is here named **PP** (commercial name ISLEN ® PP 070G2M) and possesses a melt flow rate (230 °C; 2.16 kg) of 12 g/10min. The sample with a nucleating agent is here named **PP-NA** (commercial name HD905CF) and possesses a melt flow rate (230 °C; 2.16 kg) of 6.5g/10min. These samples were employed in the experiments listed in Table 1. For isothermal crystallization from the glassy state, a commercial polylactide sample (PLA), of high molecular weight provided by NatureWorks (commercial name 4032D) was employed. Poly (ethylene oxide), PEO, with M_n = 10 kg/mol and PDI = 1.05 infiltrated in porous anodic aluminum oxide (AAO) templates, with diameter = 90 nm, and depth = 60 μm, was

employed to perform an isothermal step-crystallization in a confined system. The materials and the tests performed on these materials are shown in Table 1. The non-isothermal curves for the PP, PP-NA, and PEO/AAO templates are shown in Figure S1.

Table 1. List of materials and tests performed.

Material	Test
PP	Continuous isothermal crystallization (melt and self-nucleated state), step isothermal crystallization.
PP-NA	Continuous isothermal crystallization (melt and self-nucleated state)
PLA	Continuous isothermal crystallization (glassy state)
PEO infiltrated in AAO templates	Step-crystallization.

2.2.Polarized Light Optical Microscopy

PLOM experiments were performed in an Olympus BX51 microscope. A digital camera Canon EOS 80D was integrated into the microscope. The samples with a thickness of ~ 50 μm were sandwiched between cover glasses. The temperature is controlled in a Linkam THMS600 hot stage. The hot stage was connected to liquid nitrogen to facilitate the cooling steps and an atmosphere of ultrapure nitrogen to protect the sample.

The PP samples were first heated to around 200 °C and held for 3 min to erase the thermal history. Subsequently, the sample was cooled from the melt, at 60 °C/min, to a selected crystallization temperature, T_c. The range of T_c values was 129 °C to 145 °C and 140 to 145 °C for the PP and PP-NA.

2.3.Continuous Isothermal Crystallization by Differential Scanning Calorimetry (DSC): From the melt and glassy state.

A differential scanning calorimetry (DSC) 8500 of PerkinElmer, coupled with a cooling device of liquid nitrogen, CNL2, was used. An atmosphere of ultrapure N_2 was employed, and the DSC was calibrated with indium and zinc standards. Samples with a weight of *circa* 5 mg were used. The different protocols employed are described in detail below.

Minimum crystallization temperature, $T_{c,min}$ (melt state)

The isothermal experiments must be performed with high enough T_c and cooling rates, respectively, to avoid any crystallization during the cooling step. The correct selection of the T_c is essential. As Lorenzo et al.[9] pointed out, the incomplete isothermal curves cause erroneous values of the parameters obtained by the Avrami equation. One of the reasons for an incomplete isothermal curve is the crystallization during the previous cooling, which might occur for the selection of a low T_c. To avoid this, a simple procedure has been applied, from the melt (Scheme 3a) or the self-nucleated (Scheme 3b) state, and it is described below:

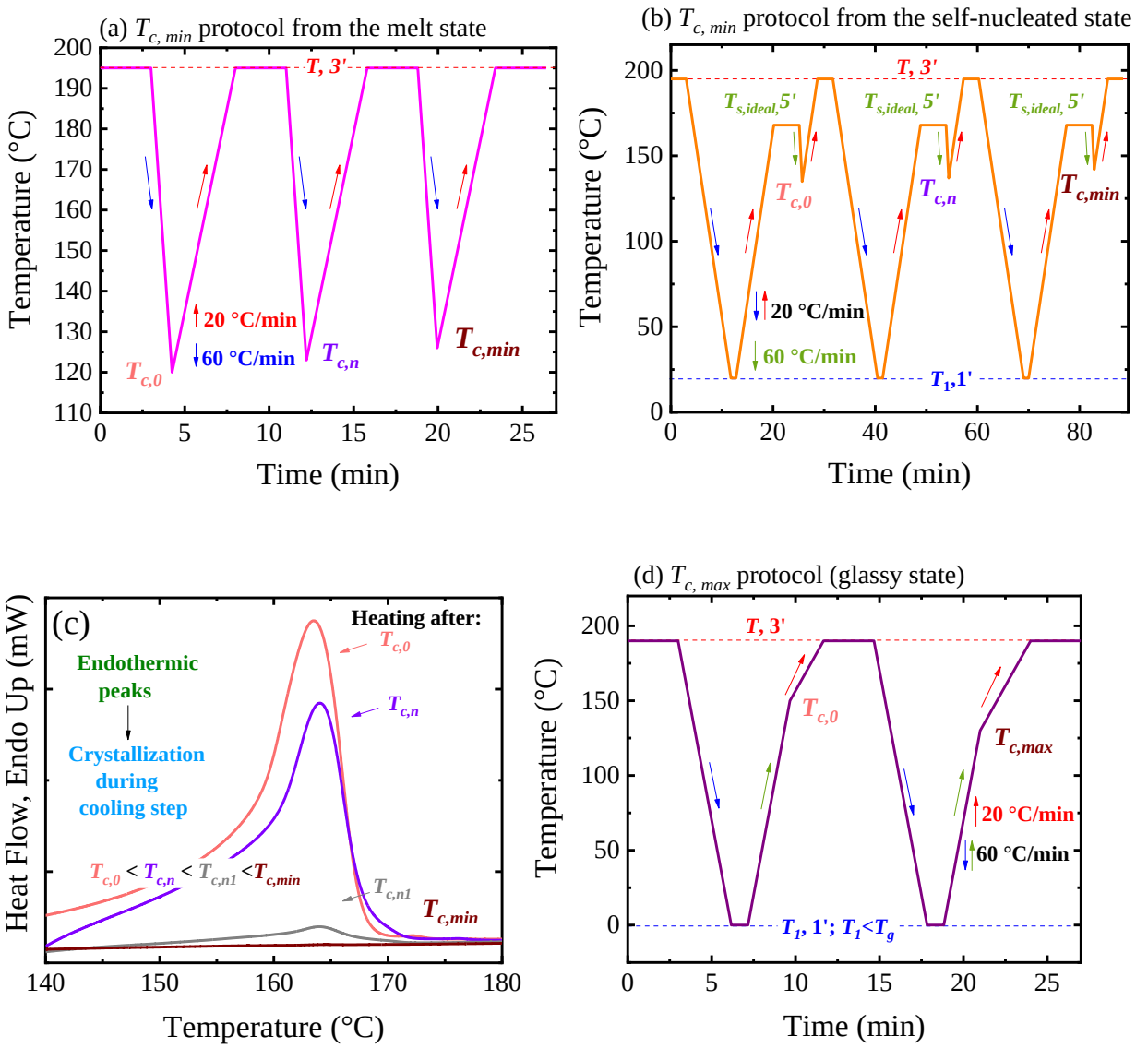

Scheme 3. Determination of the minimum crystallization temperature, $T_{c,min}$, from the (a) melt-state, and (b) self-nucleated state, using different T_c, named $T_{c,0}$, $T_{c,n}$, and $T_{c,min}$. The heating step after the cooling to T_c is schematically represented in (c), taking as an example the PP (an additional $T_{c,n1}$ was added for illustrating purposes). Note that the disappearance of the endothermic peak indicates that the selected T_c (i.e., $T_c \geq T_{c,min}$) does not generated crystallization during the cooling. In (d) the $T_{c,max}$ protocol for the glassy state is included.

Scheme 3a shows that after erasing the thermal history of the sample at T for 3 min, a fast and controlled cooling, in this case at 60 °C/min, is performed to a selected crystallization temperature, T_c. Often, the selected T_c is higher than the onset crystallization temperature, $T_{c,onset}$, obtained during the non-isothermal cooling scan. After the cooling to T_c, the sample is immediately heated to T. Let us consider the selection of a $T_{c,0}$ which is not high enough to avoid crystallization during the cooling. In this case, the heating scan will reflect an endothermic peak (see Scheme 3c) corresponding to the melt of the crystals formed during the cooling step. This implies that a higher T_c should be selected. Scheme 3c shows that as T_c increases (e.g., $T_{c,n}$ and $T_{c,n1}$) the endothermic peak enthalpy decreases until no endothermic signal is detected. This point corresponds to the $T_{c,min}$, which is the minimum crystallization temperature at which the material does not crystallize during the previous cooling step. Thus, the isothermal experiment must be performed at $T_c \geq T_{c,min}$, since those $T_c < T_{c,min}$ will generate incomplete isotherms. Here, for the crystallization from the melt, the obtained $T_{c,min}$ are 126 °C (for PP) and 134.5 °C (for PP-NA).

The $T_{c,min}$ protocol can also be applied from the self-nucleated state (see Scheme 3b). This implies that the material should be previously self-nucleated (see references 26, 27, 62 for more details). From the self-nucleated state, the fast cooling is performed, and the subsequent heating is evaluated, obtaining similar results to those schematically represented in Scheme 3c. In this case, the resulting $T_{c,min}$ of the self-nucleated material will be higher compared to the $T_{c,min}$ obtained from the melt; i.e., $T_{c,min}$ of 142 °C (for PP) and 152 °C (for PP-NA). The reasons for this behavior are explained in Section 3.3.4.

Maximum crystallization temperature, $T_{c,max}$ (glassy state)

When the crystallization is performed from the glassy state (see details below), the crystallization must be avoided during the heating to the crystallization temperature. Therefore, a

thermal protocol similar to the $T_{c,min}$ approach can be established. As in the $T_{c,min}$ approach the heating curve, after selecting a T_c, should be analyzed. The complication is the cold-crystallization contribution in the heating curve. In this case, it is considered that the material does not crystallize during the heating when the melting enthalpy (ΔH_m) and the cold-crystallization enthalpy (ΔH_{cc}) are equal ($\Delta H_m - \Delta H_{cc} = 0$). Here, the T_c before $\Delta H_m - \Delta H_{cc} > 0$ is the $T_{c,max}$(Scheme 3d), defined as the maximum crystallization temperature at which the material does not crystallize during the previous heating step. The isothermal test can be performed at $T_c \leq T_{c,max}$, to guarantee complete isothermal curves. Note that in this case, a good starting point (to find the $T_{c,max}$) is the $T_{c,end}$ of the cold-crystallization exotherm of the material. Scheme 3d shows the protocol for two T_c values; it is assumed that the $T_{c,0}$ generated crystallization during the heating, and the $T_{c,max}$ does not generate crystallization, and hence it is a suitable T_c to start the isothermal experiment (Scheme 4b).

Isothermal crystallization: From the melt.

The isothermal crystallization (from the melt) steps are illustrated for two crystallization temperatures, in Scheme 4a, and described below.

a. Erase the thermal history at T for 3 minutes.
b. Cool at 60 °C/min (or a higher controlled rate) to $T_c \geq T_{c,min}$.
c. Hold at T_c for a crystallization time, t_c, which must be enough to achieve the saturation of the crystallization. Often, a time equal to 3 times the apparent half-crystallization time (i.e., time at which the minimum heat flow value is reached) is used. After t_c, the heat flow will recover the baseline.
d. Subsequent heating, at selected heating rate (i.e., often a value of 20 °C/min is used) to T, to record the melting behavior of the crystals formed in c.
e. Repeat steps a to d as many times as possible. Often 10 points are enough to characterize the crystallization kinetics of the material. Intervals of 0.5 or 1 °C can be used for T_c.

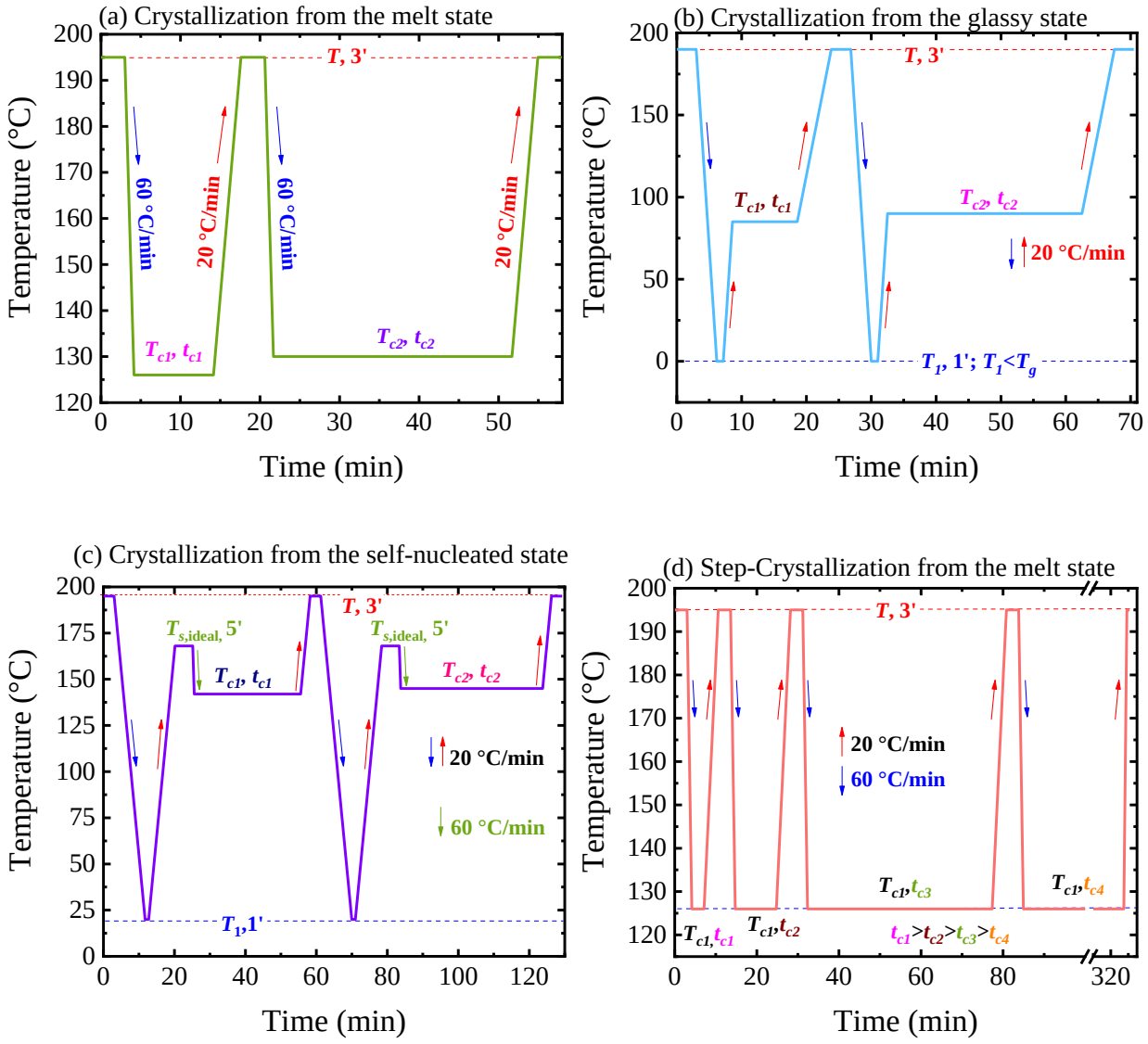

Scheme 4. Isothermal crystallization protocols from (a) the melt state; (b) the glassy state; and (c) the self-nucleated step. In (d) the step-crystallization (from the melt) protocol is represented.

Isothermal crystallization: From the glassy state.

The isothermal crystallization from the glassy state is employed for polymers with slower crystallization kinetics. The aim of crystallizing from the glassy state is to enhance the nucleation of the polymers and thus accelerate the crystallization kinetics. For instance, this procedure is applied in PLAs, where no exothermic peak can be detected during cooling from the melt. On the other hand, a cold-crystallization peak is found during the subsequent heating. This peak can be a

guide to select the starting point for the isothermal crystallization. In this case, the $T_{c,min}$ procedure cannot be applied, as the material crystallizes during the heating; therefore the $T_{c,max}$, approach can be applied instead. The procedure to apply the isothermal crystallization from the glassy state is shown schematically for two T_c (Scheme 4b), and it can be described as follows:

a. Erase the thermal history at *T* for 3 minutes
b. Cool the sample, e.g., at a cooling rate of 20 °C/min, from the melt to a temperature, T_1, below the T_g of the material, i.e., $T_1 < T_g$. It is important to remark that very fast cooling rates can inhibit the formation of nuclei. Such inhibition can generate a state similar to the melt; therefore, no enhancement will be obtained.
c. Hold 1 minute at T_1, see step b, to stabilize the DSC.
d. Heat, e.g., 20 °C/min, to the selected T_c.
e. Hold enough time at T_c to crystallize the material to saturation. Often a time of 3 times the t_c is employed.
f. Subsequent heating, e.g., at 20 °C/min, to record the melting behavior of the crystals formed at T_c.
g. Repeat steps a to f, as many times as possible, using $T_c \leq T_{c,max}$. In this case, often more temperatures can be used; therefore, intervals of 5 °C can be utilized. Note that in the isothermal crystallization from the melt state, lower intervals are used, e.g., 1 °C.

It is important to remark that the cooling rate (from the melt to the glassy state) is an essential variable in FSC, since extremely fast cooling rates, i.e., 40,000 K/s or higher, can inhibit the nucleation during vitrification. As a result, in terms of nucleation, such extremely fast rates induce a glassy state that contains a similar amount of heterogeneous nuclei as in the melt state. In contrast, the cooling rate will not be the determining step in this protocol in the standard DSC case, as rates are always comparatively slow in comparison to the nucleation rate during cooling from the melt to the glassy state.

SN followed by isothermal crystallization

Self-nucleation test was performed in the PP and PP-NA samples, according to the protocols shown in references 26, 27, 62. With this protocol, three main self-nucleation *Domains* can be obtained, and they can be briefly defined according to the cooling and melting behavior after the

holding step at the self-nucleation temperature, T_s: In *Domain I or melting domain,* the high T_s value cannot self-nucleate the sample; thus, the cooling and heating curves remains unchanged compared to the standard scans. In *Domain II or self-nucleation domain,* the T_s are lower than the ones in *Domain I*. Hence, self-nuclei are generated, enhancing the crystallization without affecting the melting behavior. Therefore, the T_c (detected during the cooling after the SN at T_s in *Domain II*) is shifted to higher values, whereas the melting behavior remains unchanged. The last *Domain* starts at the lowest T_s, which only partially melts the material. These T_s values correspond to *Domain III or self-nucleation and annealing domain*. In this case, the unmelted crystals are annealed at T_s, affecting both the crystallization and melting behavior.

Here, we perform SN experiments to determine the $T_{s,ideal}$ (i.e., T_s which generates the maximum self-nucleation without causing the annealing of the sample) of each material. The $T_{s,ideal}$ is the lowest T_s in *Domain II*. For the PP and also for the PP-NA a $T_{s,ideal}$ = 168 °C was found.

The aim of self-nucleating the sample is to generate the maximum possible number of nuclei. Therefore, in the subsequent isothermal step, the overall crystallization of the sample will be dominated by growth only, rather than nucleation + growth. From the self-nucleated state, the $T_{c,min}$ should be determined again, using the cooling curve after the SN as a reference for the $T_{c,onset}$. In this case, the $T_{c,min}$ (from the self-nucleated state) for the PP was 142 °C and for the PP-NA was 152 °C. The details of the SN followed by the isothermal tests are explained below and illustrated in Scheme 4c.

a. Erase the thermal history at T for 3 min.
b. Cool, at 20 °C/min, to T_1 to create a standard thermal history.
c. Held the sample at T_1 for 1 min to create a standard thermal history.
d. Heat, at 20 °C/min, to $T_{s,ideal}$, e.g., 168 °C, to self-nucleate the sample.
e. Held the sample at $T_{s,ideal}$ for 5 min to reach the self-nucleation of the sample.
f. Cool, at 60 °C/min to $T_{c,1}$.
g. Held the sample at $T_{c,1}$ for $t_{c,1}$ to completely crystallize the sample.
h. Heat, at 20 °C/min, to T to record the melting behavior of the crystals formed at $T_{c,1}$.

i. Repeat steps a to h using $T_c > T_{c,1}$. Note that the isothermal curves will have a weaker signal, due to the lower supercooling, than the isothermal crystallization from the melt; hence less valid points will be registered, e.g., 5 T_c instead of 10 T_c.

Step-crystallization from the melt (conventional DSC)

The step-crystallization procedure was firstly used by Galante et al.[63] and Balsamo et al.[41] for samples whose DSC signal was beyond the resolution of conventional DSC. Thus, these authors[41, 63] found that by crystallizing the material at different times at the isothermal step, the crystallization degree can be followed during the heating steps, instead. The procedure is described below and illustrated in Scheme 4d for $T_{c,1}$and different crystallization times.

a. Repeat steps (a) to (b) of the isothermal crystallization from the melt.
b. At $T_{c,1} \geq T_{c,min}$, the material will be held at a time, $t_{c,1}$, which will increase in the subsequent steps. In Scheme 4d, four different t_c are represented; $t_{c,1} < t_{c,2} < t_{c,3} < t_{c,4}$. In this context, at $t_{c,4}$ the material experienced a complete crystallization. In conventional DSC (in this work), the t_c is as low as 0.1 min (6 seconds), whereas in fast-scanning chip-calorimetry (FSC) shorter times are accessible.
c. Heat at a constant heating rate (e.g., 20 °C/min) from $T_{c,1}$ to T. The resulting melting endotherm in this step corresponds to the crystallization enthalpy of the crystals formed in (b), i.e., crystals formed during a time $t_{c,1}$ at a specific $T_{c,1}$. This step is essential to follow the crystallization kinetics of the material.
d. Repeat steps (a) to (c) at the same $T_{c,1}$ but increasing the time $t_{c,1}$ ($t_{c,1} < t_{c,2} < t_{c,3} < t_{c,4}$). The time $t_{c,1}$ should increase until the heating scan of the last t_c, e.g., $t_{c,4}$, does not change compared to the previous one, e.g., $t_{c,3}$.
e. Repeat steps (a) to (d) at different T_c, $T_{c,1} \geq T_{c,min}$.

3. RESULTS AND DISCUSSION

This Section is divided into two parts. First, the experimental aspects to consider in the different isothermal crystallization experiments are discussed. Afterward, the aspects and use of the Avrami and Lauritzen and Hoffman theories are discussed. In both parts, a particular focus on the interpretation/analysis and common mistakes is given.

3.1.CONTINUOUS ISOTHERMAL CRYSTALLIZATION: EXPERIMENTAL ASPECTS

The most common procedure to follow the crystallization kinetics of a polymer is the isothermal crystallization performed continuously. In the first part of this section, we discuss the experimental aspects of different isothermal protocols using practical examples, specifically the isothermal crystallization from the melt, the self-nucleated melt, and the glassy state. In the second part, we show how to fit the data with the Avrami equation.

3.1.1. Crystallization from the melt state

To illustrate the isothermal crystallization from the melt, we have crystallized the selected PP and PP-NA samples under different conditions. The main parameters included in the experiment are the T_c and cooling rates. The influence of those parameters will be elaborated on below.

3.1.1.1. *Ideal conditions: $T_{c,min}$ as a starting point and the use of a controlled cooling rate*

Isothermal crystallization experiments should be performed under controlled conditions, which implies using the $T_{c,min}$, as starting T_c, and a fast and controlled cooling rate to avoid the crystallization of the polymer during the cooling step.

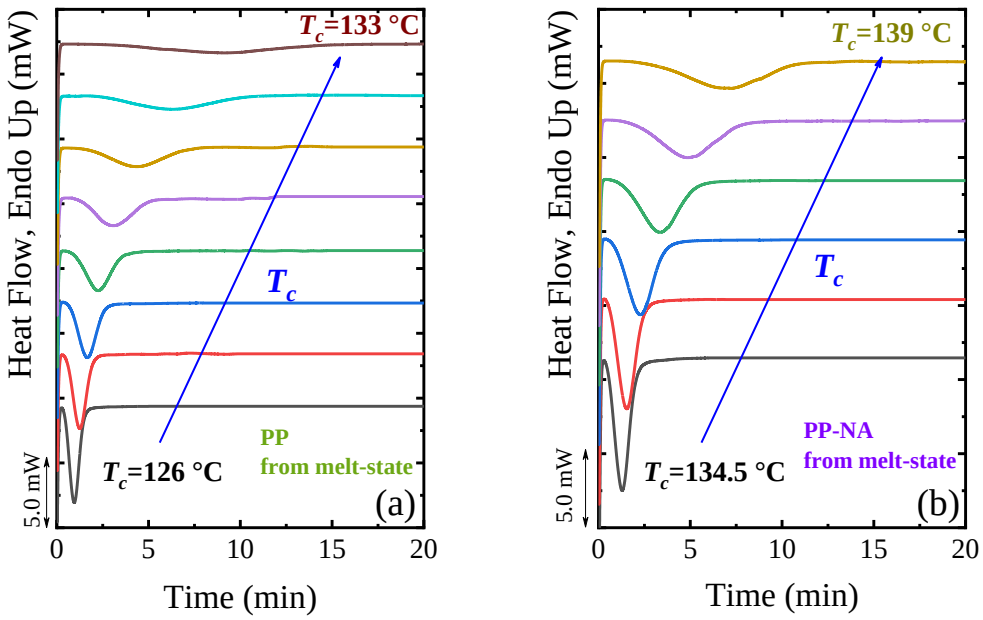

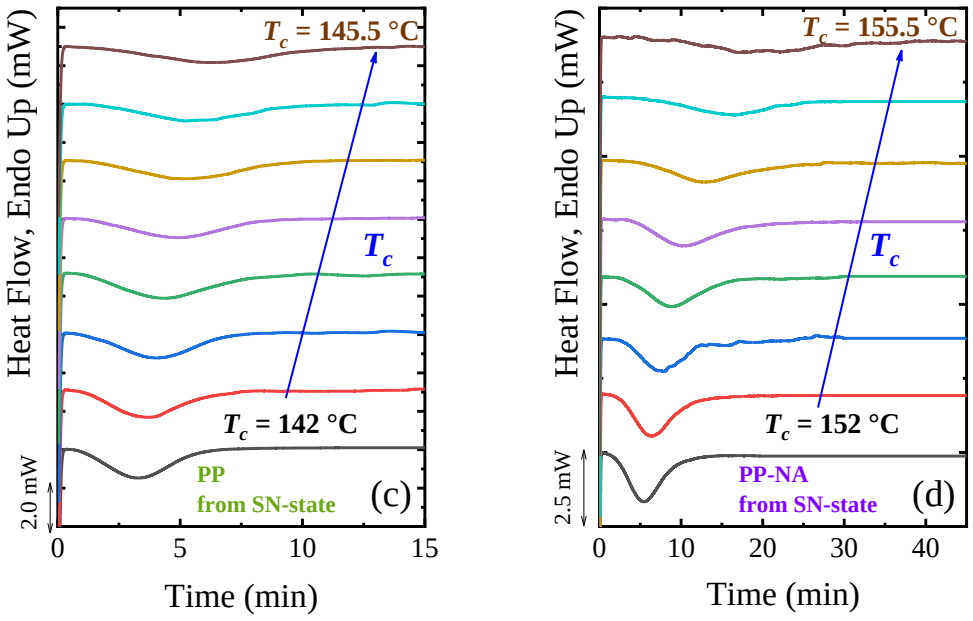

Figure 1. Isothermal curves from the melt state for (a) PP and (b) PP-NA, and from the self-nucleated state for (c) PP and (d) PP-NA. For all the plots the indicated T_c interval is shown.

Figure 1 shows the isothermal DSC curves of two PP samples for the selected T_c values, starting from the $T_{c,min}$ of each sample. These isotherms illustrated the expected curves (crystallization to saturation and no baseline deviations) when a correct procedure (i.e., use of suitable cooling rates and $T_{c,min}$) is applied. In all of them, a horizontal line can join a point at the end of the isothermal curve to a point at the beginning, e.g., τ_0, as has been proposed in the literature.[9, 64, 65]

Figure 1 further shows that as the T_c increases, the crystallization time increases. This is the typical behavior obtained at low supercoolings in most polymers with a high crystallization rate.[9] Figure 1b shows that the PP-NA crystallizes faster than the PP as reflected by the shift of the isotherms to higher T_c values (Figure 1a) due to the presence of a nucleating agent in this sample. Before illustrating the use of the Avrami theory on the isotherms, common mistakes are discussed and how they influence the isothermal curves.

3.1.1.2. Effect of selecting low T_c: $T_c < T_{c,min}$

One of the most important prerequisites of the isothermal crystallization protocol is to avoid the crystallization of the polymer during the cooling step. This is the reason for the determination of $T_{c,min}$. A common mistake is selecting an arbitrary T_c, which is below $T_{c,min}$. To illustrate the impact of this erroneous T_c selection, we have performed isothermal experiments in the PP, using inappropriately low T_c values.

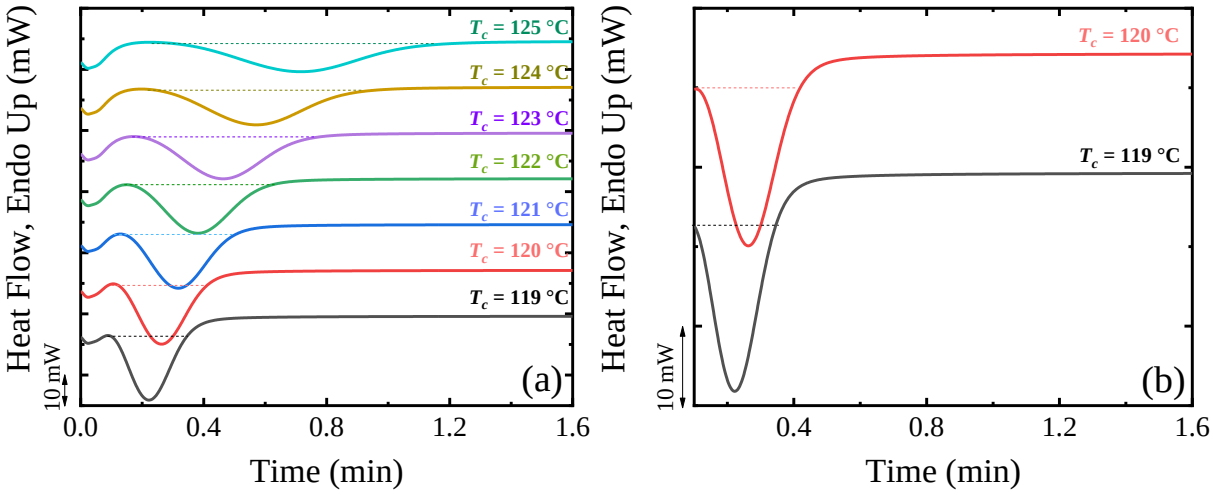

Figure 2. (a) Isothermal crystallization of PP at $T_c < T_{c,min}$. Note that T_c= 119 °C corresponds to the $T_{c,onset}$ recorded during the non-isothermal cooling scan. A horizontal dashed line illustrates the difference between the expected baseline (considering the point at which the isothermal crystallization starts) and the real baseline. In (b) the selected curves at T_c = 119 and 120 °C are plotted to emphasize the two curves.

Figure 2 shows the isotherms for $T_c < T_{c,min}$, starting at the $T_{c,onset}$. For the PP the $T_{c,onset}$ is around 119 °C (see Figure S1), whereas the $T_{c,min}$ is 126 °C. For all the curves, we have used a horizontal line from a point after the crystallization exotherm has finished to a point at the beginning.[9, 64, 65] We can see that between 119 °C and 125 °C, none of the lines fit perfectly the baseline. As shown more clearly in Figure 2b, the isothermal crystallization curves are incomplete because crystallization started during the cooling step. If the Avrami analysis is carried out on such isothermal curves, a large error may be encountered, which will be illustrated in the next section. The effect of selecting the appropriate T_c was also discussed by Lorenzo et al.[9] They proposed

Equations 12 and 13 to estimate the relative errors on the Avrami parameters, e.g., n and K, when incomplete isotherms curves are used.

$$\Delta n = 100 \left\| \frac{n_i - n_m}{n_i} \right\| \tag{12}$$

$$\Delta K = 100 \left\| \frac{K_i - K_m}{K_i} \right\| \tag{13}$$

where the subscript "i" corresponds to the ideal case, i.e., the one with a correct isothermal curve, and "m" for the measured curve under a specific condition. The Avrami parameters are the Avrami index, n, and the rate constant, K. Equations 12 and 13 are extrapolable to other parameters, such as the induction time, τ_0.

For incomplete isothermal curves, Lorenzo et al.[9] found errors in n of around 20 ~ 25 %, implying a reduction from n ~ 3.0 (spherulites that grow instantaneously) to n ~ 2. The highest errors, in magnitude, were found in K values; up to 330 %. Here, we set T_c = 126 °C (i.e., $T_{c,min}$ of PP) and a cooling rate of 60 °C/min as the "ideal" state (see Figure 1) and estimated the errors of selecting $T_c < T_{c,min}$ (see Figure 2). The relative errors on n and K are plotted as a function of T_c in Figure 3 and listed in Table S1.

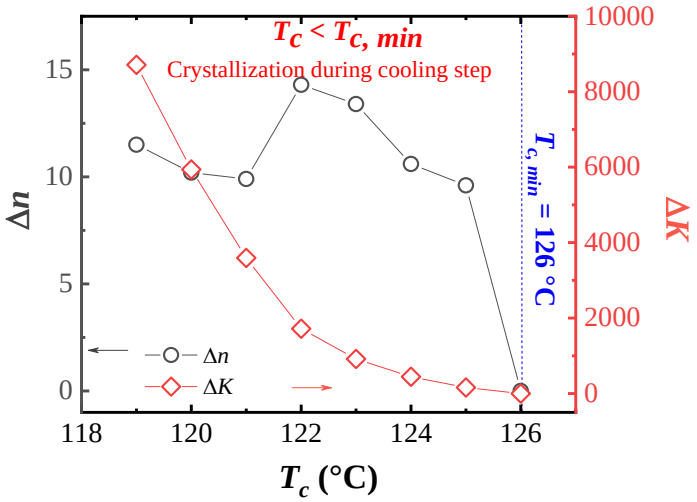

Figure 3. Relative errors (Δ) in n (left y-axis) and K (right y-axis) as a function of T_c. The results at $T_{c,min} = 126$ °C, are used as the ideal values. All the PP samples were cooling from the melt at 60 °C/min.

Figure 3 shows that the relative error of n values is between 9.6 to 14.3 %. Luckily, this error scale does not affect the physical interpretation of n for PP in this specific example. For all the cases, the obtained n can be approximated to 3, corresponding to a spherulitic morphology and instantaneous nucleation. On the other hand, remarkable errors are found for the K values (i.e., between 100 to 8700 %). The relative errors decrease as the T_c values are approaching $T_{c,min}$. These results demonstrated the importance of selecting the proper crystallization temperatures.

3.1.1.3. Effect of cooling rate

The cooling from the melt to the selected T_c must be fast enough, meanwhile, in a controlled manner. Although the nominal rates of DSC equipment may be high enough, caution must be paid as the real cooling rate may strongly deviate from the nominal rates set in the calorimeter.

The effect of the cooling rate was studied in a DSC 8500, using a CLN2 as a cooling device. For this specific DSC and cooling device, the maximum nominal rate is 750 °C/min. But is this a real cooling rate? Is it a controlled cooling rate? To answer these questions, we performed cooling scans at different cooling rates (with empty DSC pans) in a temperature range of 200 °C to – 40 °C.

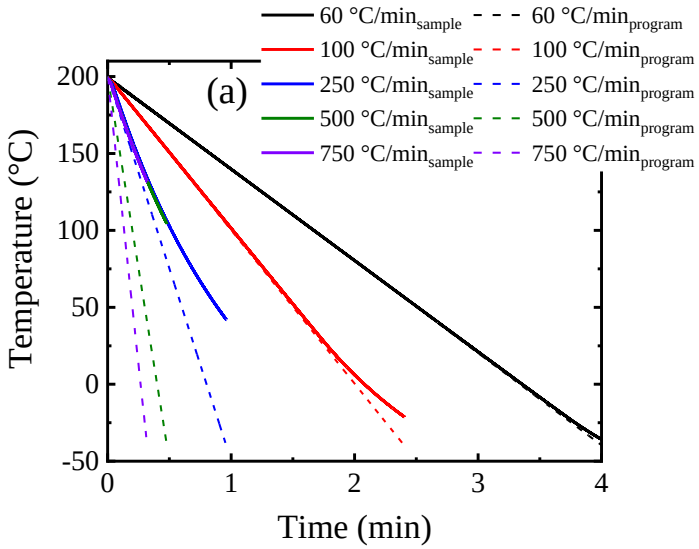

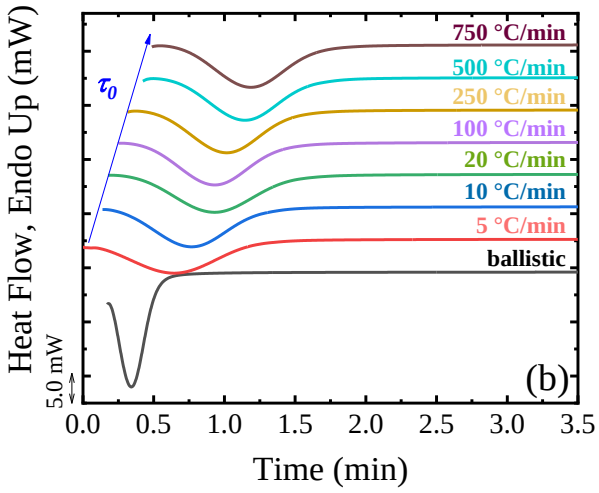

Figure 4. (a) Temperature vs. time plots of DSC curves from 200 to – 40 °C at different rates, and (b) isothermal crystallization curves for PP crystallized from the melt to T_c = 126 °C at various cooling rates, including ballistic (superfast) cooling. The arrow indicates that the induction time increases as the cooling rate increase.

As shown in Figure 4a, it is observed that, among the cooling rates between 60 – 750 °C/min, only 60 °C/min is a controlled rate because the sample temperature is almost the same as the programmed temperature in the 200 to – 20 °C temperature range. For the 100 °C/min cooling rate, significant deviations between the programmed and real temperature can be seen below 20 °C. The sample temperature curves at 250 to 750 °C/min show practically the same slope; hence, they unexpectedly have the same "real" cooling rate (see Table 2). Another important message in Figure 4 is that the cooling step finishes before reaching the set temperature if the cooling is uncontrolled because the solid lines (sample temperature) reach a temperature higher than – 40 °C ($T_{critical}$) when the dashed lines reach – 40 °C. The different $T_{critical}$ values are shown in Table 2. Note that these values depend on the equipment and cooling device and are presented here merely as an example.

Table 2. Temperature at which uncontrolled cooling conditions are reached ($T_{critical}$) and real rate (calculated from the slope of temperature vs. time curve of the sample) for different nominal cooling rates used during the cooling from 200 to – 40 °C.

Nominal Rate (°C/min)	**$T_{critical}$ (°C)**	**Real rate (°C/min)**
20	–	19.8

60	– 20.6	59.2
100	28.8	95.1
250	40.3	166.1
500	101.7	202.5
750	127.0	217.0

Table 2 shows that the nominal rate equals the real rate for 20 to 100 °C/min. For higher rates, the nominal rate is much higher than the real rate. In Table 2, the cooling rate of 20 °C/min (included for comparison purposes) is maintained for the whole temperature range, without registering a $T_{critical}$. However, often 20 °C/min is not a fast enough rate. Next, the $T_{critical}$ increases with the nominal cooling rate. For instance, for 60 °C/min, $T_{critical}$= – 20.6 °C, but for 100 °C/min, we can only cool down to 28.8 °C. In the case of a high cooling rate, e.g., 250 to 750 °C/min, the real cooling rate tends to a value of ~ 200 °C/min instead of the nominal rate. Therefore, in conventional DSC, such high rates are not recommended. To illustrate how the cooling rate affects a real sample, we isothermally crystallized PP at 126 °C, using different cooling rates, as shown in Figure 4b. Setting 60 °C/min as the "ideal" cooling rate, the relative errors of Avrami parameters were estimated and plotted in Figure 5 as a function of the nominal cooling rates. The results are also listed in Table S2 on the SI.

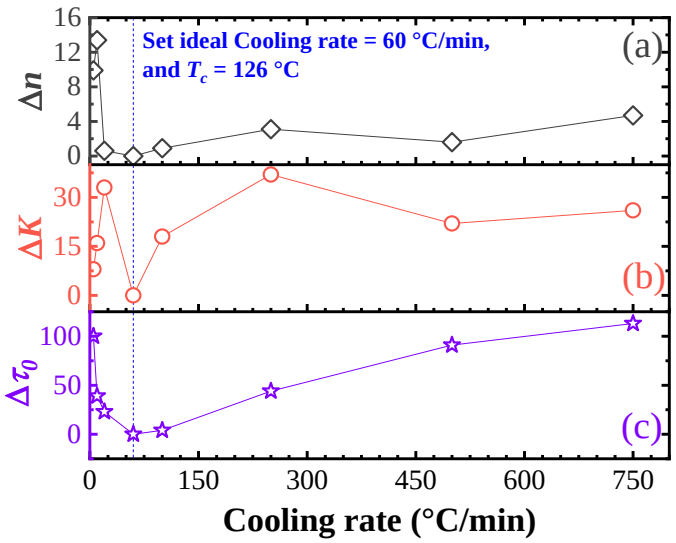

Figure 5. (a) Δn, (b) ΔK, and (c) $\Delta \tau_0$ as a function of the cooling rate. The ideal cooling rate was set as 60 °C/min. All PP samples were cooling from the melt to 126 °C. The vertical dashed line indicates the ideal cooling rate.

Fast cooling rates create a deviation between the sample temperature and the programmed temperature. When the cooling step finishes, the sample has not reached the set T_c, but the isothermal step will run immediately. As illustrated in Figure 4b, at high cooling rates, the isothermal curves are shifted to longer times (i.e., induction time) compared to the slower cooling rates. Interestingly, the DSC goes below the set T_c when the ballistic cooling option is used, i.e., temperature overshoot (i.e., undershoot), generating an incomplete crystallization. For the ballistic cooling, the cooling curve is not registered; as it is an uncontrolled cooling. For low cooling rates, the material crystallizes during the cooling step, generating errors in the measured parameters (Figure 4b and Figure 5).

The different isothermal curves (Figure 4b) can be amended (by removing the undesired overshoot signals), giving errors as high as 13.4 %, 6187 % (ballistic cooling, see Table S2), and 113% (see Table S2 and Figure 5) in the n, K and τ_0, respectively. These relative errors are in line with the values reported by Lorenzo et al.[9], who employed cooling rates as fast as 100 °C/min and as low as 10 °C/min. Figure 5 shows that the highest relative errors of induction time reach 100%. The relative errors in τ_0 illustrate an inverted bell-like behavior, in which the highest errors occur at the slowest and fastest cooling rate. This evidences that the "ideal" cooling rate should be intermediate: it must be high enough to avoid crystallization during the cooling step, and at the same time, controlled enough to avoid overshoot.

3.1.2. Isothermal crystallization from the SN state and the glassy state

The isothermal crystallization can be performed from the SN state or glassy state. Starting the isothermal crystallization from a self-nucleated (see Scheme 4c) sample is a strategy to indirectly follow the growth kinetics of the sample. This strategy was first proposed by Müller et al.[49] to study the crystallization kinetics of poly(*p*-dioxanone)-*b*-poly(ε-caprolactone) diblock copolymers and parent homopolymers.[49] Later, Lorenzo and Müller[29] applied it to poly (ε-caprolactone) (PCL), polyethylene (PE), and poly (*p*-dioxanone) (PPDX). Recently, this technique has been employed in aliphatic polycarbonates,[30] and PP.[66] The idea is to create the maximum amount of

self-nuclei by self-nucleating the sample at the $T_{s,ideal}$. As a result, in the subsequent isothermal step (see Scheme 4c), the crystallization corresponds only to the growth step instead of nucleation + growth. The self-nucleated state and subsequent isothermal crystallization are schematically represented in Scheme 5, in which a comparison with the glassy state (Schemes 5b and d) is given.

To carry out an isothermal crystallization experiment from the SN state, two important characteristic temperatures must be determined: $T_{s,ideal}$ (see references 26, 27, 62) and $T_{c,min}$ (Scheme 3b). If $T_s > T_{s,ideal}$, there is a possibility of the formation of new nuclei during the isothermal step, thus reflecting nucleation + growth kinetics. In contrast, if $T_s < T_{s,ideal}$, since crystalline structures remain, the crystallization during the cooling cannot be avoided. Thus, a careful determination of the $T_{s,ideal}$ must be done. After properly determination of the $T_{s,ideal}$, it should be noted that $T_{c,min}$ is required (see Scheme 3b). The SN of the material shifts the $T_{c,min}$ to higher values in comparison to a standard isothermal crystallization. Such a shift in T_c evidences the effective presence of self-nuclei promoting the crystallization of the material at a lower supercooling.[29] The previous SN allows crystallizing the material at lower supercooling (i.e., high T_c). Normally, fewer T_c points can be correctly followed as compared to the standard isothermal crystallization from the melt.

As an example, Figures 1c and d show the isothermal crystallization of the PP and PP-NA from the self-nucleated state, respectively. The PP and PP-NA were self-nucleated at their $T_{s,ideal}$ = 168 °C (see Section S3 and Figure S2 on the SI). The $T_{c,min}$ of PP from the self-nucleated state is 142 °C, while $T_{c,min}$ = 126 °C for crystallization from the melt state. Similarly, the $T_{c,min}$ for PP-NA is 134.5 °C for crystallization from the melt, while it is 152 °C for crystallization from the SN state. More details related to the isothermal crystallization from the self-nucleated state are shown in Section 3.3.4.

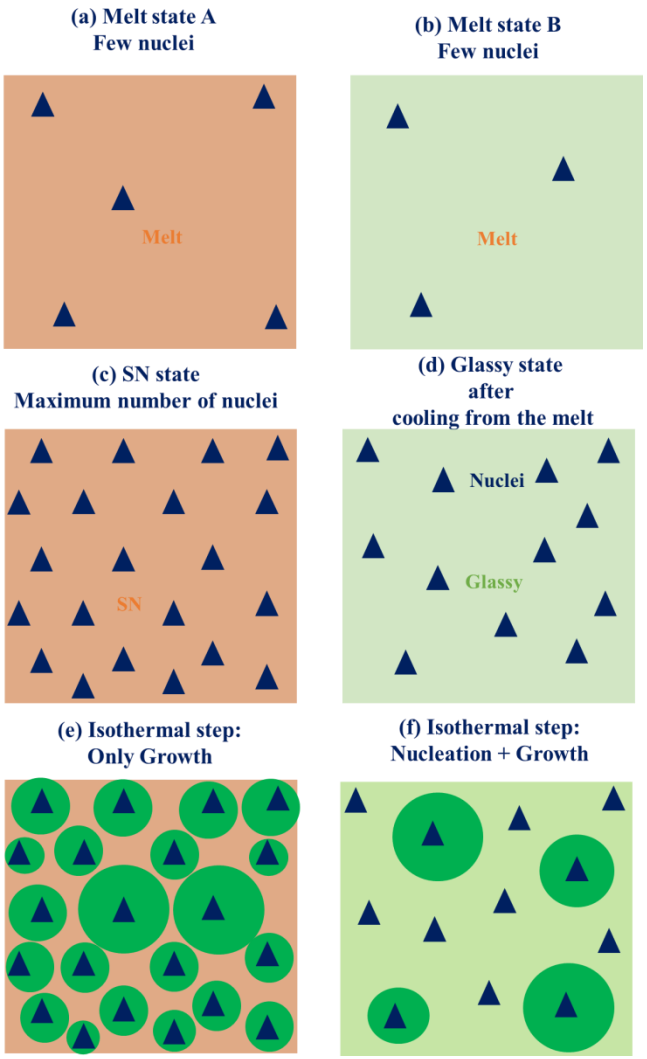

Scheme 5. Illustration of isothermal crystallization from the self-nucleated (a, c, and e) and glassy (b, d, and f) states. In both materials, few inactive nuclei are present for a material (a) melt state A, and (b) B. Then, in the SN state (c) the maximum number of nuclei is formed at $T_{s,ideal}$, and those nuclei growth during the (e) isothermal step. Note that in (e) no additional nuclei are formed. In the glassy state (d) a limited number of nuclei are formed during the cooling. Afterward, during the (f) isothermal step, the nuclei grow, and other nuclei are formed. In Scheme 5 the triangles represent the nuclei and the circles the growth of spherulites.

The crystallization of some polymers is extremely slow. One option is to follow the crystallization kinetics from the glassy state. The idea is to enhance the crystallization rate by allowing nuclei formation during the cooling from the melt to the glassy state, i.e., vitrification. Then, in the glassy state the nucleation is frozen in (see Scheme 5b),[23] as the material cannot crystallize at temperatures below T_g. In the subsequent isothermal step (after heating from the

glassy state) spherulites grow from them, and the crystallization rate is fast enough to be measured by DSC (see Scheme 5d).

It is worth noting that the employed cooling rate influences the obtained results because extremely fast cooling rates can hinder the formation of nuclei. Therefore, no enhancement effect can occur, and the crystallization kinetics from the glassy state without extra nuclei (see Scheme 5d) will be the same as that from the melt (see Scheme 5b) state.[67] In conventional DSC, fast cooling rates are not available; hence, nucleation during the cooling cannot be avoided. The crystallization from the glassy state is commonly used in PLLA.[68-70] The most critical aspect for the crystallization from the glassy state is the cooling rate, and the number of selected T_c values. Because of the slow crystallization rate of the polymer, a wide range of T_c values can be used without experimental limitations (i.e., crystallization during the cooling steps). Also, due to the slow crystallization, a determination of a $T_{c,min}$ is not required, and it is recommended to determine a $T_{c,max}$ instead. Testing a wide range of T_c is suggested. For instance, a commercial PLA can crystallize from 90 to 150 °C,[70] see Figures S3 and S4.

The PLLA nucleation has been widely studied, and its behavior illustrates the importance of the cooling rate. For PLLA, there is a critical cooling rate for suppressing nuclei formation when the sample is cooled from the melt to the glassy state. The cooling rates of conventional DSC are insufficient to suppress the nuclei formation; however, the critical cooling rate has been found through FSC. For instance, in PLLA homopolymer, with 0% of *D* isomer content, it was found that cooling rates faster than 50 K/s suppress the nuclei formation. As the *D* content increases, the nuclei formation is suppressed at lower cooling rates, e.g., 20 (for 2% of *D* content) and 10 K/s (for 4% of *D* content). Nevertheless, the suppression of the nuclei formation is not desired for the crystallization from the glassy state in standard DSC experiments where nucleation enhancement during vitrification is the objective.[68, 69]

The isothermal curves obtained for crystallization from the glassy state generally have a similar shape as in the isothermal crystallization from the melt state. However, the trend of the $\tau_{50\%}$ as a function of temperature might change. Generally, for the materials that crystallize from the glassy state, a complete bell-shaped curve of the $1/\tau_{50\%}$ vs. T_c can be obtained. Figure S4 illustrates this situation.

3.2.APPLICATION OF THE AVRAMI THEORY: CONTINUOUS FIT

Lorenzo et al. developed an Origin ® Plugin (see ref.9) that allows applying Avrami theory to isothermal crystallization data, obtaining the n and K values, the induction time, the experimental and theoretical $\tau_{50\%}$, and the ΔH_{total}. Recently, a free Origin App named Crystallization Fit[71] was developed by some of us following the previous plugin version. The correct determination of all Avrami parameters is here described. All the information obtained from the Avrami equation, together with its simplicity, makes this equation the most commonly applied treatment to study polymer crystallization. We will show, through practical examples, the correct use of the Avrami theory and all the information that can be obtained from it.

The continuous Avrami fit works with a set of heat flow vs. time data. Such isothermal curve can be obtained from any of the isothermal crystallization experiments explained above. Here we discuss the most important aspects to consider and the interpretation of the results on practical examples.

Using the data of the PP at 126 °C, Figure 6 shows the different plots obtained with the Crystallization Fit App[71](See Scheme S1). It is worth noting that the heat flow data is transformed to V_c data using Equation 6.

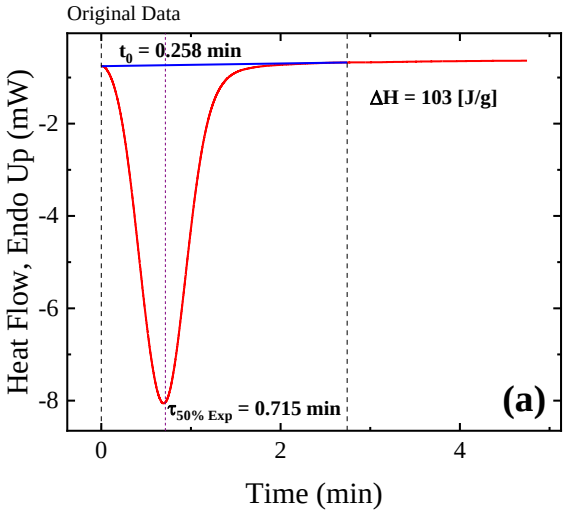
Original Data
t0 = 0.258 min
ΔH = 103 [J/g]
τ50% Exp = 0.715 min
(a)
Heat Flow, Endo Up (mW)
Time (min)

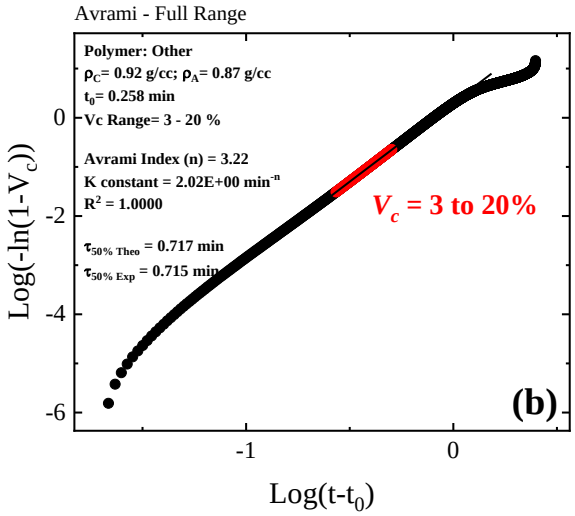
Avrami - Full Range
Polymer: Other
ρC= 0.92 g/cc; ρA= 0.87 g/cc
t0= 0.258 min
Vc Range= 3 - 20 %
Avrami Index (n) = 3.22
K constant = 2.02E+00 min-n
R2 = 1.0000
τ50% Theo = 0.717 min
τ50% Exp = 0.715 min
Vc = 3 to 20%
(b)
Log(-ln(1-Vc))
Log(t-t0)

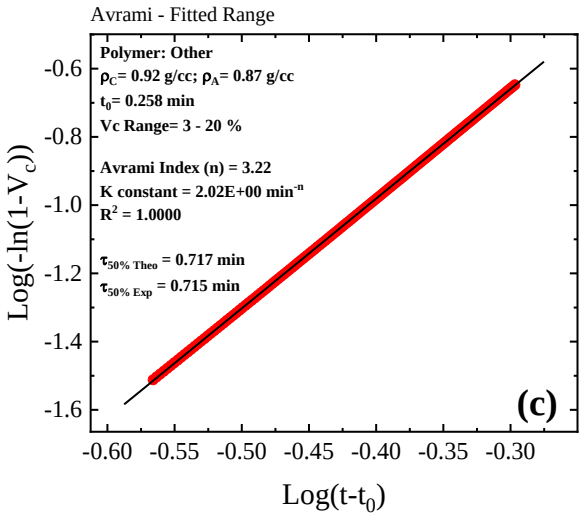
Avrami - Fitted Range
Polymer: Other
ρC= 0.92 g/cc; ρA= 0.87 g/cc
t0= 0.258 min
Vc Range= 3 - 20 %
Avrami Index (n) = 3.22
K constant = 2.02E+00 min-n
R2 = 1.0000
τ50% Theo = 0.717 min
τ50% Exp = 0.715 min
(c)
Log(-ln(1-Vc))
Log(t-t0)

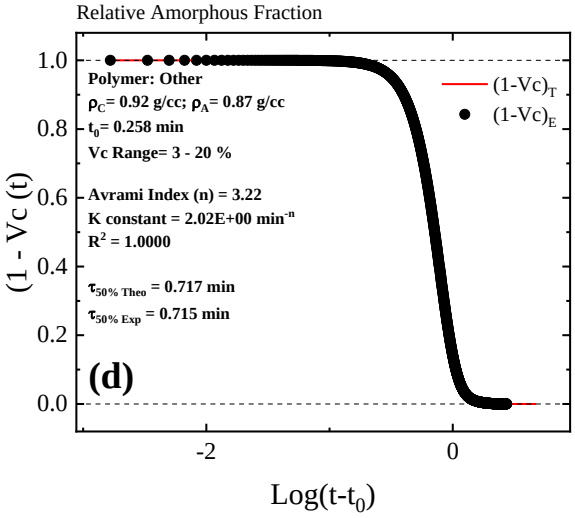
Relative Amorphous Fraction
Polymer: Other
ρC= 0.92 g/cc; ρA= 0.87 g/cc
t0= 0.258 min
Vc Range= 3 - 20 %
Avrami Index (n) = 3.22
K constant = 2.02E+00 min-n
R2 = 1.0000
τ50% Theo = 0.717 min
τ50% Exp = 0.715 min
(1-Vc)T
(1-Vc)E
(d)
(1 - Vc (t)
Log(t-t0)

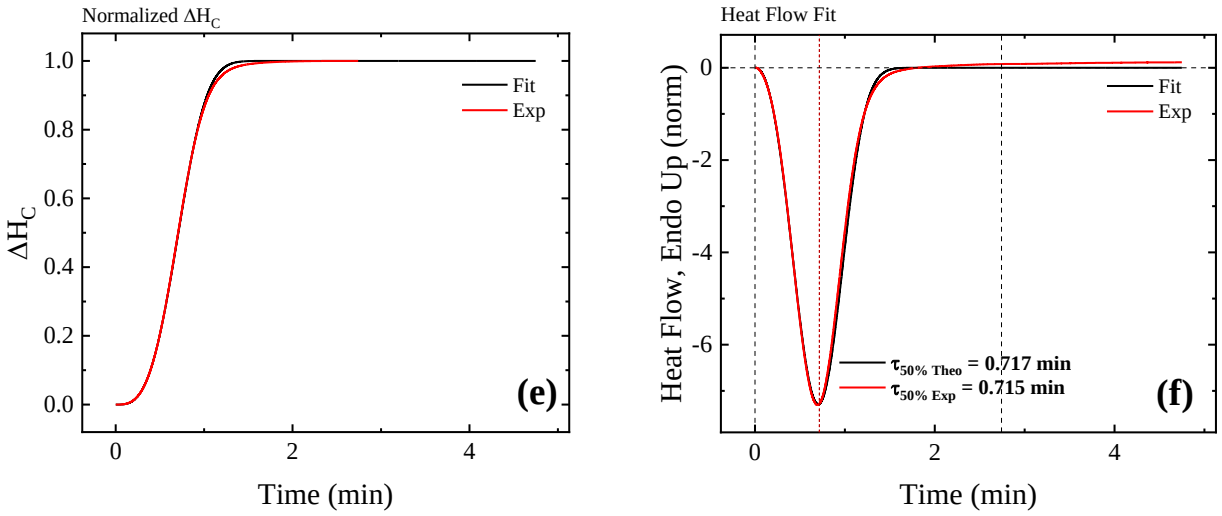

Figure 6. Plots obtained using the free Crystallization Fit App.[71] (a) Original isothermal data of PP crystallizing from the melt at 126 °C. The integration limits are indicated with vertical lines. (b) Avrami plot in the full range. Note that the theory is applied in the selected V_c = 3 to 20 %, to ensure complying with the free growth approximation valid for the primary crystallization range. (c) Avrami plot in the selected range in (b). (d) Relative amorphous fraction vs. time. (e) Normalized crystalline enthalpy (ΔH_c) vs. time, and (f) Original and fitted isothermal curve. The Avrami values (e.g., n and K) are indicated in Figures 6b to d.

Figure 6a shows the selection of the integration limits on the original data. With this selection, the induction time, τ_0, and the half-crystallization time, $\tau_{50\%}$, are determined, as well as the crystallization enthalpy of the curve, ΔH. From the original data, the heat flow is transformed into V_c (see Equations 5 and 6). To obtain a more accurate result, the amorphous (ρ_a) and crystalline (ρ_c) densities of the material are considered (see Equation 5). For Figure 6 we have used the values of ρ_a = 0. 87 g/cm^3, and ρ_c = 0.92 g/cm^3, reported in the literature for PP.[72] The amorphous and crystalline densities of the material are difficult to determine, and in some cases, they are not reported in the literature. For those cases, as an approximation, in Equation 5, the densities can be assumed equal, i.e., in practical terms, a value of 1.0 g/cm^3 can be utilized, to not modify the equation. Here, we have determined (see Section S5) that the related error (of neglecting the ρ_a and ρ_c differences) in n is around 0.3 %, and for the K values around 4.5 %, whereas for the $\tau_{50\%}$

the error is around 1.5%. Thus, this demonstrated that when the densities are not available, the assumption of $\rho_c = \rho_a$, e.g., 1, does not lead to significant errors.

Figure 6b shows the Avrami plot in the entire range. In red, it is indicated the fitting range, which is typically selected between V_c = 3 to 20 % to strictly comply with the free growth approximation. In Figure 6c, the Avrami plot can be seen (see Equation 4) in the fitted range, obtaining a correlation factor of R^2 = 1.000, which is expected for the linear character of the plot (logarithmic function is applied in the *y*- and *x*-axis). As double logarithmic linearization is employed, a high correlation coefficient must be obtained for a good fit, i.e., the R^2 value should preferably be higher than 0.995. With the original data and the Avrami fit, the relative amorphous fraction (Figure 6d), and its crystalline (Figure 6e) counterpart can be obtained. Also, the entire heat flow vs. time curve (Figure 6f) can be generated and compared to the original one. In this specific case, the original and fitted curve are very similar, even at high conversion (i.e., higher than the fixed V_c = 3 to 20%), indicating the goodness of the fitting. This is also reported in other materials, as PCL,[24, 73-75] but is not a general rule. Below (Section 3.2.3 to 3.2.6), we indicate the most important information that can be obtained from the application of the Avrami theory, using the Crystallization Fit Origin ® App.[71]

Figure 6 shows an ideal situation in which the isothermal curve and the feeding parameters to the Avrami Equation are accurate. In the previous Section, we discussed the importance of obtaining an accurate isothermal curve, and now, we will discuss how there are other parameters (i.e., feeding parameters) that can affect the Avrami results.

3.2.1. Induction time

The application of the Avrami fit needs the definition of two integration limits: just before the crystallization start and when the crystallization is completed. Here, we suggest taking the latter, as **three times** the half-crystallization time ($\tau_{50\%}$). The first limit is fundamental since it is related to the induction or incubation time, τ_0. In simple terms, τ_0 is the time interval between the moment the desire T_c is reached (i.e., holding step) to the moment while the crystallization starts. Physically, during the induction period, primary nucleation occurs before any significant calorimetric event can be detected by the DSC.[16, 76, 77] Therefore, it corresponds to the elapsed primary nucleation time before crystal growth can be detected. The nucleation process can continue after crystallization starts, especially when the nucleation of the material is sporadic.

For the correct application of the Avrami theory, the induction time should be subtracted. The Avrami equation is not defined for times at which no crystallization can be detected. Substracting the induction time, the Avrami fit will be applied only when crystallization is detected by the DSC. Lorenzo et al.[9] showed the influence of the induction time by arbitrarily adding 10 minutes to the fitted isothermal curve of a hydrogenated polybutadiene (HPB) at T_c = 93 °C. When the Avrami fit is applied with such a long τ_0, n and K values of 45.85 and 1.21x10^{-49} min^{-1} were obtained. These values are totally absurd, and it is purely caused by the fitting. When the induction time was subtracted, using the modified version of the Avrami equation (Equation 4), Lorenzo et al.[9] obtained reasonable values: n = 2.69 and K = 0.29 min^{-n}.

To show the impact of τ_0 more clearly, we have added an arbitrary time, t_a, to the isothermal curve at T_c = 126 °C employed in Figure 6; the obtained curves are shown in Figure 7a, while the Avrami parameters, i.e., n and K, from fitting the curves are plotted in Figure 7b.

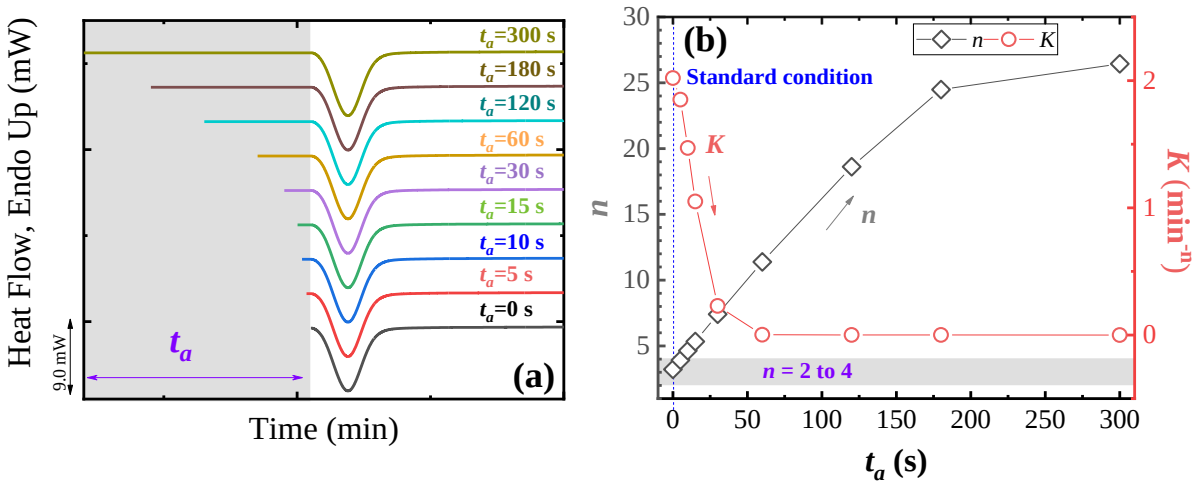

Figure 7. (a) isotherms obtained after arbitrarily adding a time, t_a; (b) n and K values obtained after fitting the curves in 7a with the Avrami equation. Note that the standard isothermal curve, i.e., t_a = 0 s, corresponds to the PP crystallizes at T_c = 126 °C (see Figure 6).

Figure 7b displays an increase in the n values, and a decrease in K values as t_a increases. In this case, no subtracting a time of 10 s already generates absurd n values, i.e., n > 4, demonstrating the importance of substracting the induction time before applying the Avrami fit.

3.2.2. Influence of the fitting conversion range

The conversion range is another key parameter of the Avrami fitting. The derivation of the Avrami equation assumes free growth of the crystals. Therefore, it can only describe the crystallization process before the impingement of the crystals (e.g., spherulites). Practically, the Avrami equation describes the overall transformation process in the primary crystallization range (V_c < 40 ~ 50%).[24]

The Avrami theory applies to a free growth situation. The highest conversion reached for free growth differs from polymer to polymer. In some cases, for instance, at 50% of conversion, probably some spherulites have already impinged on one another. However, in other cases, e.g., PP, PCL, among others,[24, 73] the free growth condition can be fulfilled even at high conversion ranges. In general, the 50% of conversion can be excessive, and for that reason, a lower conversion range is employed to fulfill the Avrami conditions for all materials.

Lorenzo et al.[9] evaluated different conversion ranges and found that the best conversion range is V_c = 3 to 20 %. These authors suggest neglecting the initial data points (V_c < 3%), because the heat flow signal at that period is mainly experimental errors caused by the stabilization of the equipment. On the top limit, Lorenzo et al.[9] pointed out that the secondary crystallization process produces nonlinearity in the Avrami plot, which is appreciable beyond V_c = 50%. In HPB such deviation was found even in a conversion of 35 %.

3.2.3. Avrami Parameters and Others

In this section, we will discuss the different parameters that can be obtained by using the Crystallization Fit App.[71] Here, we have included the Avrami parameters, i.e., n and K, and the nucleation and overall half-crystallization times which are also obtained with the App.

3.2.4. Nucleation and Overall Crystallization Rates

The induction time, τ_0, and the overall half-crystallization time, $\tau_{50\%}$, can be obtained from the isothermal curves. The inverse of them represents the nucleation rate, $1/\tau_0$, and the overall crystallization rate, $1/\tau_{50\%}$. Figures 8a and d compared the obtained $1/\tau_0$ and $1/\tau_{50\%}$ values as a function of T_c for the PP and PP-NA.

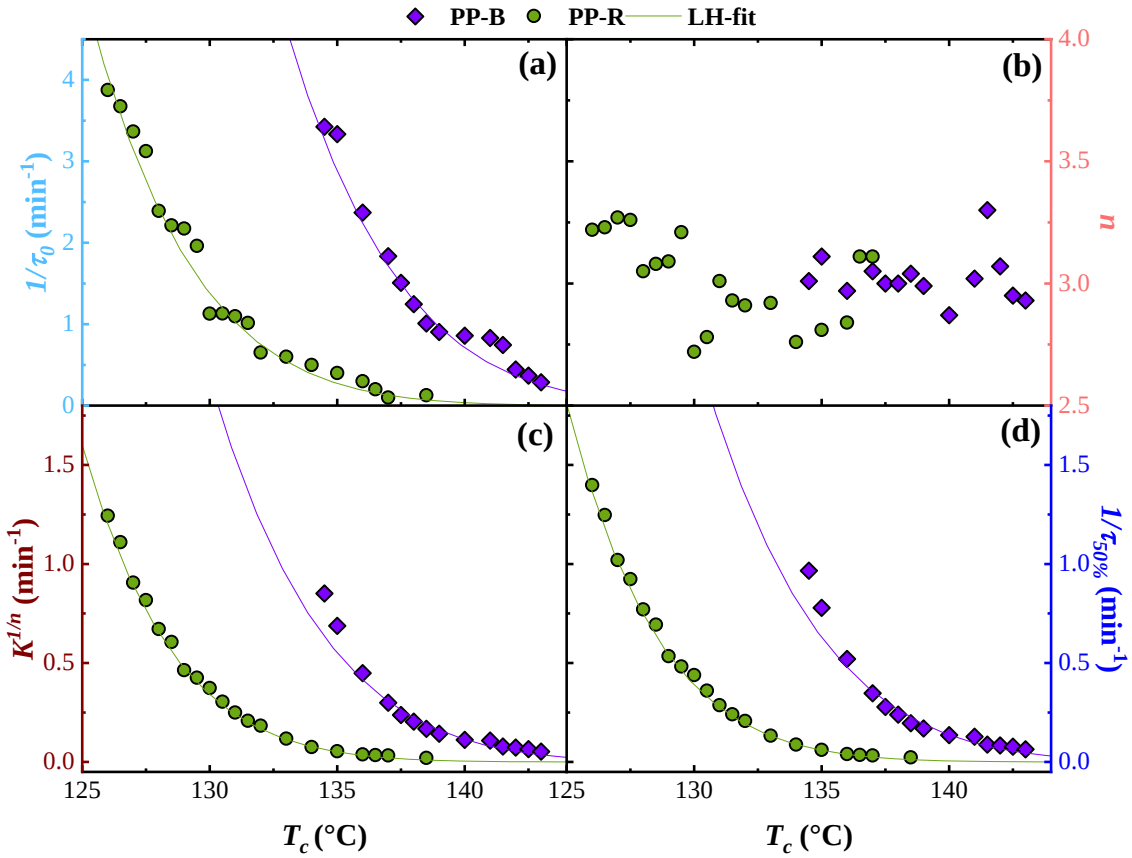

Figure 8. Experimental data points and Avrami parameters plotted vs. T_c; (a) $1/\tau_0$; (b) n, (c) $K^{1/n}$ and (d) $1/\tau_{50\%}$. The solid lines represent the LH fit.

Figures 8a and d show that PP-NA has higher nucleation and overall crystallization kinetics than the PP (see Table 3). This is explained by the presence of a nucleating agent in the PP-NA. In Table 3, we listed the equivalent T_c values needed for reaching the selected $1/\tau_0$ = 2.0 min^{-1} and $1/\tau_{50\%}$ = 1.0 min^{-1}, and the rate values (i.e., $1/\tau_0$ or $1/\tau_{50\%}$) needed to reach a selected T_c = 135 °C. The obtained results evidence faster nucleation and overall crystallization rates of the PP-NA.

Table 3. Comparisons of PP and PP-NA equivalent T_c, $1/\tau_0$ and $1/\tau_{50\%}$.

Sample	**T_c (°C) (at $1/\tau_0$=2.0 min^{-1})**	**T_c (°C) (at $1/\tau_{50\%}$=1.0 min^{-1})**	**$1/\tau_0$ (min^{-1}) (at T_c= 135 °C)**	**$1/\tau_{50\%}$ (min^{-1}) (at T_c = 135 °C)**
PP	129.5	127	0.29	0.06
PP-NA	135.8	133	3.33	0.78

The nucleation rate can be measured by PLOM since the nuclei can be counted assuming that each spherulite comes from a single heterogenous nucleus. The nucleation rate, I, is obtained from the initial slope (i.e., at short times where linear trends are obtained) of the nucleation density vs. time data. On the other hand, the DSC provides indirect information: the nucleation rate ($1/\tau_0$) before any growth starts is obtained as the inverse of the induction time, τ_0, extracted from the isothermal crystallization (Tables S3 and S4). In this section, we compare the nucleation rate obtained by PLOM and DSC in a poly (butylene succinate-*ran*-ε-caprolactone) copolymer with a 91:9 composition ($BS_{91}CL_9$), as studied previously.[78] Figure 9 compared the nucleation rate obtained through PLOM (i.e., I) and DSC (i.e., $1/\tau_0$) in the $BS_{91}CL_9$ copolymer. The two sets of data show the same trend, although the exact values are different. It must be remembered that there are experimental differences between the measurement of these two quantities, and therefore they are not quantitatively the same. Thus, the nucleation rate obtained as $1/\tau_0$ can be an alternative to the PLOM measurements, especially when the nucleation density is too high to allow PLOM determinations to be made accurately as a function of time. Recently, the $1/\tau_0$vs. T_c measurements have been employed in PLA,[70] polycarbonates,[30] among others.[28]

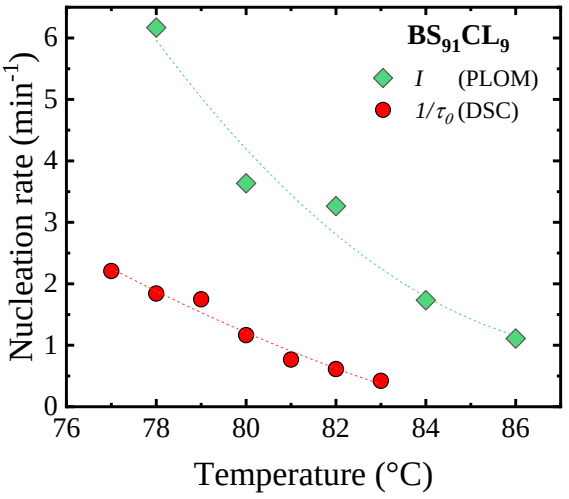

Figure 9. Comparison of the nucleation rate obtained from PLOM (i.e., I) and DSC (i.e., $1/\tau_0$) in $BS_{91}CL_9$ copolymer. The data were obtained from the previous work of Safari et al.[78]

3.2.5. Avrami index

Figure 8b shows the Avrami index, n, obtained for PP and PP-NA samples. The obtained values can be approximated to $n \sim 3.0$, corresponding to spherulites that grow instantaneously: n_{gD} = 3 and n_n= 0. These results are in line with the literature.[47] The n values of PP-NA are slightly lower than those of PP, which is attributed to the nucleating agent. It is important to remark that the n values higher than 4 are physically meaningless.[47] They may result from an erroneous analysis of the isothermal curves either experimentally or analytically.

Figure 8b shows that for both, PP and PP-NA the n values can be considered constant as T_c increases. This behavior is explained by a compensation between the n_n and n_{gD} contributions. The n values as a function of T_c, depend on the dominant mechanism: morphology vs. crystal growth. Scheme 6 illustrated how the n values change with T_c. Note that in Scheme 6a to c, the general case has been considered (i.e., $2 < n < 4$), excluding those cases with $n < 2$. Only in Scheme 6d confinement systems are considered.

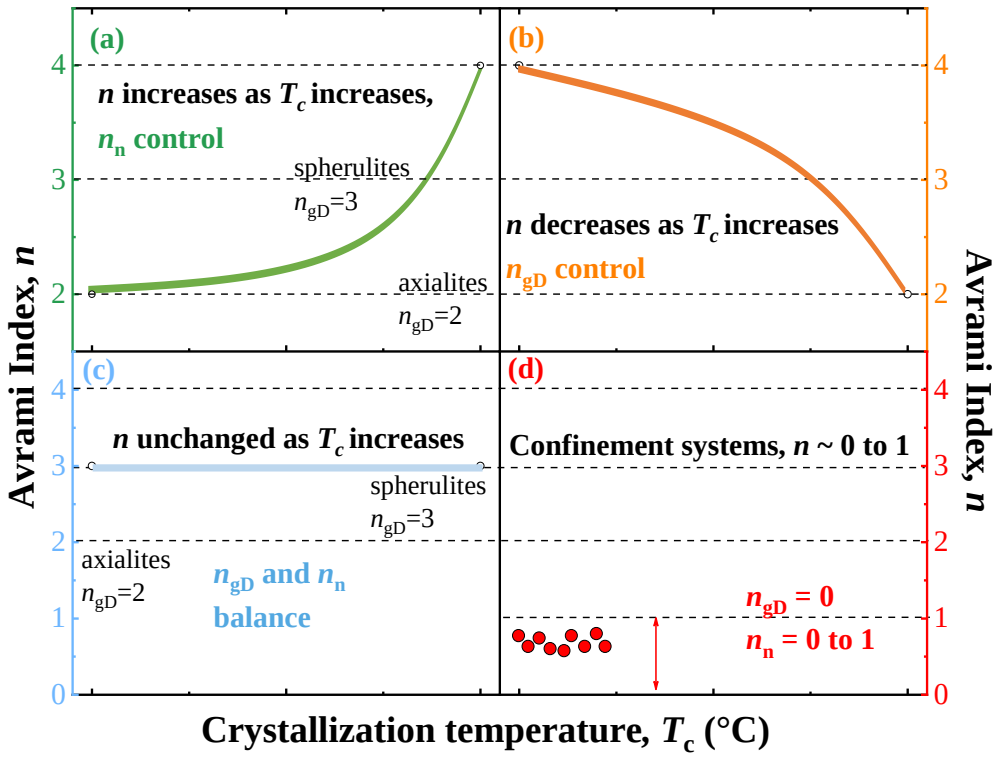

Scheme 6. Schematic representation of the behavior of the Avrami index, n, as a function of T_c. The n values can (a) increases as T_c increases; (b) decreases as T_c increases, or (c) remains unchanged as T_c increases. The horizontal dotted lines indicate the limits for the n values in

polymers. The horizontal line at n =2 indicates axialites (n_{gD}=2), and at n = 3, spherulites (n_{gD}=3). In Scheme 6d the expected n values for confinement systems are represented.

Scheme 6 shows the different expected trends of n vs T_c. Many different trends of the variation of n with respect to T_c can be found in the literature. Namely, the n values can remain unchanged, increase or decrease with T_c. The increase of n values as T_c increases (Scheme 6a) is caused by the changes in nucleation, as it is well known that nucleation tends to be more sporadic as T_c values increase (considering that no change in morphology occurs and that the polymer is always forming spherulites). Therefore, one expects n_n = 0, at high supercooling (i.e., low T_c), and increasing values of n with T_c until n_n = 1, at low supercooling (i.e., high T_c), keeping constant the n_{gD}.[79]

Scheme 6b shows an opposite trend, a decrease of n as T_c increases, which can be explained by dimensionality changes (usually spherulites at low T_c values and axialites at high T_c values) induced by T_c with a constant nucleation rate. This has been reported in low density polyethylene.[79] A similar trend has been reported when the n values are evaluated as a function of the molecular weight (MW). It has been reported in PEs n = 4 at low MW, followed by n = 3 at intermediate MW, and finally n = 2, at high MW.[40] At high MW the entanglements might affect the crystallization, leading to such a low n value.

Scheme 6c shows that the n values can remain unchanged as T_c increases. This is attributed to a balance between the nucleation and crystal dimensionality contributions. The n values can also remain unchanged with T_c in confinement systems,[44, 79] schematically represented in Scheme 6d. The n values for confinement systems, e.g., block copolymers,[41,42,80] homopolymers or copolymers confined within alumina nanoporous,[81-83] among others, e.g., polymer into micro-droplets,[66] is as low as 1.0 (or even lower).[44] For confined systems, it is considered that the nucleation is the rate-determining step in the crystallization. This argument is based on the fact that the free-energy barrier for homogenous nucleation is much higher than the one associated with crystal growth. Thus, since the growth is so fast, the crystallization kinetics is completely dominated by the nucleation process, it can be considered that n_{gD} = 0 (see Equation 2). Consequently, the n values depend only on the volume of the crystallizable microdomains and not in its dimensionality or shape, i.e., $n = n_n$ taking values between 0 and 1. The n < 1.0 implies that the nucleation is not completely sporadic, and it is somewhere in between sporadic and

instantaneous,[42] as illustrated Scheme 6d. Such low n values are also characteristic of a homogeneous nucleation mechanism.

3.2.6. $K^{1/n}$ values

A constant proportional to the overall crystallization rate, K, can be obtained from the Avrami fitting. It is important to remark that the obtained K value has units of time^{-n} (e.g., min^{-n}); therefore, unless n is a constant, its values cannot be directly compared. Thus, for comparison purposes, $K^{1/n}$ should be used instead, which are expressed in units of min^{-1}. The $K^{1/n}$ should have the same trend as the $1/\tau_{50\%}$, as long as the fitting to the Avrami equation is valid until approximately 50% conversion, as shown in Figures 8c and d.

3.3. LAURITZEN AND HOFFMAN ANALYSIS

The feeding parameters to apply the LH theory are the growth rate or overall crystallization rate vs T_c. As stated before, the general form of the LH formula (see Equation 8) can be adapted to the experiment data (i.e., PLOM vs. DSC). Thus, spherulitic growth rate (G), growth rate obtained by DSC after SN ($1/\tau_{50\%,G}$), or overall crystallization rate ($1/\tau_{50\%}$) vs. T_c data can be employed.

The equilibrium melting temperature (T_m^0) must be used in the fitting, which can be taken from the literature or estimated experimentally. The methods to estimate the T_m^0 are based on extrapolations, including the Hoffman-Weeks method,[84] using the plot of T_m versus T_c, and the Gibbs-Thomson method,[85, 86] using the T_m vs the inverse of the lamellar thickness. Recently, the maximum melting temperature after thermal fractionation (i.e., Successive Self-nucleation and Annealing[27, 87, 88]) plus an arbitrary factor have been used to estimate the T_m^0.[89] When experimental data is not available, the T_m^0 can also be estimated using the semi-empirical equations of Van Krevelen,[90] which are based on the contributions of the different groups in the repeating units. The discussion of the T_m^0 determination is beyond the scope of this work. If a set of materials is compared, special attention should be put into the T_m (i.e., from non-isothermal DSC test) and the $T_{m,SSA}$ from SSA experiments, since these values often reflect the big picture of the real trend.

The T_m^0 values affect the LH fitting results (e.g., K_g^A) generated because it affects the LH plot shape.[47]

3.3.1. Illustrating the use of the LH fit

Figures 10 and 11 show the generated plots for both PP and PP-NA samples when the LH Fitting is performed in the Crystallization Fit Origin ® App (See Scheme S2) with DSC (Figure 10) and PLOM (Figure 11) data.[71] To perform the fit, the App should be fed with various parameters. For both PP and PP-NA, we used: a_0 = 5.49 Å and b_0 = 6.26 Å;[47] U^* = 1500 cal/mol;[47] ρ_c = 0.92 g/cm^3;[72] T_m^0 = 186.1 °C,[91] T_g = –12 °C,[47] and ΔH_m^0 = 209 J/g.[47] It is worth noting that in the case of the PP, the ΔH_m^0 calculated using the contribution of groups function of Van Krevelen[90] is 207 J/g,[90], similar to that extrapolated from experimental data.

According to the literature, the PP crystallizes in two (i.e., Regimes II and III) or even three (i.e., Regimes I, II, and III) crystallization regimes depending on the molecular weight.[92, 93] Here, for illustrating purposes, we have fitted the experimental $1/\tau_{50\%}$ vs. T_c data for a T_c range of 126 to 133 °C, where the PP crystallizes in only one regime (Regime III), as shown in Figure 10. Note that often Regime II is assumed as a first trial. When a broader range of T_c (i.e., 126 to 138.5 °C) is considered, the PP crystallizes in Regime II and III (see Figure S6 on the SI). The LH analysis for the complete T_c range for PP (126 to 138.5 °C) and PP-NA (134.5 to 139 °C) is shown in Figures S6 (PP), S7 and 12b (PP-NA), respectively, and the obtained LH parameters are listed in Table 4.

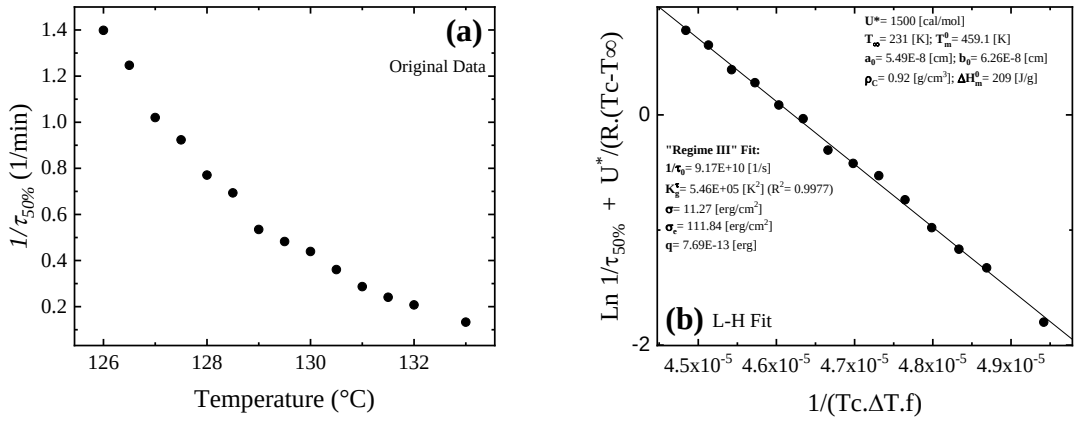

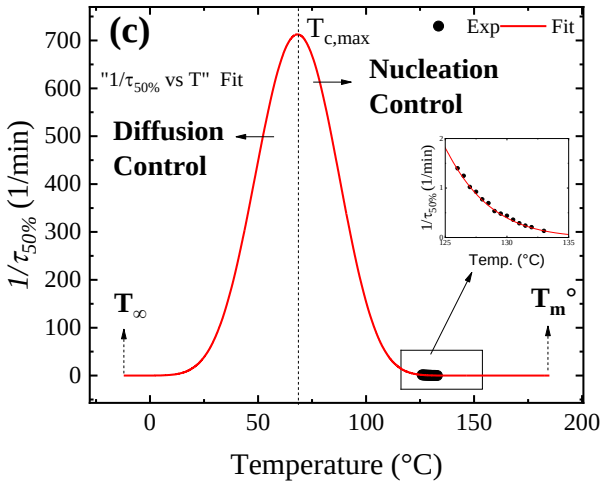

Figure 10. Plots generated by the Crystallization Fit Origin ® App for PP crystallized for a T_c range of 126 to 133 °C; (a) Experimental $1/\tau_{50\%}$ vs. T_c; (b) Lauritzen and Hoffman plot; and (c) fitted vs. experimental $1/\tau_{50\%}$ vs. T_c curves in the entire range of crystallization temperature. Note that in (b), the different LH results are listed.

Figure 10a displays the experimental data (i.e., $1/\tau_{50\%}$ vs. T_c), while the LH fit or LH plot (see Equation 8) is shown in Figure 10b. The LH results are indicated in Figure 10b and Table 4. The complete $1/\tau_{50\%}$ vs. T_c generated by the App is shown in Figure 10c. As we mentioned before, we have used Regime III as the crystallization regime for this example. In Figure S6 it is shown that the PP crystallizes in Regime II for a T_c range of 126 to 135 °C, and Regime III for T_c range of 136 to 138.5 °C.

Figure 10c compares the experimental and fitted $1/\tau_{50\%}$ vs. T_c data from T_∞ to T_m^0, displaying a bell-shape curve. At the right-hand side, crystallization is controlled by nucleation (in this case both primary and secondary nucleation, as the data was collected by DSC), i.e., the second exponential term in equation 8. As T_c becomes higher, the attach-detach events increase, reducing the crystallization rate drastically, especially at T_c close to T_m^0.[23] On the other hand, the left-hand side is controlled by chain diffusion, where the first exponential term is in charge. The crystallization will be hindered as T_c approaches T_g.

As shown in Figure 10c, the data points are located in the nucleation control region. Similar results are obtained for PP-NA as well (Figure S8). In fact, the experimental data always (in a

conventional DSC) falls in the nucleation control region for fast crystallizing polymers such as PE, PCL, among others.[9, 24] This reflects an experimental limitation of conventional DSC whose cooling rates are not fast enough to reach T_c in the diffusion control side (left-hand side of the curve) without crystallization during cooling. For slow crystallizing materials, such as the PLA, the complete curve can be obtained experimentally, even in a conventional DSC (see Figure S4).

The cooling rate limitation of conventional DSC has been overcome by FSC. Thanks to the high cooling rates (up to 40,000 K/s in the commercially available Flash DSC by Mettler but up to 500,000 K/s in custom build equipments,[22] FSC allows performing isothermal crystallization in a much broader T_c range, obtaining complete crystallization kinetics of the materials. Recently the investigations through FSC have revealed that two nucleation mechanisms can be detected in polymers: homogeneous (at high supercooling) and heterogeneous (at low supercooling) nucleation (see Section 3.6), generating two maxima in a $1/\tau_{50\%}$ vs. T_c curve. Due to the experimental limitations, conventional DSC can only record the so-called heterogeneous nucleation mechanism at low supercoolings. Moreover, the LH theory cannot fit two maxima simultaneously. For more details, see Section 3.6.

The LH fit can be applied to spherulitic growth rate, G vs. T_c. For this case, the same fitting parameters as the $1/\tau_{50\%}$ vs. T_c data are used. To illustrate the fitting, we have used the G vs. T_c data for PP in a T_c range of 129 to 145 °C. The results of the fitting are shown in Figure 11. In Figure S8 the results of the LH fit on the PP-NA are displayed.

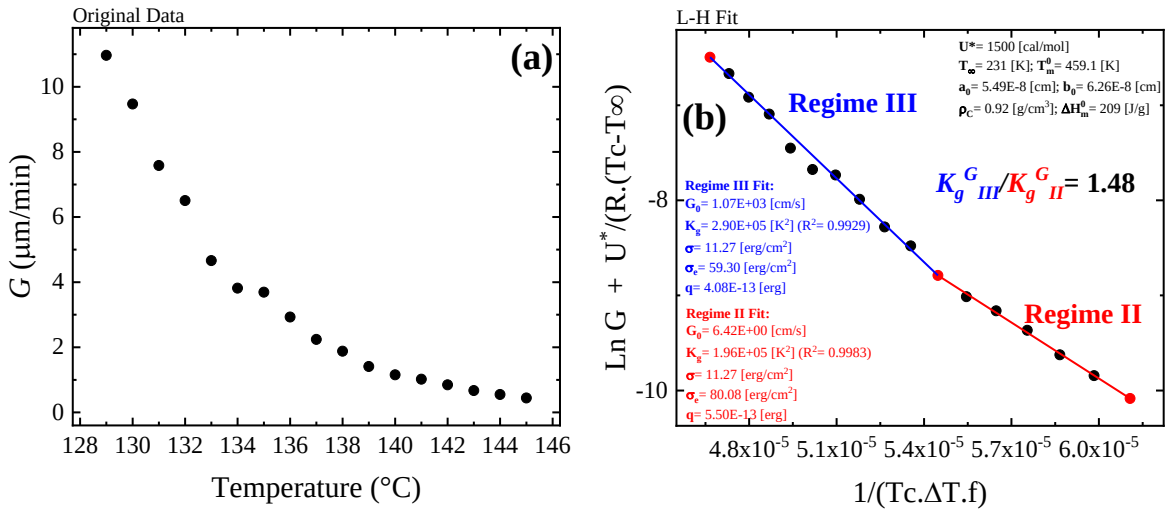

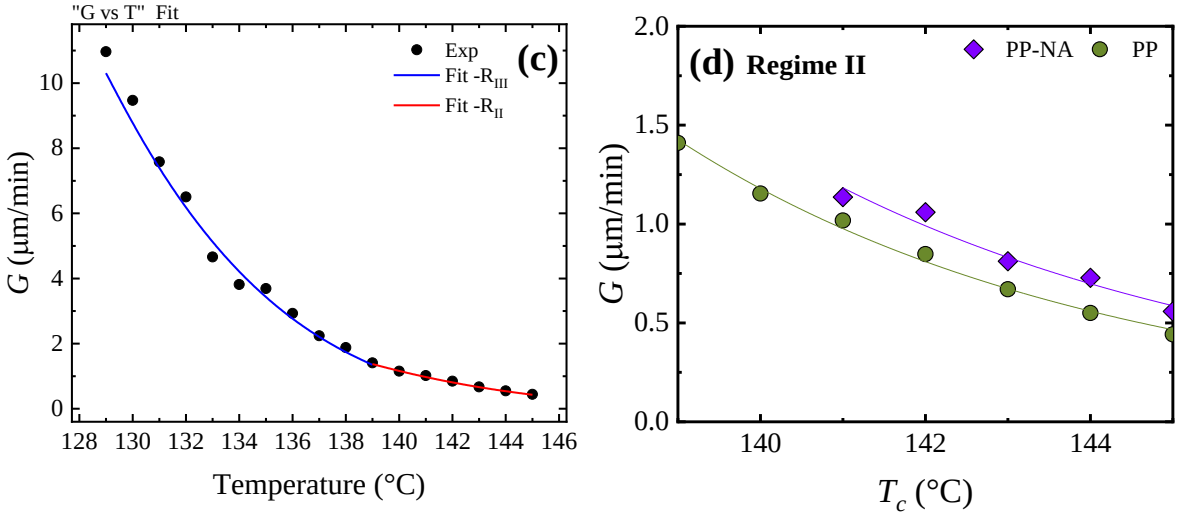

Figure 11. (a) Experimental G vs. T_c data; (b) LH plot; (c) Comparison of experimental and fitted data for PP; and (d) comparison of G vs. T_c for PP and PP-NA samples. Note that in (b) the LH results are indicated.

Figure 11 shows the experimental data and their fit according to the LH model. The Crystallization Fit Origin ® App generates three plots: the experimental G vs. T_c data (Figure 11a), the LH plot (Figure 11b), and the comparison of the experimental and fitted G vs. T_c data (Figure 11c). The PP displays two crystallization Regimes, as in the overall crystallization results (Figure S6). At T_c < 139 °C, the PP crystallizes in Regime III (i.e., much faster nucleation than spreading rate, see Section 3.3.3), and at T_c > 139 °C, in Regime II (i.e., comparable nucleation and spreading rates, see Section 3.3.3). The Regime II to III transition temperature is in line with the literature.[47, 66, 92-95] In this case, the obtained $K_{g,III}/K_{g,II}$ = 1.48 can be approximated to the theoretical value of 2, since there is vast evidence of PP crystallization in two Regimes. The K_g^G values are listed in Table 4 and indicated, together with the other LH results, in Figure 11b. In the case of the PP-NA (see Figure S8), the growth can only be followed in Regime II, at a T_c range of 140 to 145 °C. At T_c < 140 °C (Regime III), the spherulitic growth rate is hard to measure because of the high nucleation density. Figure 11d compared the G vs. T_c curves, in Regime II, for both PP and PP-NA, exhibiting slightly higher G values for the PP-NA, which can be explained by the difference in molecular weight or the presence of additives in the samples. Table 4 compares the LH parameters obtained from PLOM and DSC experiments in both PP and PP-NA samples.

Table 4. LH parameters for PP and PP-NA samples.

Sample, technique	T_c range (°C)	Rg.	K_g^τ x10^{-5} (K^2)	K_g^G x10^{-5} (K^2)	σ (erg/cm^2)	σ_e (erg/cm^2)	qx10^{13} (erg)	R^2
PP	129-138	III	-	2.90	11.3	59	4.10	0.9929
PLOM	139-145	II	-	1.96	11.3	80	5.50	0.9983
PP-NA	140-145	II	-	1.76	11.3	72	4.96	0.9795
PLOM								
PP	126-135	III	5.52	-	11.3	113	7.77	0.9990
DSC	136-138.5	II	2.64	-	11.3	108	7.44	0.9965
PP-NA	134.5-137	III	5.18	-	11.3	106	7.28	0.9997
DSC	137.5-139	II	2.73	-	11.3	112	7.69	0.9818

Table 4 shows different results that will be discussed separately in the next sections. The LH parameters, i.e., K_g, σ_e and q, obtained from PLOM experiments (only growth) are lower than the parameters obtained from DSC experiments (nucleation and growth) due to the latter involving the overall process. **It is important to remark that always the K_g^G values must be lower than the K_g^τ ones.**[29]

As mentioned above, both PP and PP-NA crystallize in Regime II and III, allowing a comparison between them. Table 4 show that $K_{g,III}^A > K_{g,II}^A$, where A refers either to G or τ. According to Equation 9, **$K_{g,III}^A$ must be higher than $K_{g,II}^A$, in a factor ~ 2**. In the case of σ_e values, there is no specific relationship of its changes with the crystallization regimes. In the literature,[47] it has been reported $\sigma_{e,II}$ is lower, equal or higher than $\sigma_{e,III}$. Here, Table 4 reflects $\sigma_{e,II} > \sigma_{e,III}$.

The K_g^G values here reported (see Table 4), are 1.76 to 1.96 x 10^5 K^2 (Regime II) and 2.90 x 10^5 K^2 (Regime III). The K_g^G values reported in the literature vary depending on the MW and the crystallization regime. Cheng et al.[92] studied low and high MW iPP. For low MW iPP, i.e., 15 kg/mol, three crystallization regimes were found, with $K_{g,I}^G$ ~ 3.0x10^5 K^2 (~ T_c > 133 °C), $K_{g,II}^G$ ~ 1.61x10^5 K^2 (122 °C < T_c < 133 °C), and $K_{g,III}^G$ ~ 3.2x10^5 K^2 (~ T_c < 122 °C). As the MW increases,

i.e., 300 kg/mol, only two crystallization regimes are reported, $K_{g,II}^{G}$ ~ 1.25x10^5 K^2 (~ T_c > 137 °C), and $K_{g,III}^{G}$ ~ 2.6x10^5 K^2 (T_c < 137 °C). Hoffman and Clark,[94] recompiled the information of different works reported in the literature and found $K_{g,II}^{G}$ ~ 1.6x10^5 K^2 (~ T_c > 140 °C) and $K_{g,III}^{G}$ ~ 3.1 to 3.6x10^5 K^2 (~ T_c < 140 °C).

Table 4 shows that the K_g^{τ}, σ_e and q values are lower (in Regime III) for the PP-NA than those of PP due to the action of the nucleating agent in PP-NA. In this case, the σ values are the same, due to the same a_0, b_0 and ΔH_m^0 (see Equation 10) were taken for both samples. The LH parameters can be affected by any factor that influences the material's crystallization kinetics. The overall crystallization (nucleation + growth) can be affected by MW differences, the presence of plasticizers agents or other polymers that acts as a plasticization-like agent, nucleating agents, e.g., nanocomposites, comonomers, different topologies, e.g., cyclic vs. linear, and different molecular architecture, among others. Accelerating the crystallization kinetics leads to lower K_g^{τ}, σ_e, and q. Although, it should be noted that the growth process, e.g., K_g^{G}, would be affected only by those factors that affect the mobility of the chains (e.g., plasticization agents). In general, a classic nucleating agent will not affect the growth process.

3.3.2. LH parameters: U^* values, T_m^0, and Regime Selection

The most common value of U^* reported in the literature is 1500 cal/mol; in the following lines, we refer to this value as the reference or standard one (U_r^*). However, other values are also reported, for instance, ~ 6000 cal/mol.[47] The employed U^* value will influence on the K_g^{τ}, σ_e, and q values, but not significantly. The experimental $1/\tau_{50\%}$ vs. T_c data of Figure 10 was fitted using arbitrary U^* values of 375 and 6000 cal/mol (Figure S9a and Table S5), which are four times lower and four times higher than U_r^*, respectively. The K_g^{τ}, σ_e, and q values decrease in factor of 1.1 (for U^* = 375 cal/mol) and increases in a factor of 1.2 (U^* = 6000 cal/mol) compared to the standard case. Therefore, the assumption of U^* = 1500 cal/mol is a good approximation when the U^* value cannot be experimentally obtained.

The discussion on the T_m^0 is complicated and beyond the scope of this paper. However, to illustrate the T_m^0 influence, the $1/\tau_{50\%}$ vs. T_c data of Figure 10, was fitted using T_m^0 = 176.1 and 196.1 (see Figure S9b and Table S5), i.e., T_m^0 = 186.1 ± 10 °C (representing a factor of only 1.05). In this case, the K_g^{τ}, σ_e, and q values decrease in a factor of 1.5 (T_m^0 = 176.1 °C) and increase in a

factor of 1.4 (T_m^0 = 196.1 °C) compared to the standard case (T_m^0 = 186.1 °C). Therefore, the T_m^0 is one of the most influential factors in the LH fitting. To sum up, **the T_m^0 causes the major changes, whereas minor changes are related to U^* and T_g.**

The crystallization Regime selection depends on the polymer. In general, most polymers crystallize in Regime II when they are cooled from the melt at intermediate supercoolings (i.e., comparable nucleation and spreading rates); for that reason, Regime II is assumed in most cases.[47] For illustrating purposes, in Figure S10, Regime II was selected instead. The K_g^τ value depends on the slope of the $\ln 1/\tau_{50\%} + U^*/R\,.\,(T_c - T_\infty)$ vs. $1/(T_c.\Delta T.f)$ curve (see Figures 10 and S10); hence, for the same set of $1/\tau_{50\%}$ vs. T_c data, and assuming only one crystallization Regime, the K_g^τ is independent (i.e., $K_{g,II}^\tau = K_{g,III}^\tau$) of the Regime selection. But, $\sigma_{e,II}$ and q_{II} will be higher than their analogous in Regime III by a factor of 2 (see Equation 9). The same differences will be found if Regime I and II are compared, whereas Regime III and I lead to the same results.

If the analyzed material possesses more than one crystallization regimes, it will be noticed in the slope of the LH plot, since $K_{g,III}^A/K_{g,II}^A$ and $K_{g,I}^A/K_{g,II}^A$ = 2.0 (see Equation 9). When two crystallization regimes are present, probably the assumption of one crystallization regime instead of 2 leads to a poor R^2, as demonstrated in Figure S11 Below we present more details regarding the crystallization regimes.

3.3.3. Changes in Regime of crystallization

The iPP crystallizes in Regime II and III, as was shown in Figures 11, S6, and S7. To further analyze the changes in the crystallization regime, Figure 12 shows two examples: (a) the regime transition induced in PCL by multi-walled carbon nanotubes (MWCNT), and (b) the regime changes in PP-NA inherent to the polymer.

The growth of lamellar crystals is dictated by two processes: lateral spreading growth, with its respective rate, g, and secondary nucleation, with a rate i. The relation between the rate of these processes, i vs. g, defines the crystallization regime. At low ΔT, i.e., T_c close to T_m^0, Regime I takes place. In Regime I, the formation process of secondary nuclei is much slower than their growth, i.e., $g >> i$. At intermediate ΔT, the rate of each process is comparable, i.e., $g \sim i$; defining Regime II. At high ΔT, the formation of secondary nuclei is much faster than their growth, $g << i$, defining Regime III. Further details of the crystallization regimes can be found in the literature.

[11, 12, 15-17, 73, 92-94,96] For PP, the regime transition temperature depends on the crystallographic form (α vs. β) and the MW. Only for low MW fractions of the α-form, it is reported that the transition between Regimes II to I occurs at 155 °C, besides the transition of Regime III to II. At high MW, the Regime III to II occurs at around 137 to 138 °C, for the α-form, and 123 to 129.5 °C, for the β-form.[93] If pressure is applied, e.g., 150 MPa, high MW iPP displays all the regimes.[47]

The regime change is characterized by a variation in the slope of the LH plot. In some instances, the regime change has a clear morphological manifestation. In particular, for PE, it is reported a spherulitic morphology for Regime II and an axilitic one in Regime I.[17]

To illustrate the variation in the slope of the LH plot, we have applied the LH theory to the experimental data Trujillo et al.[73] in PCL/MWCNT nanocomposites (Figure 12a) and our data in the PP-NA (Figure 12b). The LH plot is shown for both cases in Figure 12.

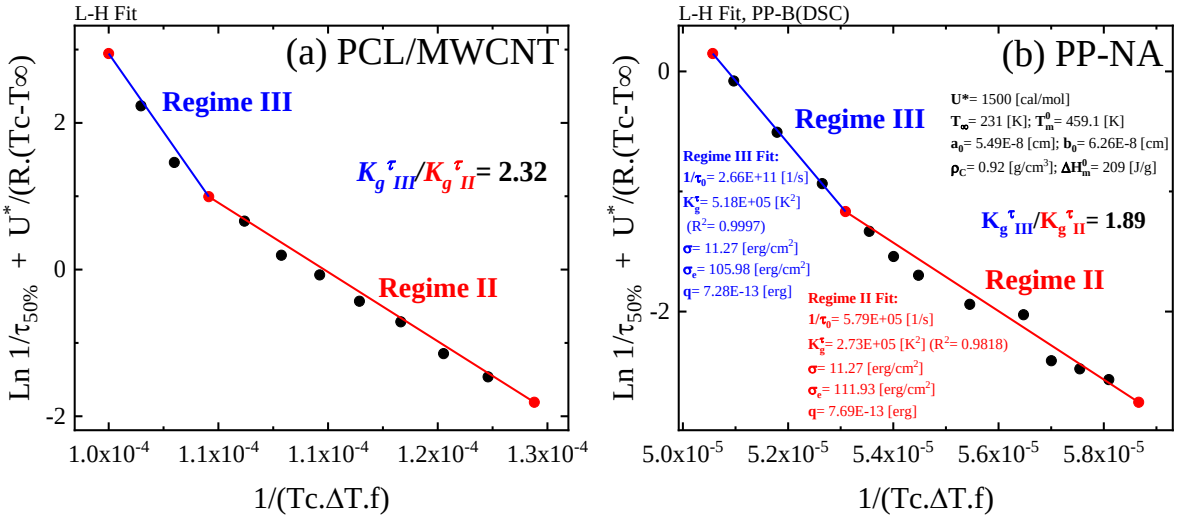

Figure 12. Illustration of regime changes for (a) PCL/MWCNT studied by Trujillo et al.,[73] and (b) PP obtained in this work. Note that the $K_{g,III}^{\tau}/K_{g,II}^{\tau}$ is ~ 2.0.

Figure 12 shows that in both cases, the slope changes by a factor of approximately 2. This indicates a change from Regime III to Regime II. For the PCL/MWCNT, the Regime III (i.e., $i >> g$) is induced by the very strong nucleating effect, i.e., in this case, the MWCNTs acts as supernucleating agents of the PCL, of the MWCNTs on PCL. In fact, the neat PCL only crystallizes in Regime II.[73, 75] In contrast, the Regime II to III transition is inherent to iPP, because both iPP

with and without nucleating agents displays the same transition, in line with the literature.[66, 92-94] It is important to remark that in iPP the regime change detection is possible only if a wide range of T_c is employed. In addition, the additives in the material might prevent the detection of the regime change. For instance, the high nucleation density in the PP-NA, difficult following the spherulitic growth at T_c < 140 °C. Thus, Regime III cannot be detected by PLOM for the PP-NA. Note that Regime III can be detected by PLOM for PP, which does not contain a nucleating agent.

When the LH theory is applied, the first assumption is that the polymer crystallizes in only one Regime, which generally corresponds to Regime II. In Figure 12b, if such assumption is made in the PP-NA, a poor R^2 of 0.9576 (see Figure S11) is obtained. However, by assuming two regimes, the R^2 improves significantly, and the ratio $K_{g,III}/K_{g,II}$ is practically 2.

3.3.4. Individual contributions on the overall crystallization process: Nucleation and growth

The Crystallization Fit Origin ® App allows the application of the LH model on spherulitic growth rate (G) vs T_c measured by PLOM as well. The generated plots for PP are shown in Figures 11 and S8. In the case of the PP-NA, the high nucleation density prevented the G measurements at T_c < 140 °C.

Lorenzo and Müller[29] proposed an alternative method to follow the growth kinetics through isothermal DSC measurements from the self-nucleated state (see Scheme 4c). The self-nucleation step performed at the ideal self-nucleation temperature generates so many nuclei (of the order of 10^{13} to 10^{14} nuclei/cm^3) that the nucleation stage can be considered essentially complete. Thus, the subsequent isothermal step (performed in the DSC) will register only the growth response instead of the nucleation + growth as in the overall isothermal crystallization from the isotropic melt. Here, through practical examples, we illustrate how to follow the growth in a DSC (see Scheme 4c) and how to separate the different contributions of the overall crystallization process.

The isothermal crystallization from the self-nucleated state was applied in both PP and PP-NA samples. The isothermal curves were shown in Figures 1c and d, and fitted with the Avrami theory (see the result in Section S7 on the Supporting information). From these curves, the half-growth times denoted here as $\tau_{50\%}^{G}$, were extracted; therefore, the growth rate from these measurements is

indicated as $1/\tau_{50\%}^{G}$. Different comparisons were made with the $1/\tau_{50\%}^{G}$vs. T_c data, as displayed in Figure 13.

Figure 13a illustrates the experimental data and the corresponding LH fits for the overall crystallization rate and growth rate vs. T_c curves using the PP as an example. The prediction shows that the bell-shape $1/\tau_{50\%}^{G}$ vs. T_c curve is shifted to higher T_c values than the $1/\tau_{50\%}$ vs. T_c curve due to the promotion of the crystallization at low supercooling caused by the self-nucleation. Such a shift is indicative of the effective SN of the material. The same behavior (not shown) was also observed for the PP-NA. Figure 13b compares the $1/\tau_{50\%}^{G}$ vs. T_c curves for the PP and PP-NA samples. The curves of the PP-NA are displayed at higher T_c, indicating that the PP-NA also shows a higher growth rate than the PP, in line with the G vs T_c curves in Figure 11b. In this case, the presence of nucleating agents should not influence the growth; therefore, the difference between the materials might be related to different reasons, e.g., MW, defects distribution, among others.

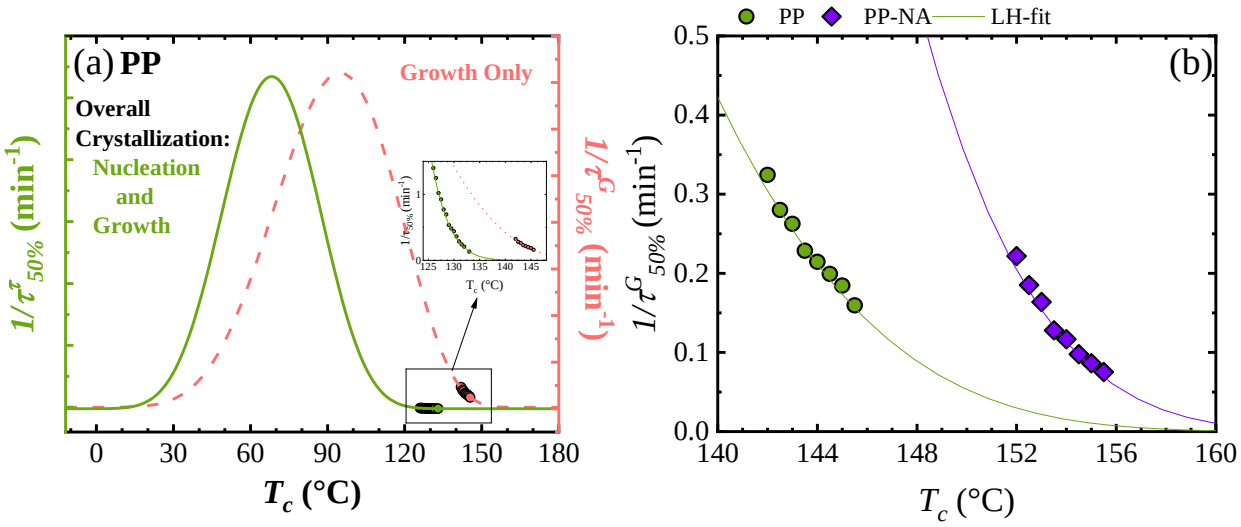

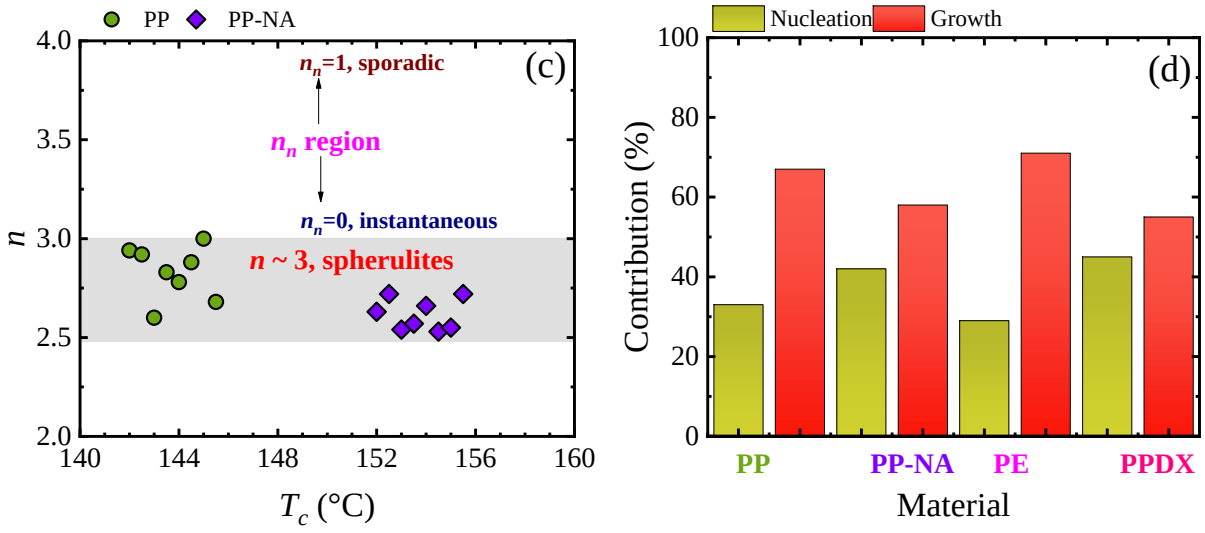

Figure 13. (a) Comparison of the overall and growth (DSC) crystallization kinetics of the PP- neat; (b) Comparison of the growth rates (DSC) for the PP and PP-NA; (c) Avrami index obtained from isothermal crystallization from the self-nucleated state for PP and PP-NA; and (d) nucleation and growth contribution for PP and PP-NA estimated in this work, and their comparison with the PE and PPDX obtained in the literature.[9]

Figure 13c shows the Avrami index, n, determined from the self-nucleated samples. The SN process forces the material to crystallize instantaneously; hence the nucleation term, n_n, is equal to zero. Both samples crystallize as spherulites (Figure S13); therefore, the obtained n values can be approximated to n = 3. Note that these n values are lower than those obtained from the isothermal crystallization from the melt, in which the nucleation term contribution was present, generating n values higher than 3 (Figure 8b). The reduction of the n values is an expected behavior when the material is isothermally crystallized from the self-nucleated state.

As previously indicated, the LH fit allows estimating the K_g^A, which is the energy proportional to a specific process, e.g., overall crystallization or spherulitic growth. For the overall crystallization kinetics, K_g^τ is obtained, corresponding to a factor proportional to the overall crystallization energy barrier, including contributions from nucleation and growth. When the spherulitic growth is followed in the PLOM, a K_g^G value is obtained, and it is only attributed to the spherulitic growth process. From the results of Figure 13, the LH allows determining $K_{g,SN}^\tau$, here defined as a factor proportional to the energy barrier for the growth process obtained by DSC (i.e.,

isothermal crystallization from the self-nucleated state). Below, it is demonstrated that comparable K_g^G and $K_{g,SN}^\tau$ values are obtained, validating the isothermal crystallization from the self-nucleation state.

Considering the different K_g^A values, the nucleation and growth contributions to the overall crystallization process can be estimated. The evaluation of the individual nucleation and growth contributions was proposed by Lorenzo and Müller[29] in a pioneer work, estimating the contributions of each process in different polymers, using the isothermal crystallization from the melt and the self-nucleated state. The method is based on the principle that the $K_g^\tau = K_g^{nucleation} + K_{g,SN}^\tau$ (or K_g^G). Thus, the overall crystallization is equal to nucleation (i.e., indirectly estimated) and growth contributions, like is shown in Figure 13d for different materials, including the PP and PP-NA (used in this work). This procedure has been employed in the literature.[29, 30, 66]We applied the same process for PP and PP-NA samples. Due to the regime transitions, these samples are novel for the above-described methodology. The obtained K_g^G, K_g^τ and $K_{g,SN}^\tau$, as well as the separated contributions are shown in Table 5.

Table 5. K_g^A values obtained from different methods (PLOM, DSC neat, and self-nucleated state), and the estimated individual contributions in the nucleation and growth process. The T_c range in which the experiments were performed is also indicated.

Sample	**Method**	**T_c range (°C)**	**K_g^A x10^{-5} (K^2)**	**Nucleation contribution (%)**	**Growth contribution (%)**
PP	PLOM	129-138	2.90 (RIII)	-	-
		139-145	1.96 (RII)	-	-
	Neat, DSC	126-135	5.52 (RIII)	47*	53*
		136-138.5	2.64 (RII)	26*	74*
	Self-nucleated at 168 °C, DSC	142-145.5	1.78 (R-II)	33	67
PP-NA	PLOM	140-145	1.76 (R-II)	-	-
	Neat, DSC	134.5-137	5.18 (R-III)	-	-
		137.5-139	2.73 (R-II)	35*	65*

	Self-nucleated at 168 °C, DSC	152-155.5	1.61 (R-II)	41	59

*Obtained by using the K_g^G values.

The SN process before the isothermal steps provokes a shift to a higher T_c range, due to the nucleation effect of the self-nuclei. In this case, i.e., iPPs, such shift (T_c > 140 °C) imply that the growth process only occurs in Regime II. Table 5 shows that the $K_{g,SN}^{\tau}$ values of 1.61 and 1.78x10^5 K^2 for the PP-NA and PP samples, respectively, are in good correlation with its homologous K_g^G values of 1.78x10^5 and 1.96x10^5 K^2, respectively. This proof the goodness of the method, as shown by Lorenzo and Müller[29] in PPDX, reporting K_g^G = 1.72x10^5 K^2 and $K_{g,SN}^{\tau}$ = 1.70x10^5 K^2, and PCL, with K_g^G = 0.615x10^5 and $K_{g,SN}^{\tau}$ = 0.609x10^5 K^2.

The obtained $K_{g,SN}^{\tau}$, as well as K_g^G , values are in line with the values of K_g^G reported in the literature for iPP in Regime II, K_g^G = 1.25 to 1.64 x 10^5 K^2. [92-94] The $K_{g,SN}^{\tau}$ values here obtained are also comparable to the values reported by Kang et al.[95] These authors isothermally crystallized the iPP from the self-nucleated state ($T_{s,ideal}$ = 167 °C), obtaining $K_{g,SN}^{\tau}$ = 2.1 and 2.7 x 10^5 K^2 (T_c = 145 to 149 °C)[95] assuming a crystallization in Regime II. Wang et al.,[66] in iPP microdroplets in immiscible blends obtained at $K_{g,SN}^{\tau}$ = 2.65x10^5 K^2 after self-nucleating the sample at $T_{s,ideal}$ = 160 °C. As we mentioned before, for the specific case of the iPP, it is important to remark that the SN technique limits the $K_{g,SN}^{\tau}$ vs. K_g^{τ} comparison to only one regime, i.e., Regime II. Other cases will be easier to analyze since the materials already crystallize in only one regime, i.e., Regime II.

The nucleation and growth contribution estimation should be performed by comparing the data in the same crystallization Regime. For the $K_{g,SN}^{\tau}$ the contributions can only be made in Regime II, while in the case of K_g^G values in PP, the nucleation and growth contributions can be estimated in Regime II and III. Table 5 show that both PP and PP-NA samples have similar nucleation and growth contributions (see Figure 13d) in Regime II. As expected, when the effect of the nucleation agents is suppressed by better nuclei (i.e., self-nuclei), both PP and PP-NA exhibited similar growth kinetics due to their similar MWs. The obtained nucleation and growth contributions indicate that the growth is the rate-determining step in the overall crystallization process. Interestingly, the nucleation contribution increases with the Regime II to III transition for the PP.

The values here obtained are similar to those reported by Lorenzo and Müller[29] in PPDX (see Figure 13d).

The estimated contributions agree with the expected behavior in homopolymers. In the case of iPP microdroplets in immiscible blends, considering the $K_{g,SN}^{\tau}$ = 2.65x10^5 K^2 and K_g^G = 19.3x10^5 K^2 values reported by Wang et al.,[66] the nucleation contribution is 86%, and the growth one is 14%. Such ratio indicates that the nucleation is the rate-determining step of the overall crystallization process, as expected in polymers ideally confined in isolated micro – or nanodomains.

The determination of the growth rate using SN followed by isothermal experiments significantly depends on the T_s selection. Wang et al.[66] self-nucleated the PP microdroplets at T_s > $T_{s,ideal}$, and found an increase of the $K_g^{\tau}{}_{SN}$. At the lowest limit, corresponding to the $T_{s,ideal}$ = 160 °C the authors obtained a $K_{g,SN}^{\tau}$ = 2.65x10^5 K^2. This value increases to 3.65 and 4.05x10^5 K^2 for T_s = 161 and 162 °C (in *Domain II*), respectively. In the highest limit, T_s = 210 °C (*Domain I*) a $K_{g,SN}^{\tau}$ = 19.3x10^5 K^2 was registered, demonstrating the more important contribution of primary nucleation to the overall crystallization rate as T_s increased.[66] It is expected that as T_s increases, the $K_{g,SN}^{\tau}$ increases until it reaches the limit value of K_g^{τ} at T_s in *Domain I*, as we illustrated in Scheme 7a. The effect of self-nucleating the sample at different T_s, before the isothermal crystallization, has been reported by Feng and Yin[97] in PP and low ethylene content propylene-ethylene copolymers. They found that the T_c and $1/\tau_{50\%}$ values increase as T_s decreases, whereas n and σ_e decreased. Such behavior denotes the importance of performing the isothermal crystallization from the self-nucleated state using the $T_{s,ideal}$. To illustrate the effect of self-nucleating the sample at different T_s, we arbitrarily selected K_g values (see Scheme 7a) between the estimated $K_{g,SN}^{\tau}$ (bottom limit) and K_g^{τ} (upper limit) of the PP-NA (used here as reference). Then we calculated the corresponding nucleation and growth contributions (Scheme 7b). The results of using different K_g values is schematically represented in Scheme 7b.

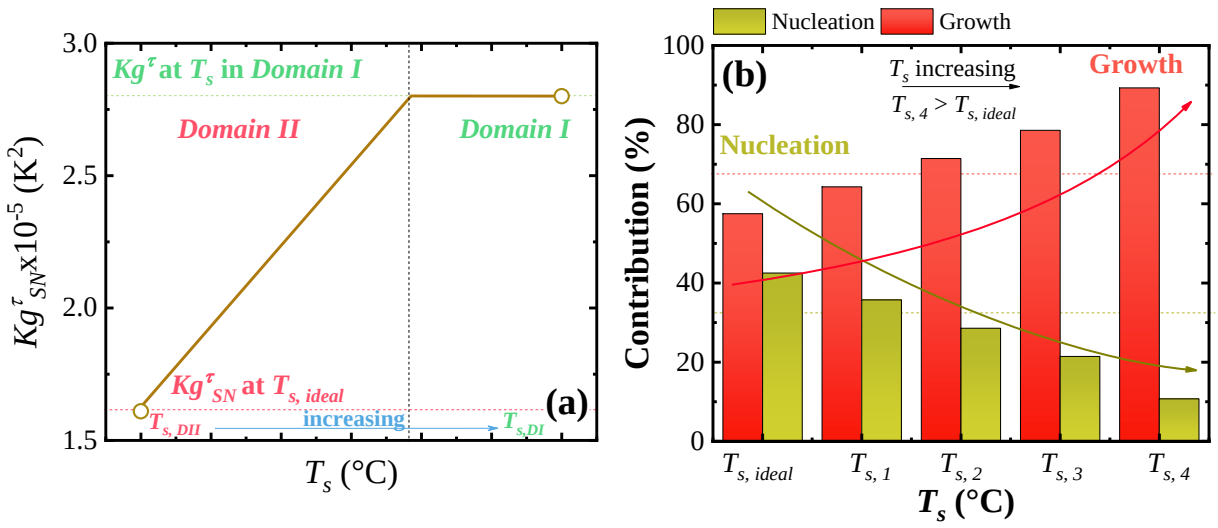

Scheme 7. Schematic representation of the $K^{\tau}_{g,SN}$ values as a function of T_s. The limit $K^{\tau}_{g,SN}$ values were obtained experimentally at $T_{s,ideal}$and a T_s in *Domain I*; (b) Schematic representation of the nucleation and growth contributions as a function of T_s, assuming arbitrary $K^{\tau}_{g,SN}$ values between the experimental obtained $K^{\tau}_{g,SN}$ values at $T_{s,ideal}$ and higher T_s in *Domain I*. The K^{τ}_{g} and $K^{\tau}_{g,SN}$ values employed as a reference corresponds to the PP-NA (see Table 5).

Scheme 7a shows the expected trend when the sample is previously self-nucleated at T_s as low as $T_{s,ideal}$, and as high as T_s in the self-nucleation *Domain I*. For this purpose, we arbitrarily selected values in between the $K^{\tau}_{g,SN}$ and the K^{τ}_{g} values of the PP-NA. At $T_{s,ideal}$, the K_g corresponds only to the growth (i.e., see Table 5). As T_s increases, the $K^{\tau}_{g,SN}$ not only corresponds to the growth and starts having nucleation contributions, increasing its value, as it has been reported by Wang et al.[66] who employed different T_s. The T_s in *Domain I* should not generate any self-nuclei; hence the crystallization from this state should be the same as in the isotropic melt, as evidence the same K_g (see straight line in *Domain I* in Scheme 7a) values, i.e., $K^{\tau}_{g,SN} = K^{\tau}_{g}$. In Scheme 7b, the nucleation and growth contribution are represented. The $K^{\tau}_{g,SN}$ increases as the T_s increases, leading to an "artificial" increment of the growth contribution. But, if the SN was not performed at $T_{s,ideal}$, such increment is caused by the nucleation component instead. Thus, Scheme 7 demonstrates that selecting T_s different to $T_{s,ideal}$, affects the K_g value (Scheme 7a) and the balance between the nucleation and growth contribution (Scheme 7b), leading to an erroneous interpretation of the overall crystallization contribution.

3.4.ISOTHERMAL CRYSTALLIZATION: CONTINUOUS VS. STEP APPROACH

Continuous isothermal crystallization generates a curve of heat flow vs. time at a specific T_c. When the signal of heat flow is too low to be detected (see Figure 14a), the step-crystallization approach can be used instead. The step-crystallization procedure can be visualized as the division of such heat flow vs. time curve in different steps until encompassing the crystallization of the material until saturation. The step-crystallization has been used to follow the crystallization kinetics in confined systems, for instance, PP microdroplets in PP/PS 15/85 blends;[66] PE in triblock copolymers,[41] and confined polymer and copolymers in templates.[20, 21, 24, 44, 82] The step-crystallization has also been employed at high crystallization temperatures, in which the exothermic signal of continuous isothermal crystallization cannot be measured.[63] The isothermal step crystallization technique is commonly used in FSC measurements because the heat flow under isothermal conditions is usually very low due to the very small sample mass.[22]

Figure 14 shows two examples of the step-crystallization performed using a conventional DSC. On the one hand, PEO infiltrated in an AAO template was crystallized from the melt (continuous approach) at T_c = – 3 °C for 30 min. Figure 14a evidence that the signal (heat flow) is not detected. But the subsequent heating clearly shows an endothermic peak (Figure 14b), corresponding to the melting of the crystals formed at the isothermal step. Thus, in this case, step-crystallization emerges as an alternative to follow the crystallization kinetics. On the other hand, for comparison purposes, the PP was crystallized by step-crystallization (Figures 14c and d) and compared to the continuous case (see Figure 1).

The PP was crystallized at 133 °C for different time intervals, starting from 0.1 min (minimum value allowed in the instrument) with increments of 0.1 min until reaching approximately 30 min. After each isothermal step, the material was subsequently heated, recording the heat flow vs. temperature for a specific crystallization time. The heat flow was followed until it reached a saturation value, in which the peak area is independent of the crystallization time. In Figure 14b, we divided the heat flow by the weight of the sample, obtaining the enthalpy (ΔH) as a function of the crystallization time. This curve represents the evolution of the crystallinity with time, and it can be used to apply the Avrami fit (see Section 3.2).

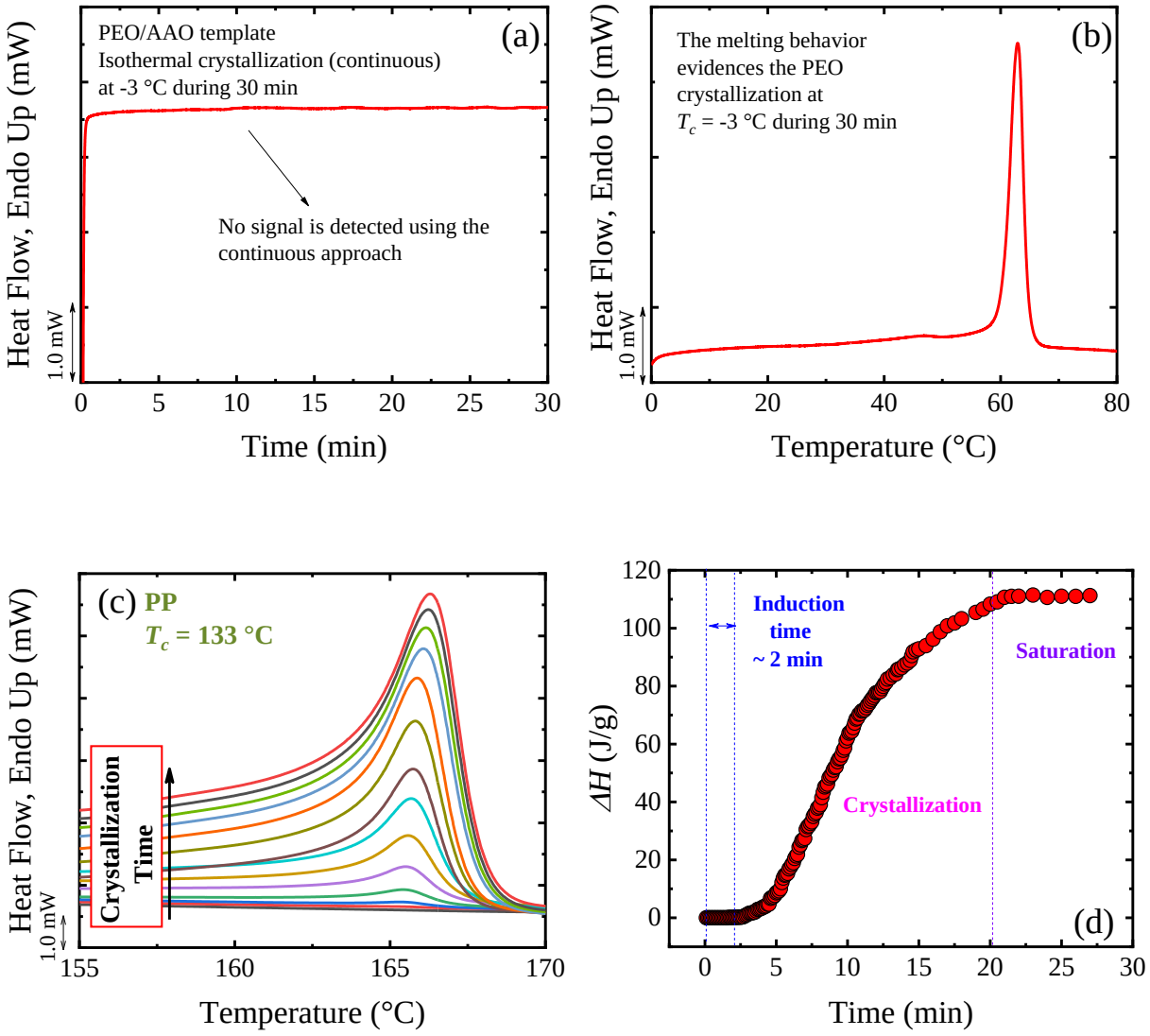

Figure 14. (a) Isothermal continuous crystallization of PEO/AAO template and its subsequent (b) DSC non-isothermal heating curve. (c) Melting after isothermal step crystallization of the PP at 133 °C at different times, and (d) melting enthalpy (ΔH) calculated from (c) as a function of the corresponding crystallization time. In (d) the region at shorter times between the dashed lines represents the induction time. The vertical dashed line at longer times divides the crystallization region from the saturation region (a maximum ΔH value is reached, and it does not change as the time increases).

Figure 14c shows how the heat flow of the endothermic curves increases as the crystallization time increases. In other techniques, the evolution of a property (P) related to the crystalline state as a function of time is registered, e.g., the intensity of the principal crystallographic planes (WAXS), and main absorption bands (FT-IR) vs. time. Even though the crystallization occurs

continuously in these techniques, its analysis is by step due to the data acquisition. Thus, curves similar to Figure 14d can be obtained, representing the evolution of the crystallinity with time. Therefore, the step-crystallization analysis can be performed through different techniques and fitted with the Avrami theory, as shown below.

From Figure 14d (ΔH vs. time), it is essential to consider an induction time, τ_0, involved. In this case, at short times, the enthalpy registered in the subsequent heating curves is approximately equal to zero, indicating that growth does not occur at such times. The τ_0 can be estimated as the interception between the linear extrapolation of the initial crystallization data and the time axis (x-axis).[66] The τ_0 must be considered in the step-crystallization Avrami analysis.

The ΔH evolution in Figure 14d is transformed to V_c (see Equations 5 and 6), allowing applying the Avrami fit. Even if a different technique is used, the step-crystallization analysis with the Avrami fit can be employed. For them, the following equation can be utilized as an approximation to V_c:

$$V_c = \frac{P(t)}{P(total)} \tag{14}$$

where P is a physical property of the crystalline state evaluated at a specific time, $P(t)$, and $P(total)$ corresponds to the maximum value of the considered property. For instance, P can be equal to the crystallinity determined by WAXS experiments; and being analyzed using the Crystallization Fit Origin ® App. When the App is employed in other techniques, it will be fed with P vs. time data. Afterward, to avoid extra mathematical operations, the sample weight entry (in the App) should be filled with a value of 1.0; the App will transform the data to V_c as shown in Equation 14. If the amorphous and crystalline densities are not known, a value of 1.0 can be taken, i.e., equal densities principle, without generating significant errors, as was previously shown. Thus, the Crystallization Fit Origin ® App is a powerful tool for crystallization kinetics analysis through the Avrami (using continuous or by-step approach) and Lauritzen and Hoffman theories.

3.5.APPLICATION OF THE AVRAMI THEORY: STEP-CRYSTALLIZATION

The Crystallization Fit Origin ® App[71] developed from the original plug-in of Lorenzo and Müller[9] can also fit the data generated by a **step-crystallization** (See Scheme S3). As in the

continuous fit, the following data should be provided: (a) heat flow vs. time, obtained by step-crystallization, (b) amorphous and crystalline densities, and (c) the weight of the sample. It is important to remark that the induction time should be subtracted. If the enthalpy is already normalized in the DSC program, 1.0 should be input for the weight of the sample. In this way, the already calculated enthalpy will not be divided again by the weight of the sample. Figure 15 shows the curves generated by the step-crystallization Avrami fit for the step-crystallization of the PP at 133 °C. Step-crystallization experiments were also performed and analyzed for the PP at 126 °C, as shown in Figure S14 in the supporting information.

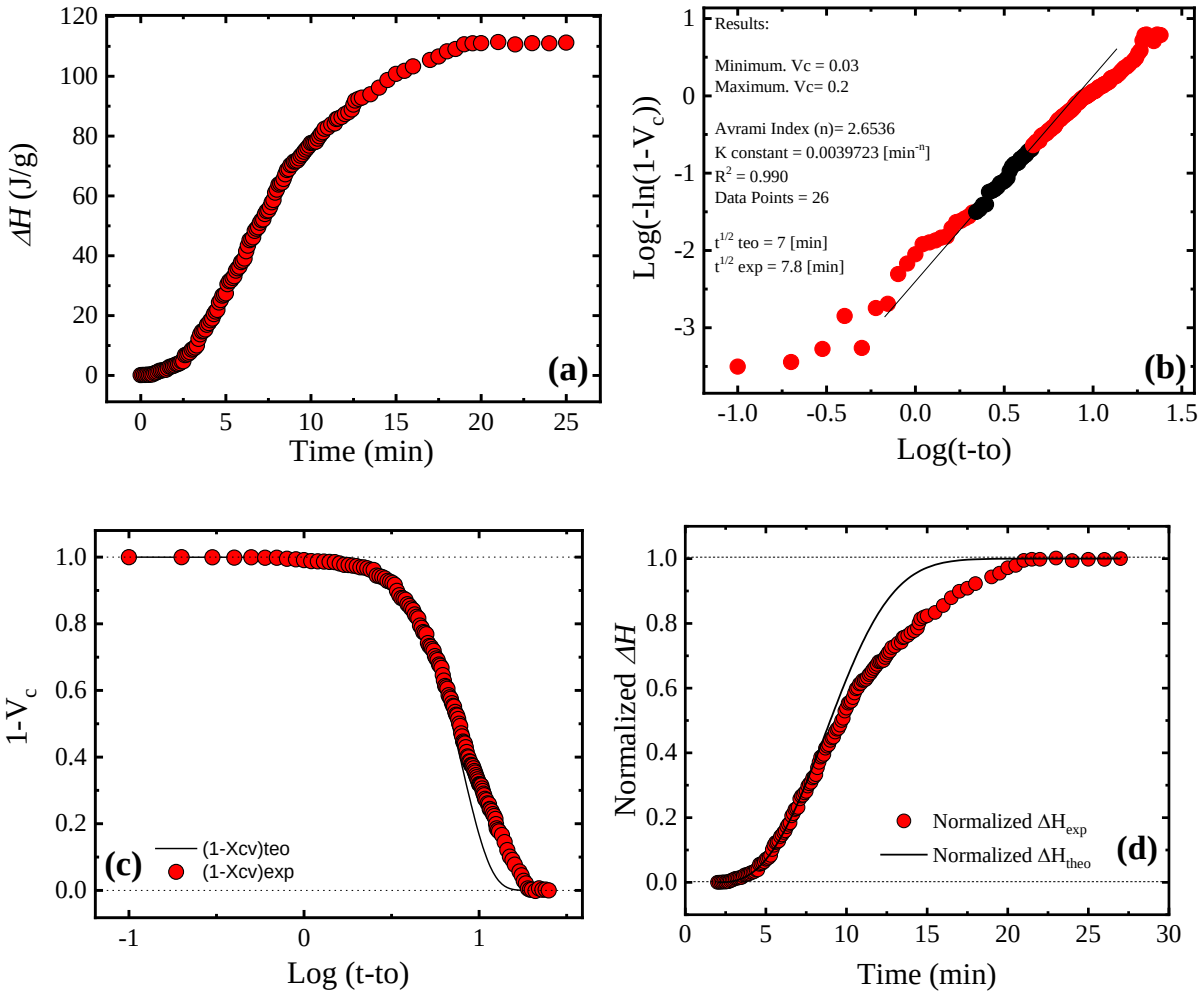

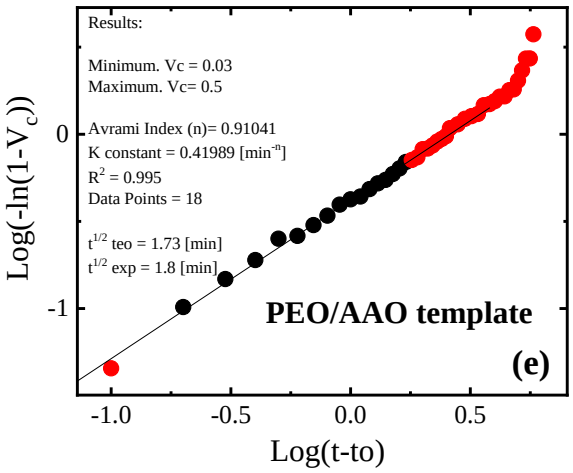

Figure 15. Plots generated by the Crystallization Fit Origin ® App when the step-crystallization Avrami fit is employed: (a) ΔH vs. time, (b) Avrami plot; (c) Relative amorphous fraction (1-V_c) vs. time, and (d) Normalized ΔH vs. time. In (e) the Avrami plot for the PEO/AAO template is included for comparison purposes. In Figure (b) the obtained Avrami results are indicated. Note that the experimental data for (a to d) corresponds to the PP crystallized at 133 °C, and for (e) to PEO/AAO template at –3 °C.

To correctly perform the Avrami fit, those points in which $\Delta H \sim 0$ (from Figure 14d) must be removed because they correspond to the induction time, τ_0. Figure 14d indicates that τ_0 is approximately 2.0 minutes, in line with the τ_0 = 1.57 minutes obtained in the continuous fit. Thus, the fit was performed on the experimental data of Figure 15a. Note that for the App the point zero corresponds to the starting time, in this case, 2 minutes. The Avrami step-crystallization fitting generated the Avrami plot (Figure 15b), the relative amorphous fraction (Figure 15c), and normalized ΔH vs. time (Figure 15d) plots. In Figures 15c and d, it is clearly observed that the obtained theoretical curves can fit the experimental data up to ~ 40% of conversion, indicating the goodness of the fit as in the continuous Avrami fit.

Figure 15b shows that from the Avrami fit for V_c = 3 to 20 %, the following results are generated: $\tau_{50\%}$ = 7.8 min, n = 2.65; and K = 0.0040 min^{-n}. These values are similar to those obtained for the continuous Avrami fit at the same T_c: $\tau_{50\%}$ = 7.54 min, n = 2.92; and K = 0.0019 min^{-n}. The maximum deviation, i.e., calculated through Equations 12 and 13, compared to the continuous approach (see Table 7) is related to the K values; however, the $K^{1/n}$ is the same (0.125 min^{-1}). Moreover, the related error (~ 9 %) with the n values does not change its physical meaning

since it still indicates that the crystallization is characterized by instantaneously nucleated spherulites. The similarity of the obtained results indicates the goodness of the fitting performed either by step-crystallization or continuous Avrami fit. Thus, the step crystallization applied correctly provides the same results as the continuous crystallization. It is a useful solution for those cases in which the signal of continuous crystallization is not well resolved. It should be remarked that if both types of crystallization can be performed in the same temperature range, continuous crystallization is preferred because it provides the same result in significantly shorter times and with greater precision.

Figure 15e represents a particular case since the crystallization occurs under confinement. As mentioned previously, the crystallization under confinement is dominated by nucleation, and there is no growth contribution. The results in Figure 15e indicate n = 0.91 in line with the expected values for confined systems (see Scheme 6). In this case, the step-crystallization is the solution to study a complex system, such as confined polymeric systems.[20, 21, 24, 26, 41, 42, 80, 82, 83, 98-106]

3.5.1. Related errors: Induction times and number of points

The induction time should be considered in the step-crystallization analysis. Figure 14b shows the region of the curve that corresponds to the induction period. If the induction time is not removed (Figures S15b and c), the following parameters are obtained: $\tau_{50\%}$ = 9.7 min, n = 4.20, and K = 9.15x10^{-5} min^{-n} with R^2 = 0.988. The obtained n value is ~ 4, which completely changes the physical interpretation of the kinetics. The relative errors have been estimated considering the previous results (removing τ_0) as the "ideal" condition, and listed in Table 7. It is important to remark that a $T_{c,min}$, and a proper cooling rate must be used in the step-crystallization since it is also affected by the crystallization during cooling, generating similar errors than the continuous crystallization.

The continuous crystallization approach generates a continuous heat flow vs. time curve, in which the number of data points is not a problem. Usually, around 300 data points are generated in a standard DSC equipment during a continuous isothermal crystallization experiment lasting 35 minutes; however, this depends on the data acquisition rate of the equipment. But, in the step-crystallization approach, the data points are fixed by the user. Here, we performed isothermal crystallization every 0.1 min. This means the first step involves an isothermal crystallization of

0.1 min, the second step 0.2 min, and so on until reaching saturation. To understand the importance of recording enough data points, we have varied the crystallization time intervals, using 0.5 min and 1.0 min for comparisons. The different curves generated by the Avrami by-step fit are shown in Figure S16. Table 7 lists the Avrami parameters and their relative errors compared to those obtained by using intervals of 0.1 min. The results of the continuous Avrami fit and the by-step fit (using intervals of 0.1 min) are also listed, estimating the latter's errors using the continuous fit as an "ideal" condition.

Table 6. Avrami parameters and the relative errors (Δ) for different crystallization conditions. Avrami index, n; constant proportional to the crystallization rate, K^n, theoretical half-crystallization time, $\tau_{50\%,t}$, experimental half-crystallization time, $\tau_{50\%,exp}$.

Condition	**Parameter**					Δ			
	n	Kx10^3 (min^{-n})	$\tau_{50\%,t}$ (min)	$\tau_{50\%,exp}$ (min)	**Dat P.**	Δn	ΔK	$\Delta\tau_{50\%,t}$	$\Delta\tau_{50\%,exp}$
Continuous	2.92	1.93	7.49	7.54	-	-	-	-	-
Interval 0.1 min	2.65	3.97	7.00	7.80	26	9.1^{+}	106^{+}	6.6^{+}	3.5^{+}
Interval 0.5 min	2.69	3.71	7.00	8.0	6	1.3*	6.9*	0.1*	2.6*
Interval 1.0 min	2.50	4.83	7.31	8.0	3	6.0*	21.4*	4.6*	2.6*
Unsubstrated τ_0	4.20	0.0915	8.38	9.70	26	58.3*	97.7*	19.9*	24.4*

$^{+}$Relative errors estimated using the continuous fit results as "ideal" condition. *Relative errors estimated using the interval 0.1 min as "ideal" condition. See Equations 13 and 14.

Table 7 shows that as the interval of time increases, the relative error increases. Thus, it is suggested to obtain data points as many as possible in the conversion region to correctly apply the Avrami fit. As in the continuous crystallization approach, the fit to curves without subtracting τ_0 leads to significant errors, as high as 98 %, and n values higher than 4.0. Also, in this case (unsubtracted τ_0), even considering $K^{1/n}$ values the errors are still higher than 30%.

3.6. FLASH DSC: APPLICATION OF THE AVRAMI AND LAURITZEN AND HOFFMAN THEORIES

The FSC is a growing technique that brings new insights related to polymer crystallization. The study of crystallization kinetics by FSC is advantageous because of extremely fast heating and cooling rates. The continuous crystallization approach has been considered in FSC experiments; but the required minimal sample mass generated, under isothermal conditions, a low heat flow.[22] This makes the step-crystallization the preferred approach (in FSC). For the step-crystallization approach the same considerations explained in previous sections, e.g., the number of points, induction times, among others, must be taken into consideration. Considering the low T_c reached with FSC, the number of points at the low conversion range is essential to apply the Avrami fit, as shown in Table 7. Thus, more points can be collected at shorter time intervals to guarantee a better Avrami fit.

In Section 3.5, the continuous and step-crystallization were compared using a conventional DSC. The Avrami fit leads to similar results in both cases. Experimentally, longer testing times are required for the step-crystallization approach. The time consumption problem is overcome in the FSC due to its faster cooling and heating rates, making proper the use of the step-crystallization and the Avrami fit with the FSC. The step-crystallization experimental protocol with an FSC is similar to the one shown in Scheme 4d, except for the scanning rates. The scanning rates in the FSC allow obtaining amorphous samples from the melt (in most but not all cases), i.e., suppressing the crystallization by fast cooling until vitrification occurs. The critical rate to get such a state depends on the material; for instance, the critical rate for iPP is 1000 K/s, while for the PLLA, it is only 0.5 K/s.[22] Such fast scanning rates allow the study of crystallization kinetics in a significantly broad range of supercooling. However, in the case of linear polyethylene, even cooling rates as fast as 500,000 K/s are not fast enough to quench it into the amorphous state.[22]

In a recent contribution, Schick and Androsh[22] presented examples of $\tau_{50\%}$ vs. T_c curves for different materials, including iPP, illustrating the occurrence of two distinct crystallization rate maxima. To illustrate how the APP can be applied to FSC data, we replotted the reported data[22] and fitted them with the LH equation, as shown in Figure 16.

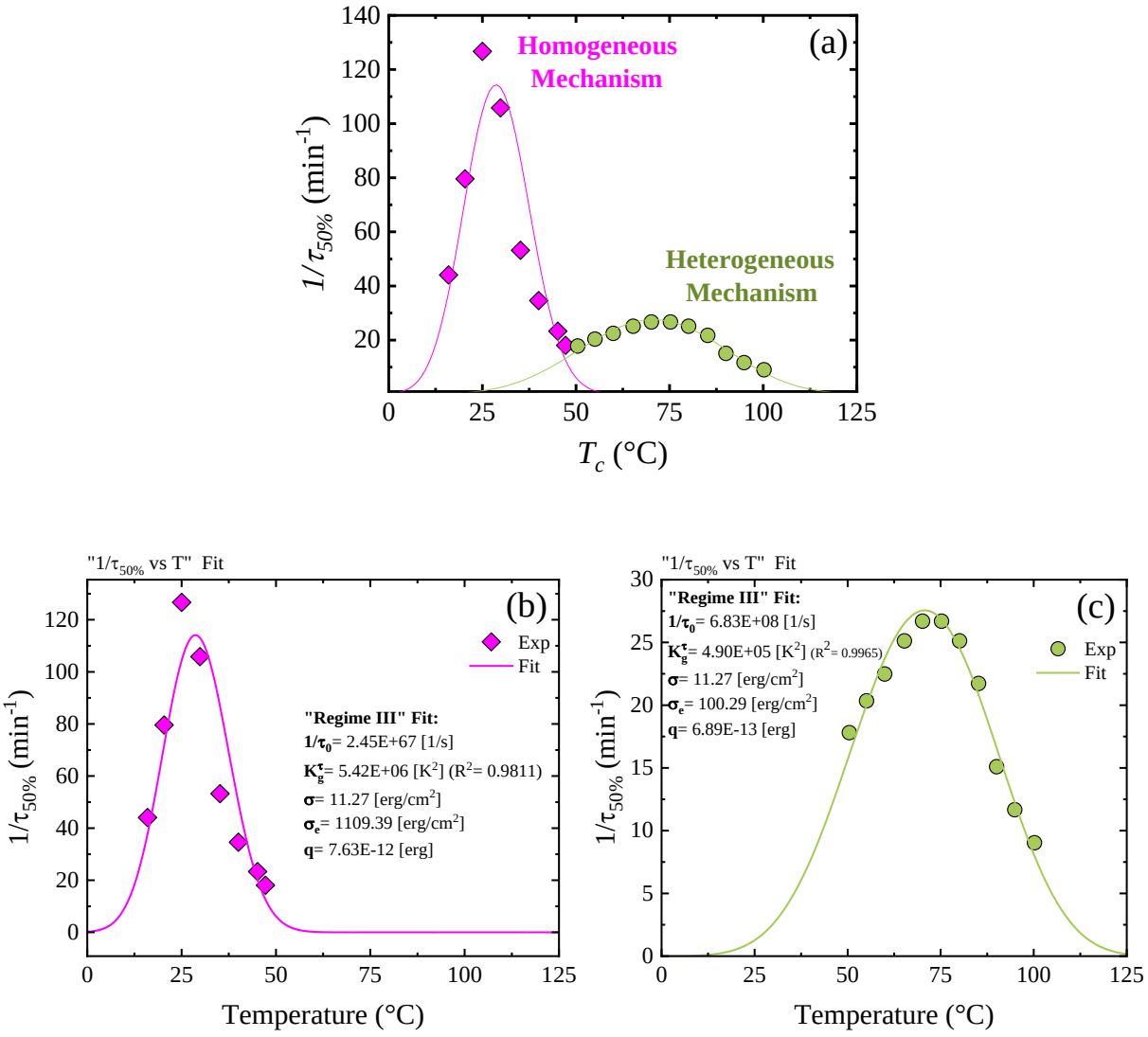

Figure 16. (a) $1/\tau_{50\%}$ vs. T_c data for iPP taken from reference 22. Each nucleation mechanism was fitted with the LH model. The $1/\tau_{50\%}$ vs. T_c data and the results of the LH fitting are shown in (b) homogenous mechanism; and (c) heterogeneous mechanism.

Figure 16a shows that a broader range of ΔT can be covered in the FSC for iPPs. The two maxima have been related to the homogeneous (at high ΔT, i.e., low T_c) and heterogeneous (at low ΔT, i.e., high T_c) nucleation mechanism. At low ΔT, the crystallization from the melt proceeds via spherulitic growth of lamellae. The heterogeneous nucleation mechanism was explained above (see Figure 10), and its maxima is related to the diffusion vs. nucleation control. At high ΔT takes place the formation of small ordered domains or crystals, which are not forming higher-ordered

superstructures; instead, a nodular morphology has been reported. Thus, the homogeneous nucleation mechanism at high ΔT seems to be independent of the growth. The homogeneous nucleation mechanism has been experimentally supported by a significantly higher nucleation density (at low ΔT) than the heterogeneous nucleation region.[22] In PBT it was found nucleation density values in the order of 10^6 (low ΔT, heterogeneous) and 10^{15} nuclei/mm^3 (high ΔT, homogeneous).[107] Additionally, it has been found that nucleating agents purposely added are active at low ΔT (heterogenous mechanism region). In contrast, they do not significantly affect the homogeneous region (high ΔT), suggesting that the crystallization in this region takes place by a homogenous nucleation mechanism.[22] The homogeneous nucleation has also been reported in "droplet experiments" in which droplets or domains clean of heterogeneities can be obtained.[19] Such droplets have been reported in immiscible polymer blends, block copolymers with microphase-separated microdomains, and polymers infiltrated in alumina templates.[20, 21, 41-44, 80, 81, 83, 102, 104,108]

The two maxima shown in Figure 16a cannot be simultaneously fitted with the LH approach. Here, we provide the first attempt to fit the data by separating the LH approaches in two, assuming the same feeding parameters as in Section 3.3.1. The obtained values for the heterogeneous region are comparable with the literature and the values here obtained for the PP and PP-NA. The K_g^τ values are higher for the homogeneous nucleation curve, in one order of magnitude, which is expected because homogeneous nucleation has a higher free energy barrier than heterogeneous nucleation. The LH fit performed in the heterogeneous area, in Figure 16c, proves that this approach is suitable for FSC data. Even though the LH fit was also achieved in the homogeneous area, its analysis requires further investigation.

4. CONCLUSIONS

Crystallization kinetics is intrinsic to polymeric materials and of importance to their applications. This contribution provides a guideline on how to obtain information on crystallization kinetics correctly. The discussion was divided into two aspects (a) experimental and (b) interpretation and analysis of isothermal crystallization, by using real data from common polymers (iPP and PLA) with different thermal protocols. The experimental data were analyzed with Avrami, and LH theories only from a practical point of view, using a Crystallization Fit Origin ® App[71] recently developed by us. Various common experimental and analytical mistakes were

simulated, and their errors were calculated, showing the importance of working and analyzing the ideal conditions. In addition, key messages related to the FSC were given in this contribution, providing a complete picture of the crystallization kinetics.

Experimentally, the success of an isothermal crystallization is evidenced in the measurement of complete isothermal curves. This implies that the crystallization during the cooling steps (before the isothermal step) must be avoided. The only way to prevent crystallization during the cooling rates is by using appropriate cooling rates and crystallization temperatures (e.g., above $T_{c,min}$). It is recommended to carefully study the testing conditions (e.g., $T_{c,min}$ protocol) before the isothermal test.

With ideal experimental data, the Avrami theory can be easily applied. Here, it is vital to consider (remove) the induction time since it dramatically affects the Avrami results. Also, a careful determination of the induction time allows indirect measurements of the nucleation rate through the inverse of the induction time.

The LH theory was applied with the Crystallization Fit Origin ® App, obtaining results in line with the literature. Here we show the versatility of the LH theory by employing the fit to experimental data obtained from PLOM, DSC, and FSC (homogenous and heterogeneous nucleation mechanism). The analysis with the LH model of isothermal crystallization from the melt and the self-nucleation state allows us to determine the overall crystallization kinetics, and the growth kinetics, respectively, through DSC measurements.

ACKNOWLEDGEMENTS

This work was supported by the National Natural Science Foundation of China (21922308, 51820105005) and the National Key R&D Program of China (2017YFE0117800). We would also like to acknowledge the financial support from the BIODEST project; this project has received funding from the European Union's Horizon 2020 research and innovation programme under the Marie Skłodowska-Curie grant agreement No. 778092. The funding of MICINN (Spain) through grant PID2020-113045GB-C21 is gratefully acknowledged. G.L. is grateful to the Youth Innovation Promotion Association of the Chinese Academy of Sciences (Y201908). Mr. Ming Wang is thanked for preparing the AAO infiltrated sample. Dr. Maryam Safari is thanked for the fruitful discussions and data related to random copolymers, and Mr. Sam Fang and Dr. Easwar R.

Iyer from OriginLab Corporation for their help transforming our plug-in (ref.9) into an updated APP (ref. 71).

Conflicts of Interest: The authors declare not conflict of interest.

REFERENCES

[1] Xu, J.; Reiter, G.; Alamo, R. G. Concepts of Nucleation in Polymer Crystallization. *Crystals* **2021,** 11 (3), 304.
[2] Ozawa, T. Kinetics of non-isothermal crystallization. *Polymer* **1971,** 12 (3), 150-158 DOI: https://doi.org/10.1016/0032-3861(71)90041-3.
[3] Toda, A. A reinterpretation of the Ozawa model for non-isothermal crystallization at fixed scan rates. *Thermochimica Acta* **2021**, 707, 179086 DOI: https://doi.org/10.1016/j.tca.2021.179086.
[4] Di Lorenzo, M. L.; Silvestre, C. Non-isothermal crystallization of polymers. *Progress in Polymer Science* **1999,** 24 (6), 917-950 DOI: https://doi.org/10.1016/S0079-6700(99)00019-2.
[5] Avrami, M. Granulation, Phase Change, and Microstructure Kinetics of Phase Change. III. *The Journal of Chemical Physics* **1941,** 9 (2), 177-184 DOI: 10.1063/1.1750872.
[6] Avrami, M. Kinetics of Phase Change. I General Theory. *Journal of Chemistry Physics* **1939,** 7 (12), 1103-1112 DOI: 10.1063/1.1750380.
[7] Avrami, M. Kinetics of Phase Change. II Transformation‐Time Relations for Random Distribution of Nuclei. *The Journal of Chemical Physics* **1940,** 8 (2), 212-224 DOI: 10.1063/1.1750631.
[8] Fanfoni, M.; Tomellini, M. The Johnson-Mehl- Avrami-Kohnogorov model: A brief review. *Il Nuovo Cimento D* **1998,** 20 (7), 1171-1182 DOI: 10.1007/BF03185527.
[9] Lorenzo, A. T.; Arnal, M. L.; Albuerne, J.; Müller, A. J. DSC isothermal polymer crystallization kinetics measurements and the use of the Avrami equation to fit the data: Guidelines to avoid common problems. *Polymer Testing* **2007,** 26 (2), 222-231 DOI: https://doi.org/10.1016/j.polymertesting.2006.10.005.
[10] Piorkowska, E.; Galeski, A.; Haudin, J.-M. Critical assessment of overall crystallization kinetics theories and predictions. *Progress in Polymer Science* **2006,** 31 (6), 549-575 DOI: https://doi.org/10.1016/j.progpolymsci.2006.05.001.
[11] Hoffman, J. D.; Lauritzen, J. I. Crystallization of Bulk Polymers With Chain Folding: Theory of Growth of Lamellar Spherulites *J. Res. Natl. Bur. Stand., Sect. A* **1961,** 65A (4), 297-336 DOI: http://dx.doi.org/10.6028/jres.065A.035.
[12] Lauritzen, J. I.; Hoffman, J. D. Theory of Formation of Polymer Crystals with Folded Chains in Dilute Solution. *J. Res. Natl. Bur. Stand., Sect. A* **1960,** 64A (1), 73-102 DOI: http://dx.doi.org/10.6028/jres.064A.007.
[13] Muthukumar, M.; Welch, P. Modeling polymer crystallization from solutions. *Polymer* **2000,** 41 (25), 8833-8837 DOI: https://doi.org/10.1016/S0032-3861(00)00226-3.
[14] Zhang, M. C.; Guo, B.-H.; Xu, J. A Review on Polymer Crystallization Theories. *Crystals* **2017,** 7 (1), 4.
[15] Hoffman, J. D.; Miller, R. L. Kinetic of crystallization from the melt and chain folding in polyethylene fractions revisited: theory and experiment. *Polymer* **1997,** 38 (13), 3151-3212 DOI: https://doi.org/10.1016/S0032-3861(97)00071-2.

[16] Baltá-Calleja, F. J.; Ezquerra, T. A., Polymer Crystallization: General Concepts of Theory and Experiments. In *Encyclopedia of Materials: Science and Technology*, Buschow, K. H. J., Cahn, R. W., Flemings, M. C., Ilschner, B., Kramer, E. J., Mahajan, S., Veyssière, P., Eds. Elsevier: Oxford, 2001; pp 7244-7252.
[17] Gedde, U. W.; Hedenqvist, M. S., Crystallization Kinetics. In *Fundamental Polymer Science*, Springer International Publishing: Cham, 2019; pp 327-386.
[18] Wypych, G., *Handbook of Nucleating Agents*. ChemTec Publishing: 2016; pp 1-3.
[19] Sangroniz, L.; Cavallo, D.; Müller, A. J. Self-Nucleation Effects on Polymer Crystallization. *Macromolecules* **2020,** 53 (12), 4581-4604 DOI: 10.1021/acs.macromol.0c00223.
[20] Michell, R. M.; Blaszczyk-Lezak, I.; Mijangos, C.; Müller, A. J. Confinement effects on polymer crystallization: From droplets to alumina nanopores. *Polymer* **2013,** 54 (16), 4059-4077 DOI: https://doi.org/10.1016/j.polymer.2013.05.029.
[21] Michell, R. M.; Blaszczyk-Lezak, I.; Mijangos, C.; Müller, A. J. Confined crystallization of polymers within anodic aluminum oxide templates. *Journal of Polymer Science Part B: Polymer Physics* **2014,** 52 (18), 1179-1194 DOI: https://doi.org/10.1002/polb.23553.
[22] Schick, C.; Androsch, R., New Insights into Polymer Crystallization by Fast Scanning Chip Calorimetry. In *Fast Scanning Calorimetry*, Schick, C., Mathot, V., Eds. Springer International Publishing: Cham, 2016; pp 463-535.
[23] Cavallo, D.; Müller, A. J., Polymer Crystallization. In *Macromolecular Engineering: From Precise Synthesis to Macroscopic Materials and Applications*, 2nd Edition ed.; Matyjaszewski, K., Gnanou, Y., Hadjichristidi, N., Muthukumar, M., Eds. John Wiley & Sons, Inc.: 2022.
[24] Müller, A. J.; Michell, R. M.; Lorenzo, A. T., Isothermal Crystallization Kinetics of Polymers. In *Polymer Morphology*, 2016; pp 181-203.
[25] Fillon, B.; Wittmann, J. C.; Lotz, B.; Thierry, A. Self‐nucleation and recrystallization of isotactic polypropylene (α phase) investigated by differential scanning calorimetry. *Journal of Polymer Science Part B: Polymer Physics* **1993,** 31 (10), 1383-1393 DOI: 10.1002/polb.1993.090311013.
[26] Michell, R. M.; Mugica, A.; Zubitur, M.; Müller, A. J., Self-Nucleation of Crystalline Phases Within Homopolymers, Polymer Blends, Copolymers, and Nanocomposites. In *Polymer Crystallization I: From Chain Microstructure to Processing*, Auriemma, F., Alfonso, G. C., de Rosa, C., Eds. Springer International Publishing: Cham, 2017; pp 215-256.
[27] Müller, A. J.; Michell, R. M.; Pérez, R. A.; Lorenzo, A. T. Successive Self-nucleation and Annealing (SSA): Correct design of thermal protocol and applications. *European Polymer Journal* **2015,** 65, 132-154 DOI: https://doi.org/10.1016/j.eurpolymj.2015.01.015.
[28] López-Barrón, C. R.; Hagadorn, J. R.; Throckmorton, J. A. Isothermal Crystallization Kinetics of α-Olefin Molecular Bottlebrushes. *Macromolecules* **2020,** 53 (17), 7439-7449 DOI: 10.1021/acs.macromol.0c01282.
[29] Lorenzo, A. T.; Müller, A. J. Estimation of the nucleation and crystal growth contributions to the overall crystallization energy barrier. *Journal of Polymer Science Part B: Polymer Physics* **2008,** 46 (14), 1478-1487 DOI: 10.1002/polb.21483.
[30] Pérez-Camargo, R. A.; Meabe, L.; Liu, G.; Sardon, H.; Zhao, Y.; Wang, D.; Müller, A. J. Even–Odd Effect in Aliphatic Polycarbonates with Different Chain Lengths: from Poly (Hexamethylene Carbonate) to Poly (Dodecamethylene Carbonate). *Macromolecules* **2020,** 54 (1), 259-271 DOI: 10.1021/acs.macromol.0c02374.

[31] Zhang, S.; Wang, Z.; Guo, B.; Xu, J. Secondary nucleation in polymer crystallization: A kinetic view. *Polymer Crystallization* **2021,** 4 (3), e10173 DOI: https://doi.org/10.1002/pcr2.10173.
[32] Androsch, R.; Toda, A.; Furushima, Y.; Schick, C. Insertion-Crystallization-Induced Low-Temperature Annealing Peaks in Melt-Crystallized Poly(l-Lactic Acid). *Macromol. Chem. Phys.* **2021,** 222 (18), 2100177 DOI: https://doi.org/10.1002/macp.202100177.
[33] Wutz, C.; Bark, M.; Cronauer, J.; Döhrmann, R.; Zachmann, H. G. Simultaneous measurements of small angle x-ray scattering, wide angle x-ray scattering, and light scattering during phase transitions in polymers. *Review of Scientific Instruments*. **1995,** 66 (2), 1303-1307 DOI: 10.1063/1.1145959.
[34] Gedde, U. W., *Polymer Physics*. Springer Netherlands: 1999; p 298.
[35] Nogales, A.; Ezquerra, T. A.; Batallán, F.; Frick, B.; López-Cabarcos, E.; Baltá-Calleja, F. J. Restricted Dynamics in Poly(ether ether ketone) As Revealed by Incoherent Quasielastic Neutron Scattering and Broad-Band Dielectric Spectroscopy. *Macromolecules* **1999,** 32 (7), 2301-2308 DOI: 10.1021/ma9815758.
[36] Murthy, N. S., Chapter 3 - Experimental Techniques for Understanding Polymer Crystallization. In *Crystallization in Multiphase Polymer Systems*, Thomas, S., Arif P, M., Gowd, E. B., Kalarikkal, N., Eds. Elsevier: 2018; pp 49-72.
[37] Rueda, D. R.; Viksne, A.; Malers, L.; Calleja, F. J. B.; Zachmann, H. G. Influence of morphology on the microhardness of poly(ethylene naphthalene-2,6-dicarboxylate). *Macromol. Chem. Phys.* **1994,** 195 (12), 3869-3876 DOI: https://doi.org/10.1002/macp.1994.021951213.
[38] Baltá Calleja, F. J.; Fakirov, S., *Microhardness of Polymers*. Cambridge University Press: Cambridge, 2000.
[39] Mandelkern, L., *Crystallization of Polymers: Volume 1: Equilibrium Concepts*. 2 ed.; Cambridge University Press: Cambridge, 2002; Vol. 1.
[40] Ergoz, E.; Fatou, J. G.; Mandelkern, L. Molecular Weight Dependence of the Crystallization Kinetics of Linear Polyethylene. I. Experimental Results. *Macromolecules* **1972,** 5 (2), 147-157 DOI: 10.1021/ma60026a011.
[41] Balsamo, V.; Urdaneta, N.; Pérez, L.; Carrizales, P.; Abetz, V.; Müller, A. J. Effect of the polyethylene confinement and topology on its crystallisation within semicrystalline ABC triblock copolymers. *European Polymer Journal* **2004,** 40 (6), 1033-1049 DOI: https://doi.org/10.1016/j.eurpolymj.2004.01.009.
[42] Müller, A. J.; Balsamo, V.; Arnal, M. L., Nucleation and Crystallization in Diblock and Triblock Copolymers. In *Block Copolymers II*, Abetz, V., Ed. Springer Berlin Heidelberg: Berlin, Heidelberg, 2005; pp 1-63.
[43] Su, C.; Chen, Y.; Shi, G.; Li, T.; Liu, G.; Müller, A. J.; Wang, D. Crystallization Kinetics of Poly(ethylene oxide) under Confinement in Nanoporous Alumina Studied by in Situ X-ray Scattering and Simulation. *Langmuir* **2019,** 35 (36), 11799-11808 DOI: 10.1021/acs.langmuir.9b01968.
[44] Michell, R. M.; Müller, A. J. Confined crystallization of polymeric materials. *Progress in Polymer Science* **2016,** 54-55, 183-213 DOI: https://doi.org/10.1016/j.progpolymsci.2015.10.007.
[45] Fisher, J. C.; Hollomon, J. H.; Turnbull, D. Nucleation. *Journal of Applied Physics* **1948,** 19 (8), 775-784 DOI: 10.1063/1.1698202.
[46] Lauritzen Jr, J.I.; Hoffman, J. D. Formation of Polymer Crystals with Folded Chains from Dilute Solution. *J. Chem.Phys.* **1959,** 31 (6), 1680-1681 DOI: 10.1063/1.1730678.

[47] Patki, R.; Mezghani, K.; Phillips, P. J., Crystallization Kinetics of Polymers. In *Physical Properties of Polymers Handbook*, Mark, J. E., Ed. Springer New York: New York, NY, 2007; pp 625-640.
[48] Mandelkern, L., *Crystallization of Polymers: Volume 2: Kinetics and Mechanisms*. 2 ed.; Cambridge University Press: Cambridge, 2004; Vol. 2.
[49] Müller, A. J.; Albuerne, J.; Marquez, L.; Raquez, J.-M.; Degée, P.; Dubois, P.; Hobbs, J.; Hamley, I. W. Self-nucleation and crystallization kinetics of double crystalline poly(p-dioxanone)-b-poly(ε-caprolactone) diblock copolymers. *Faraday Discussions* **2005,** 128 (0), 231-252 DOI: 10.1039/b403085k.
[50] Sabino, M. A.; Albuerne, J.; Müller, A. J.; Brisson, J.; Prud'homme, R. E. Influence of in Vitro Hydrolytic Degradation on the Morphology and Crystallization Behavior of Poly(p-dioxanone). *Biomacromolecules* **2004,** 5 (2), 358-370 DOI: 10.1021/bm034367i.
[51] Sadler, D. M.; Gilmer, G. H. Rate-Theory Model of Polymer Crystallization. *Physical Review Letters* **1986,** 56 (25), 2708-2711 DOI: 10.1103/PhysRevLett.56.2708.
[52] Hu, W.; Frenkel, D.; Mathot, V. B. F. Intramolecular Nucleation Model for Polymer Crystallization. *Macromolecules* **2003,** 36 (21), 8178-8183 DOI: 10.1021/ma0344285.
[53] Strobl, G. From the melt via mesomorphic and granular crystalline layers to lamellar crystallites: A major route followed in polymer crystallization? *The European Physical Journal E* **2000,** 3 (2), 165-183 DOI: 10.1007/s101890070030.
[54] Kundagrami, A.; Muthukumar, M. Continuum theory of polymer crystallization. *The Journal of Chemical Physics* **2007,** 126 (14), 144901 DOI: 10.1063/1.2713380.
[55] Li, C. Y. The rise of semicrystalline polymers and why are they still interesting. *Polymer* **2020,** 211, 123150 DOI: https://doi.org/10.1016/j.polymer.2020.123150.
[56] Zhang, S.; Wang, Z.; Guo, B.; Xu, J. Secondary nucleation in polymer crystallization: A kinetic view. *Polymer crystallization* **2021,** 4 (3), e10173 DOI: https://doi.org/10.1002/pcr2.10173.
[57] Hu, W. Growth rate equations of lamellar polymer crystals. *Polymer Crystallization*. **2018,** 1 (4), e25831 DOI: https://doi.org/10.1002/pcr2.10038.
[58] Armitstead, K.; Goldbeck-Wood, G.; Keller, A., Polymer crystallization theories. In *Macromolecules: Synthesis, Order and Advanced Properties*, Springer Berlin Heidelberg: Berlin, Heidelberg, 1992; pp 219-312.
[59] Hiemenz, P. C.; Lodge, T. P., *Polymer Chemistry* Second Edition ed.; CRC Press: 2007.
[60] Liang, G.; Bao, S.; Zhu, F., Chapter 2 - Theoretical Aspects of Polymer Crystallization in Multiphase Systems. In *Crystallization in Multiphase Polymer Systems*, Thomas, S., Arif P, M., Gowd, E. B., Kalarikkal, N., Eds. Elsevier: 2018; pp 17-48.
[61] Thomas, D. G.; Staveley, L. A. K. 889. A study of the supercooling of drops of some molecular liquids. *Journal of the Chemical Society (Resumed)* **1952,** (0), 4569-4577 DOI: 10.1039/JR9520004569.
[62] Lorenzo, A. T.; Arnal, M. L.; Sánchez, J. J.; Müller, A. J. Effect of annealing time on the self-nucleation behavior of semicrystalline polymers. *Journal of Polymer Science Part B: Polymer Physics* **2006,** 44 (12), 1738-1750 DOI: 10.1002/polb.20832.
[63] Galante, M. J.; Mandelkern, L.; Alamo, R. G.; Lehtinen, A.; Paukker, R. Crystallization kinetics of metallocene type polypropylenes. *Journal of thermal analysis* **1996,** 47 (4), 913-929 DOI: 10.1007/BF01979439.
[64] Hay, J. N.; Mills, P. J. The use of differential scanning calorimetry to study polymer crystallization kinetics. *Polymer* **1982,** 23 (9), 1380-1384 DOI: https://doi.org/10.1016/0032-3861(82)90283-X.

[65] Hay, J. N.; Booth, A. The effect of a secondary process on the course of polymer crystallisation. *British Polymer Journal* **1972,** 4 (1), 19-26 DOI: https://doi.org/10.1002/pi.4980040104.
[66] Wang, B.; Utzeri, R.; Castellano, M.; Stagnaro, P.; Müller, A. J.; Cavallo, D. Heterogeneous Nucleation and Self-Nucleation of Isotactic Polypropylene Microdroplets in Immiscible Blends: From Nucleation to Growth-Dominated Crystallization. *Macromolecules* **2020,** 53 (14), 5980-5991 DOI: 10.1021/acs.macromol.0c01167.
[67] Androsch, R.; Di Lorenzo, M. L. Crystal Nucleation in Glassy Poly(l-lactic acid). *Macromolecules* **2013,** 46 (15), 6048-6056 DOI: 10.1021/ma401036j.
[68] Androsch, R.; Schick, C.; Di Lorenzo, M. L., Kinetics of Nucleation and Growth of Crystals of Poly(l-lactic acid). In *Synthesis, Structure and Properties of Poly(lactic acid)*, Di Lorenzo, M. L., Androsch, R., Eds. Springer International Publishing: Cham, 2018; pp 235-272.
[69] Müller, A. J.; Ávila, M.; Saenz, G.; Salazar, J., CHAPTER 3 Crystallization of PLA-based Materials. In *Poly(lactic acid) Science and Technology: Processing, Properties, Additives and Applications*, The Royal Society of Chemistry: 2015; pp 66-98.
[70] Ruiz, M. B.; Pérez-Camargo, R. A.; López, J. V.; Penott-Chang, E.; Múgica, A.; Coulembier, O.; Müller, A. J. Accelerating the crystallization kinetics of linear polylactides by adding cyclic poly (L-lactide): Nucleation, plasticization and topological effects. *International Journal of Biological Macromolecules* **2021,** 186, 255-267 DOI: https://doi.org/10.1016/j.ijbiomac.2021.07.028.
[71] OriginLab Crystallization Fit. https://www.originlab.com/fileExchange/details.aspx?fid=597 (March 09, 2021),
[72] Kholodovych, V.; Welsh, W. J., Densities of Amorphous and Crystalline Polymers. In *Physical Properties of Polymers Handbook*, Mark, J. E., Ed. Springer New York: New York, NY, 2007; pp 611-617.
[73] Trujillo, M.; Arnal, M. L.; Müller, A. J.; Mujica, M. A.; Urbina de Navarro, C.; Ruelle, B.; Dubois, P. Supernucleation and crystallization regime change provoked by MWNT addition to poly(ε-caprolactone). *Polymer* **2012,** 53 (3), 832-841 DOI: https://doi.org/10.1016/j.polymer.2011.12.028.
[74] Pérez, R. A.; Córdova, M. E.; López, J. V.; Hoskins, J. N.; Zhang, B.; Grayson, S. M.; Müller, A. J. Nucleation, crystallization, self-nucleation and thermal fractionation of cyclic and linear poly(ε-caprolactone)s. *Reactive and Functional Polymers* **2014,** 80, 71-82 DOI: https://doi.org/10.1016/j.reactfunctpolym.2013.10.013.
[75] Pérez, R. A.; López, J. V.; Hoskins, J. N.; Zhang, B.; Grayson, S. M.; Casas, M. T.; Puiggalí, J.; Müller, A. J. Nucleation and Antinucleation Effects of Functionalized Carbon Nanotubes on Cyclic and Linear Poly(ε-caprolactones). *Macromolecules* **2014,** 47 (11), 3553-3566 DOI: 10.1021/ma5005869.
[76] Imai, M.; Mori, K.; Mizukami, T.; Kaji, K.; Kanaya, T. Structural formation of poly (ethylene terephthalate) during the induction period of crystallization: 1. Ordered structure appearing before crystal nucleation. *Polymer* **1992,** 33 (21), 4451-4456 DOI: https://doi.org/10.1016/0032-3861(92)90399-H.
[77] Imai, M.; Mori, K.; Mizukami, T.; Kaji, K.; Kanaya, T. Structural formation of poly(ethylene terephthalate) during the induction period of crystallization: 2. Kinetic analysis based on the theories of phase separation. *Polymer* **1992,** 33 (21), 4457-4462 DOI: https://doi.org/10.1016/0032-3861(92)90400-Q.

[78] Safari, M.; Mugica, A.; Zubitur, M.; Martínez de Ilarduya, A.; Muñoz-Guerra, S.; Müller, A. J. Controlling the Isothermal Crystallization of Isodimorphic PBS-ran-PCL Random Copolymers by Varying Composition and Supercooling. *Polymers* **2020,** 12 (1), 17.
[79] Córdova, M. E.; Lorenzo, A. T.; Müller, A. J.; Gani, L.; Tencé-Girault, S.; Leibler, L. The Influence of Blend Morphology (Co-Continuous or Sub-Micrometer Droplets Dispersions) on the Nucleation and Crystallization Kinetics of Double Crystalline Polyethylene/Polyamide Blends Prepared by Reactive Extrusion. *Macromol. Chem. Phys.* **2011,** 212 (13), 1335-1350 DOI: https://doi.org/10.1002/macp.201100039.
[80] Müller, A. J.; Arnal, M. L.; Balsamo, V., Crystallization in Block Copolymers with More than One Crystallizable Block. In *Progress in Understanding of Polymer Crystallization*, Reiter, G., Strobl, G. R., Eds. Springer Berlin Heidelberg: Berlin, Heidelberg, 2007; pp 229-259.
[81] Shi, G.; Wang, Z.; Wang, M.; Liu, G.; Cavallo, D.; Müller, A. J.; Wang, D. Crystallization, Orientation, and Solid–Solid Crystal Transition of Polybutene-1 Confined within Nanoporous Alumina. *Macromolecules* **2020,** 53 (15), 6510-6518 DOI: 10.1021/acs.macromol.0c01384.
[82] Liu, G.; Müller, A. J.; Wang, D. Confined Crystallization of Polymers within Nanopores. *Accounts of Chemical Research* **2021,** 54 (15), 3028-3038 DOI: 10.1021/acs.accounts.1c00242.
[83] Sangroniz, L.; Wang, B.; Su, Y.; Liu, G.; Cavallo, D.; Wang, D.; Müller, A. J. Fractionated crystallization in semicrystalline polymers. *Progress in Polymer Science* **2021,** 115, 101376 DOI: https://doi.org/10.1016/j.progpolymsci.2021.101376.
[84] Hoffman, J. D.; Weeks, J. J. Melting process and the equilibrium melting temperature of polychlorotrifluoroethylene. *J. Res. Natl. Bur. Stand. Sect. A* **1962,** 66A (1), 13-28 DOI: http://dx.doi.org/10.6028/jres.066A.003.
[85] Alamo, R. G.; Viers, B. D.; Mandelkern, L. A Re-examination of the Relation between the Melting Temperature and the Crystallization Temperature: Linear Polyethylene. *Macromolecules* **1995,** 28 (9), 3205-3213 DOI: 10.1021/ma00113a024.
[86] Toda, A.; Taguchi, K.; Nozaki, K. Gibbs–Thomson, Thermal Gibbs–Thomson, and Hoffman–Weeks Plots of Polyethylene Crystals Examined by Fast-Scan Calorimetry and Small-Angle X-ray Scattering. *Crystal Growth & Design* **2019,** 19 (4), 2493-2502 DOI: 10.1021/acs.cgd.9b00209.
[87] Müller, A. J.; Arnal, M. L. Thermal fractionation of polymers. *Progress in Polymer Science* **2005,** 30 (5), 559-603 DOI: https://doi.org/10.1016/j.progpolymsci.2005.03.001.
[88] Müller, A. J.; Hernández, Z. H.; Arnal, M. L.; Sánchez, J. J. Successive self-nucleation/annealing (SSA): A novel technique to study molecular segregation during crystallization. *Polymer Bulletin* **1997,** 39 (4), 465-472 DOI: 10.1007/s002890050174.
[89] Arandia, I.; Mugica, A.; Zubitur, M.; Iturrospe, A.; Arbe, A.; Liu, G.; Wang, D.; Mincheva, R.; Dubois, P.; Müller, A. J. Application of SSA thermal fractionation and X-ray diffraction to elucidate comonomer inclusion or exclusion from the crystalline phases in poly(butylene succinate-ran-butylene azelate) random copolymers. *Journal of Polymer Science Part B: Polymer Physics* **2016,** 54 (22), 2346-2358 DOI: 10.1002/polb.24146.
[90] Van Krevelen, D. W., CHAPTER 5 - CALORIMETRIC PROPERTIES. In *Properties of Polymers (Third Edition)*, Van Krevelen, D. W., Ed. Elsevier: Amsterdam, 1997; pp 109-127.
[91] Yamada, K.; Hikosaka, M.; Toda, A.; Yamazaki, S.; Tagashira, K. Equilibrium Melting Temperature of Isotactic Polypropylene with High Tacticity: 1. Determination by Differential Scanning Calorimetry. *Macromolecules* **2003,** 36 (13), 4790-4801 DOI: 10.1021/ma021206i.
[92] Cheng, S. Z. D.; Janimak, J. J.; Zhang, A.; Cheng, H. N. Regime transitions in fractions of isotactic polypropylene. *Macromolecules* **1990,** 23 (1), 298-303 DOI: 10.1021/ma00203a051.

[93] Pawlak, A.; Galeski, A., Crystallization of Polypropylene. In *Polypropylene Handbook: Morphology, Blends and Composites*, Karger-Kocsis, J., Bárány, T., Eds. Springer International Publishing: Cham, 2019; pp 185-242.
[94] Clark, E. J.; Hoffman, J. D. Regime III crystallization in polypropylene. *Macromolecules* **1984,** 17 (4), 878-885 DOI: 10.1021/ma00134a058.
[95] Kang, J.; Li, J.; Chen, S.; Peng, H.; Wang, B.; Cao, Y.; Li, H.; Chen, J.; Gai, J.; Yang, F.; Xiang, M. Investigation of the crystallization behavior of isotactic polypropylene polymerized with different Ziegler-Natta catalysts. *J. Appl. Polym. Sci.* **2013,** 129 (5), 2663-2670 DOI: https://doi.org/10.1002/app.38984.
[96] Point, J. J.; Dosière, M. Crystal growth rate as a function of molecular weight in polyethylene crystallized from the melt: an evaluation of the kinetic theory of polymer crystallization. *Polymer* **1989,** 30 (12), 2292-2296 DOI: https://doi.org/10.1016/0032-3861(89)90264-4.
[97] Feng, Y.; Jin, X. Effect of self-nucleation on crystallization and melting behavior of polypropylene and its copolymers. *J. Appl. Polym. Sci.* **1999,** 72 (12), 1559-1564 DOI: https://doi.org/10.1002/(SICI)1097-4628(19990620)72:12<1559::AID-APP8>3.0.CO;2-F.
[98] Carmeli, E.; Fenni, S. E.; Caputo, M. R.; Müller, A. J.; Tranchida, D.; Cavallo, D. Surface Nucleation of Dispersed Polyethylene Droplets in Immiscible Blends Revealed by Polypropylene Matrix Self-Nucleation. *Macromolecules* **2021,** 54 (19), 9100-9112 DOI: 10.1021/acs.macromol.1c01430.
[99] Habel, C.; Maiz, J.; Olmedo-Martínez, J. L.; López, J. V.; Breu, J.; Müller, A. J. Competition between nucleation and confinement in the crystallization of poly(ethylene glycol)/ large aspect ratio hectorite nanocomposites. *Polymer* **2020,** 202, 122734 DOI: https://doi.org/10.1016/j.polymer.2020.122734.
[100] Wang, H.; Keum, J. K.; Hiltner, A.; Baer, E. Crystallization Kinetics of Poly(ethylene oxide) in Confined Nanolayers. *Macromolecules* **2010,** 43 (7), 3359-3364 DOI: 10.1021/ma902780p.
[101] Wen, X.; Su, Y.; Shui, Y.; Zhao, W.; Müller, A. J.; Wang, D. Correlation between Grafting Density and Confined Crystallization Behavior of Poly(ethylene glycol) Grafted to Silica. *Macromolecules* **2019,** 52 (4), 1505-1516 DOI: 10.1021/acs.macromol.8b02007.
[102] Palacios, J. K.; Mugica, A.; Zubitur, M.; Müller, A. J., Chapter 6 - Crystallization and Morphology of Block Copolymers and Terpolymers With More Than One Crystallizable Block. In *Crystallization in Multiphase Polymer Systems*, Thomas, S., Arif P, M., Gowd, E. B., Kalarikkal, N., Eds. Elsevier: 2018; pp 123-180.
[103] Müller, A. J.; Michell, R. M., Differential Scanning Calorimetry of Polymers. In *Polymer Morphology*, 2016; pp 72-99.
[104] Müller, A. J.; Arnal, M. L.; Lorenzo, A. T., Crystallization in Nano-Confined Polymeric Systems. In *Handbook of Polymer Crystallization*, 2013; pp 347-378.
[105] Córdova, M. E.; Lorenzo, A. T.; Müller, A. J.; Gani, L.; Tencé-Girault, S.; Leibler, L. The Influence of Blend Morphology (Co-Continuous or Sub-Micrometer Droplets Dispersions) on the Nucleation and Crystallization Kinetics of Double Crystalline Polyethylene/Polyamide Blends Prepared by Reactive Extrusion. *Macromolecular Chemistry and Physics* **2011,** 212 (13), 1335-1350 DOI: https://doi.org/10.1002/macp.201100039.
[106] Castillo, R. V.; Müller, A. J. Crystallization and morphology of biodegradable or biostable single and double crystalline block copolymers. *Progress in Polymer Science* **2009,** 34 (6), 516-560 DOI: https://doi.org/10.1016/j.progpolymsci.2009.03.002.

[107] Androsch, R.; Rhoades, A. M.; Stolte, I.; Schick, C. Density of heterogeneous and homogeneous crystal nuclei in poly (butylene terephthalate). *European Polymer Journal* **2015,** 66, 180-189 DOI: https://doi.org/10.1016/j.eurpolymj.2015.02.013.
[108] Wang, M.; Li, J.; Shi, G.; Liu, G.; Müller, A. J.; Wang, D. Suppression of the Self-Nucleation Effect of Semicrystalline Polymers by Confinement. *Macromolecules* **2021,** 54 (8), 3810-3821 DOI: 10.1021/acs.macromol.1c00485.